

Editor-in-Chief B.E.Paton

Editorial board:

Yu.S.Borisov	V.F.Khorunov
A.Ya.Ishchenko	I.V.Krivtsun
B.V.Khitrovskaya	L.M.Lobanov
V.I.Kyrian	A.A.Mazur
S.I.Kuchuk	Yatsenko
Yu.N.Lankin	I.K.Pokhodnya
V.N.Lipodaev	V.D.Poznyakov
V.I.Makhnenko	K.A.Yushchenko
O.K.Nazarenko	A.T.Zelnichenko
I.A.Ryabtsev	

International editorial council:

N.P.Alyoshin	(Russia)
U.Diltey	(Germany)
Guan Qiao	(China)
D. von Hofe	(Germany)
V.I.Lysak	(Russia)
N.I.Nikiforov	(Russia)
B.E.Paton	(Ukraine)
Ya.Pilarczyk	(Poland)
G.A.Turichin	(Russia)
Zhang Yanmin	(China)
A.S.Zubchenko	(Russia)

Promotion group:

V.N.Lipodaev, V.I.Lokteva
A.T.Zelnichenko (exec. director)

Translators:

A.A.Fomin, O.S.Kurochko,
I.N.Kutianova, T.K.Vasilenko

Editor:

N.A.Dmitrieva

Electron galley:

D.I.Sereda, T.Yu.Snegiryova

Address:

E.O. Paton Electric Welding Institute,
International Association «Welding»,
11, Bozhenko str., 03680, Kyiv, Ukraine

Tel.: (38044) 200 82 77

Fax: (38044) 200 81 45

E-mail: journal@paton.kiev.ua

http://www.nas.gov.ua/pwj

State Registration Certificate
KV 4790 of 09.01.2001

Subscriptions:

\$324, 12 issues per year,
postage and packaging included.
Back issues available.

All rights reserved.

This publication and each of the articles
contained herein are protected by copyright.
Permission to reproduce material contained in
this journal must be obtained in writing from
the Publisher.

Copies of individual articles may be obtained
from the Publisher.

CONTENTS

SCIENTIFIC AND TECHNICAL

<i>Makhnenko V.I., Olejnik O.I. and Paltsevich A.P.</i> Hydrogen behaviour in repair welding of the main pipelines under pressure	2
<i>Turichin G.A., Tsybulsky I.A., Zemlyakov E.V., Valdajtseva E.A. and Kuznetsov M.V.</i> Development of the technology and equipment for laser and laser-arc welding of aluminium alloys	10
<i>Kah P., Hiltunen E. and Martikainen J.</i> Experimental investigation of hot cracking susceptibility of wrought aluminum alloys	16
<i>Tarassenko Yu.P., Berdnik O.B. and Tsaryova I.N.</i> Optimization of conditions of reduction heat treatment of blades of alloy KhN65VMTYu after long-term service	22
<i>Pereplyotchikov E.F. and Ryabtsev I.A.</i> Properties of iron-base alloys for plasma powder hard-facing of sealing surfaces of fittings	27
<i>Pokhodnya I.K., Karmanov V.I., Yavdoshchin I.R., Gubanya I.P., Khizhun O.Yu. and Khobta I.V.</i> Particle dispersity and manganese valence in welding aerosol	31

INDUSTRIAL

<i>Paton B.E., Lakomsky V.I. and Braginets V.I.</i> Welded electric contacts of dissimilar conductors	34
<i>Nesterenkov V.M., Bondarev A.A., Arkhangelsky Yu.A. and Zagornikov V.I.</i> Electron beam welding of bodies of drill bits with modifying of weld metal by zirconium	40
<i>Pokhmursky V.I., Student M.M., Gvozdetsky V.M. and Pokhmurskaya A.V.</i> Flux-cored wires of FMI series for coating deposition by electric arc spraying (Review)	44

BRIEF INFORMATION

<i>Ryzhkov S.S., Blintsov V.S., Egorov G.V., Zhukov Yu.D., Kvasnitsky V.F., Koshkin K.V., Krivtsun I.V., Nekrasov V.A., Sevryukov V.V. and Solonichenko Yu.V.</i> Development of versatile transport ships and ocean engineering facilities	49
---	----

NEWS

Foundation of the E.O. Paton Chinese-Ukrainian Welding Institute	51
--	----



HYDROGEN BEHAVIOUR IN REPAIR WELDING OF THE MAIN PIPELINES UNDER PRESSURE

V.I. MAKHNENKO, O.I. OLEJNIK and A.P. PALTSEVICH

E.O. Paton Electric Welding Institute, NASU, Kiev, Ukraine

Possibility of diffusion hydrogen penetration from hydrocarbon gas transported through the gas pipeline during repair welding performance on an operating pipeline has been analyzed. It is shown that at partial pressure of diffusion hydrogen on the inner surface of steel pipe in the range of 0.10–0.75 MPa at residual wall thickness in the defect zone of more than 5 mm increase of the parameter of hydrogen (cold) cracking risk is not higher than 5–11 %. Values of experimental measurements of diffusion hydrogen flow through the pipe wall in operating pipelines are given.

Keywords: repair arc welding, operating gas pipelines, diffusion hydrogen, gas pipeline wall, hydrogen cracks, risk of formation

A typical problem in repair welding of the main gas pipelines in stringent modes (low heat input) is the risk of appearance of cold (hydrogen) cracks, the formation of which is essentially affected by diffusion hydrogen in the welded joint metal. Application of consumables with a low hydrogen content in combination with reliable protection of the weld pool from the environment allows an essential lowering of the content of diffusion hydrogen in the HAZ. However, there still remains one more source of diffusion hydrogen – natural gas transported through the pipeline, which contains hydrogen in the form of chemical compounds (methane, propane, ethane, butane), or in the molecular form H_2 which does not diffuse into the pipeline wall metal. However, depending on pressure and temperature, natural gas can be in the two-phase state, i.e. the liquid phase also exists alongside

the gas phase. Figure 1 gives the two-phase state diagram of natural gas, from which it follows that at working pressures of about 7.5 MPa and temperatures of 40–50 °C the liquid phase is equal to approximately 20 % of the mixture volume. In the liquid phase free hydrogen can dissolve in the atomic form. Considering the high degree of gas turbulization in the main gas pipeline, higher density of the liquid phase and lower temperature in the pipe section at its walls, it can be assumed that the liquid phase concentrates at the pipe walls and from the liquid phase the dissolved atomic hydrogen diffuses into the pipe wall metal, respectively. Under the stationary conditions of natural gas transportation, hydrogen flow J through the wall can be presented in the following form [1]:

$$J = -D \frac{\partial C}{\partial r} \text{ (ml/(cm}^2\text{·s))}, \quad (1)$$

where D is the average coefficient of hydrogen diffusion through the pipe wall metal; $C(r)$ is the concentration of diffusion hydrogen across the pipe wall thickness (coordinate r).

At the stationary flow and small wall thicknesses

$$J \approx \frac{C(R_{\text{out}}) - C(R_{\text{in}})}{\delta} D, \quad (2)$$

where $C(R_{\text{out}})$ is the hydrogen concentration on the outer surface $r = R_{\text{out}}$; $C(R_{\text{in}})$ is the same on the pipe inner surface $r = R_{\text{in}}$.

Assuming that $C(R_{\text{out}}) \approx 0$, and $C(R_{\text{in}}) \approx \sqrt{P_{H_2}} K(T)$ according to Sievert's law, where P_{H_2} is the partial pressure of hydrogen on the surface $r = R_{\text{in}}$, ata; $K(T)$ is the diffusivity of hydrogen in the pipe wall metal at temperature T (Figure 2), $\text{cm}^3 / (100 \text{ g} \cdot \text{ata}^{1/2})$, we obtain

$$C(R_{\text{in}}) = J \frac{\delta}{D(T)} \text{ (ml/100 g)} \quad (3)$$

or in the most often used dimension

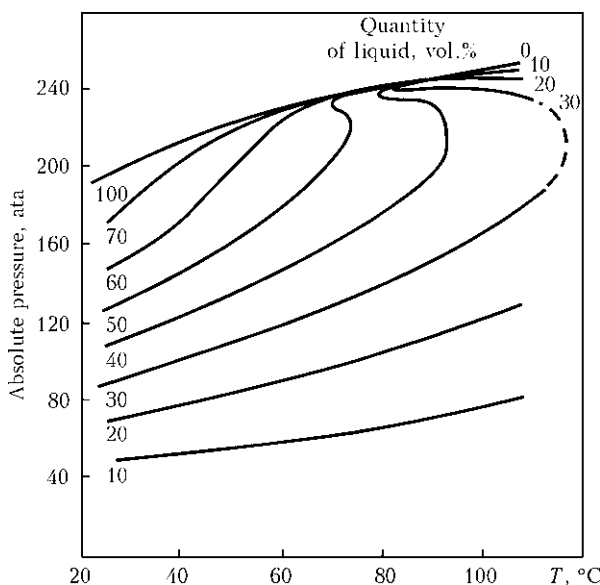


Figure 1. Phase diagram characteristic for natural hydrocarbon mixture



Table 1. Calculated values of $J\delta$ depending on T and P_{out}

$T, ^\circ\text{C}$	$D \cdot 10^6, \text{cm}^2/\text{s}$	$K, \text{ml}/(100 \text{ g} \cdot \text{ata}^{1/2})$	$J\delta \cdot 10^3, \text{ml}/(\text{cm}^2 \cdot \text{h}), \text{ at } P_{out}, \text{ ata}$				
			1	4	6	8	10
20	0.20	1.9	0.1069	0.214	0.262	0.302	0.338
40	0.46	1.8	0.2320	0.464	0.570	0.659	0.736
60	0.98	1.7	0.4680	0.938	1.147	1.325	1.482
80	1.91	1.6	0.8590	1.721	2.105	2.431	2.718

$$\overline{C}(R_{in}) = J \frac{\delta}{D(T)} \frac{100 \text{ g}}{\gamma} \text{ (ml/100 g)},$$

where γ is the specific weight of pipe wall steel (7.8 g/cm^3).

From the data in Figure 2 (Sievert's law), it follows that at the same partial pressure of hydrogen P_{out} hydrogen concentration on the pipe inner surface $C(R_{in})$, and, therefore, across the wall thickness can rise significantly, at the expense of increase of metal temperature in repair welding. This is, naturally, valid provided P_{out} remains constant, i.e. convective supply of hydrogen in the near-wall region rather quickly compensates its diffusion removal into the pipe wall.

Using data from [2, 3] of relative value D at temperature T of pipe wall in the form of

$$D(T) = 0.12 \exp\left(-\frac{3900}{T + 273}\right), \quad T < 200 \text{ } ^\circ\text{C},$$

we obtain from (1)–(3), allowing for the data of Figure 2 at $20 \leq T \leq 80 \text{ } ^\circ\text{C}$, the dependence of value $J\delta \cdot 3600, \text{ ml}/(\text{cm}^2 \cdot \text{h})$ on P_{out} (Table 1), where

$$J\delta = K \sqrt{P_{out}} D \frac{\gamma}{100} \cdot 3600 \text{ (ml}/(\text{cm}^2 \cdot \text{h})). \quad (4)$$

From the data of Table 1 it is seen that at $\delta = 1 \text{ cm}$, the magnitude of hydrogen flow J from $1 \text{ cm}^2/\text{h}$ area essentially depends on wall temperature, and at $T = 40 \text{ } ^\circ\text{C}$ and $P_{out} = 1 \text{ ata}$ it does not exceed $0.232 \cdot 10^{-3} \text{ ml}/(\text{cm}^2 \cdot \text{h})$, and at $P_{out} = 10 \text{ ata}$ this value does not exceed $0.736 \cdot 10^{-3} \text{ ml}/(\text{cm}^2 \cdot \text{h})$, i.e. sufficiently sensitive equipment is required to record such flows and determine values P_{out} and $C(R_{in})$, respectively, particularly within the limits of $P_{out} < 5 \text{ ata}$ and $T < 40 \text{ } ^\circ\text{C}$.

In the total volume of pumped gas, these losses through the wall of $1420 \times 20 \text{ mm}$ pipe at the pressure $P = 75 \text{ ata}$, $P_{out} = 8 \text{ ata}$ and transportation velocity $v = 10 \text{ m/s} = 36,000 \text{ m/h}$ are equal ($T = 80 \text{ } ^\circ\text{C}$) to just $0.25 \cdot 10^{-10} \%$, i.e. they are of little concern for gas producers.

In this connection the purpose of this work is drawing the attention of researchers to the problem of hydrogenation of pipeline wall at the expense of diffusion hydrogen flow from the transported hydrocarbons. It should be noted that this question is quite actively discussed in foreign publications [4, et al.]. Therefore,

this paper considers P_{out} influence on diffusion hydrogen distribution at welding heating in the zone of pipe wall thinning, depending on its thickness in the welding heating region, when making the first pass by arc welding in the following modes: $I = 90 \text{ A}$, $U = 24 \text{ V}$, $v_w = 0.2 \text{ cm/s}$. Pipe material is steel of 17G1S type.

Hydrogen distribution should be considered allowing for distribution of metal microstructure and its stressed state in the joint zone at welding heating. High stress level in the considered repair pressure welding in the HAZ metal is quite obvious, and as regards microstructural changes, their distribution is of a quite local nature, and requires the respective correlation with diffusion hydrogen distribution.

Calculations were performed using «ArcWeldSys» computer system developed at PWI [1, 3], which was applied to determine by successive tracing in time t (starting from the moment $t = 0$) of the arc passing through this cross-section, the temperature field $T(x, y, z)$, base metal fusion zone (FZ) characterized by isotherms of maximum temperatures $T_{max}(x, y) = T_L$, $T_{max}(x, y) = T_S$, where T_L and T_S are the temperatures of liquidus (about $1490 \text{ } ^\circ\text{C}$) and solidus (about $1420 \text{ } ^\circ\text{C}$), zone of microstructural changes characterized by isotherm $T_{max}(x, y) = 800 \text{ } ^\circ\text{C}$, for the mid-section along the deposited pass $z = \text{const}$ in plane x ,

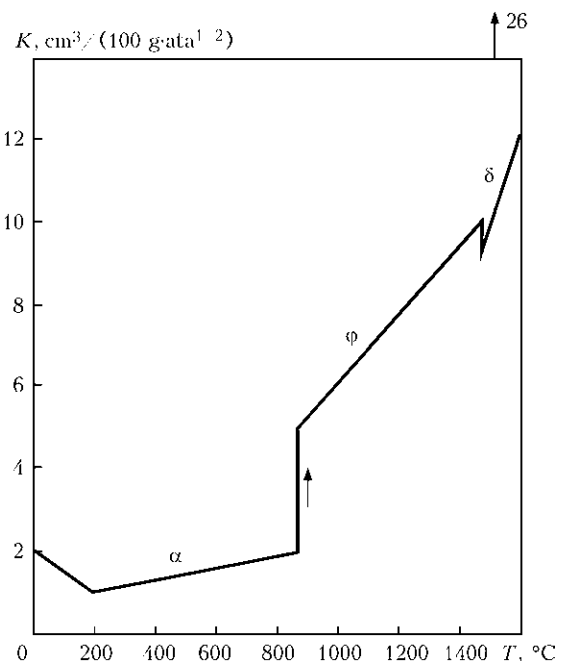


Figure 2. Temperature influence on hydrogen solubility K in iron

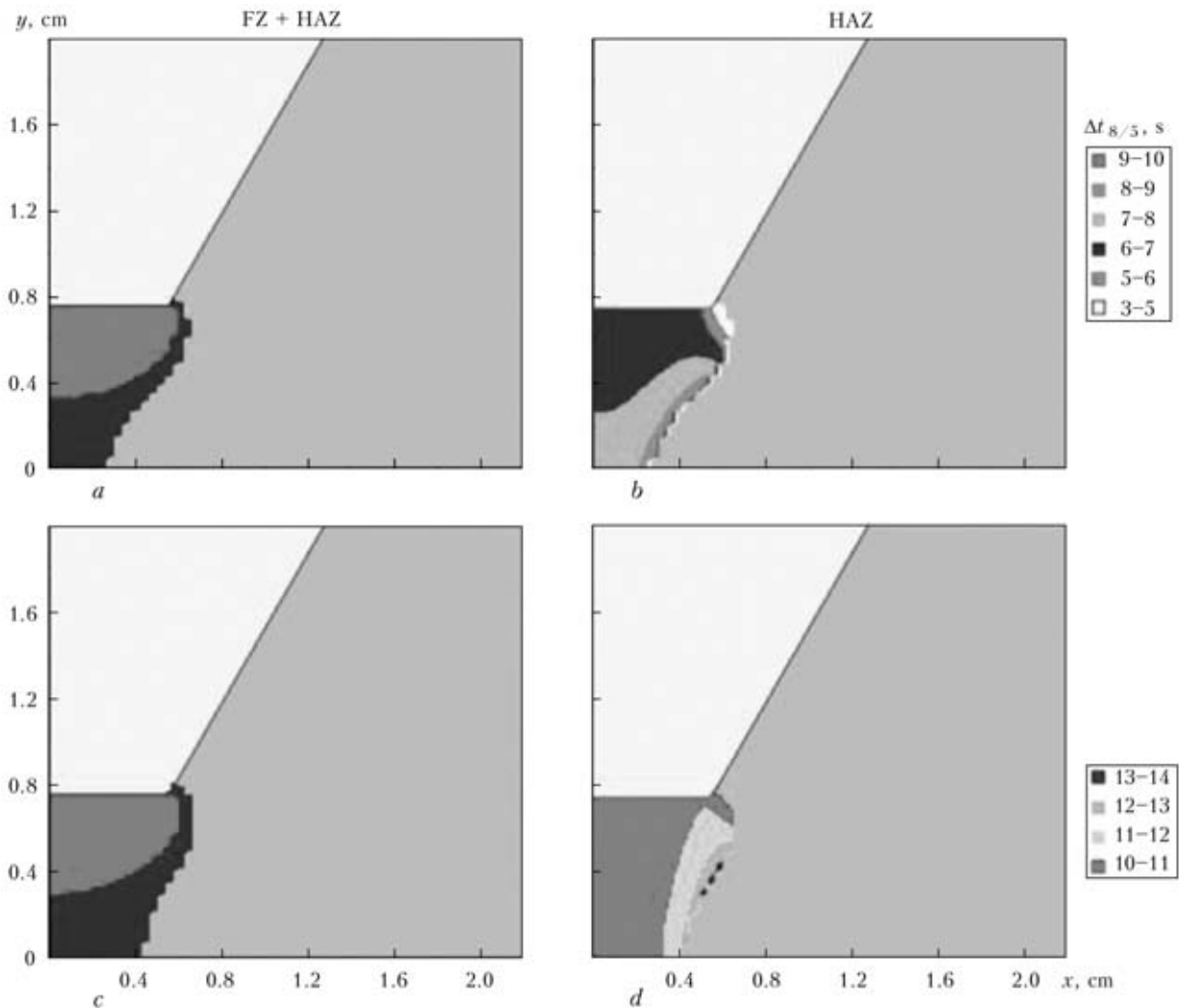


Figure 3. Results of calculation of FZ and HAZ dimensions (a), $\Delta t_{8/5}$ (b) for the first pass of arc welding-up of groove defect along the pipe circumference at $\delta_{\min} = 5$ mm, $P_{H_2} = 7.5$ ata and gas velocity in the pipe of 6 m/s (without preheating), and the same but at preheating to 150 °C (c, d)

y . In the HAZ $\Delta t_{8/5}$ – time of metal staying in the temperature range of 800–500 °C in the FZ and HAZ at cooling, was calculated. Figure 3 gives the calculation data associated with heating in the zone with minimum metal thickness $\delta_{\min} = 5$ mm without preheating, i.e. $T_0 = 20$ °C and with preheating up to $T_0 = 150$ °C. Velocity of gas motion in the pipe on the level of 6 m/s and coefficient of heat exchange on the inner surface [5] equal to 0.05 J/(cm²·s·°C), respectively, were taken into account. Figure 4 gives the calculation data of $\Delta t_{8/5}$ for the zone with minimum thickness $\delta_{\min} = 10$ mm without preheating and with preheating to $T_0 = 150$ °C.

Table 2 gives the calculation data of $\Delta t_{8/5}$ for four variants, which in combination with APA diagram [6] for 17G1S steel in Figure 5 allow judging the quantity of martensite V_M and bainite V_B in the microstructure of HAZ metal at cooling. These data show that the microstructural condition in the welding heating zone in the considered steel in repair welding is sufficiently favourable in terms of formation of cold cracks in the presence of the appropriate content of diffusion hydrogen in the HAZ metal (condition of high tensile

stresses in the considered repair pressure welding is always observed). Calculation data are given below.

Figures 6–9 give the kinetics of variation in time t of hydrogen concentration in the weld cross-section for two thicknesses of pipe wall in the defect zone (welding) at $P_{H_2} = 0$ and 7.5 ata at its content of 10 cm³/100 g in the deposited metal. It is seen that at the considered welding heating in the zone of small pipe wall thicknesses (Figure 6, a, b) and intensive restoration of partial pressure of hydrogen $P_{H_2} = 7.5$ ata a considerable saturation of metal by diffusion hydrogen occurs inside the pipe in the zone of the wall local heating (concentration reaches values of approximately 26 cm³/100 g), compared to the variant, when $P_{H_2} = 0$ and respective concentration of hydrogen reaches values of approximately 4 cm³/100 g. At metal cooling, however, this high concentration of hydrogen drops abruptly and already at $t = 58$ s it differs not so significantly for both the cases.

Increase of δ_{\min} to 10 mm (Figure 9, a, b) noticeably lowers the influence of hydrogen flow from the

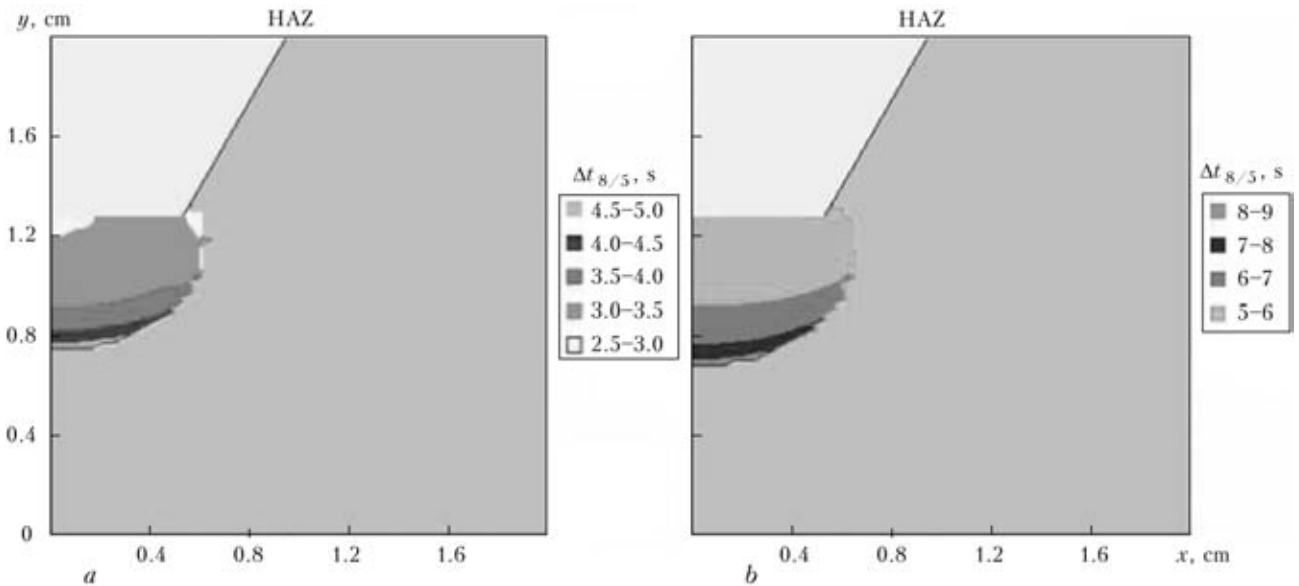


Figure 4. Time of metal staying in the HAZ at cooling $\Delta t_{8/5}$ for zone of thickness $\delta_{min} = 10$ mm, $T_0 = 20$ (a), 150 (b) °C

pipe at $P_{H_2} = 7.5$ ata on distribution of the latter in the HAZ metal, as this zone is located markedly farther from the pipe inner surface. Eventually, maximum concentration reaches not more than $7 \text{ cm}^3/100 \text{ g}$ (Figure 9, b) compared to $26 \text{ cm}^3/100 \text{ g}$ in Figure 8, b.

As regards the conditions of cold crack formation, analysis of the data in Figures 6, 7 and Table 2 leads to the following conclusions.

For variant 1 in the HAZ metal at $\Delta t_{8/5} = 3-5$ s in point 1 diffusion hydrogen content $[H] \approx 2.0 \text{ cm}^3/100 \text{ g}$ at $V_M = 100 \%$, and at $\Delta t_{8/5} = 7-8$ s and $v_M = 35 \%$, $[H] \approx 1.5 \text{ cm}^3/100 \text{ g}$ (see Figure 6, a, point 2), i.e. the most stringent conditions for hydrogen are observed in HAZ metal in the corner of weld metal surface meeting the base metal (point 1).

According to [7] sensitivity index

$$\varphi = 12P_{cm} + \log H, \quad (5)$$

where

$$P_{cm} = C + \frac{Si}{30} + \frac{Mn + Cu + Cr}{20} + \frac{Ni}{60} + \frac{Mo}{15} + \frac{V}{10} + 5 B; \quad (6)$$

Table 2. Values of $\Delta t_{8/5}$ and volume fraction of microstructural components in the HAZ metal for the four variants

Parameter	Variant			
	1 (Figure 3, a, b)	2 (Figure 3, c, d)	3 (Figure 4, a)	4 (Figure 4, b)
$\Delta t_{8/5}, \text{ s}$	7-8	11-12	4-5	6-8
$V_M, \text{ vol.}\%$	35-40	25-30	55-60	50-40
$V_B, \text{ vol.}\%$	65-60	75-70	45-40	50-60

H is the content of diffusion hydrogen in the deposited metal.

For the considered steel (see Figure 5) at $P_{H_2} = 0$ $P_{cm} = 0.272$; for point 1 in Figure 6, a, $P_1 = 4.264$, respectively. In the case of $P_{H_2} = 7.5$ ata (Figure 6, b) at the same microstructure local concentration of diffusion hydrogen $[H]_{loc}$ changes markedly: in point 1 $[H]_{loc} = 3.0 \text{ cm}^3/100 \text{ g}$, in point 2 $[H] = 4.9 \text{ cm}^3/100 \text{ g}$. Accordingly, equivalent value H_{eq} for formula (5), allowing for linear dependence of results in Figures 6 and 7 on hydrogen in the deposited metal ($10 \text{ cm}^3/100 \text{ g}$) can be determined from the following dependence:

$$H_{eq} = 10 \text{ cm}^3/100 \text{ g} \frac{[H]_{loc}(7.5)}{[H]_{loc}(0)}, \quad (7)$$

where $[H]_{loc}(7.5)$, $[H]_{loc}(0)$ are the local concentrations in points 1 and 2 at $P_{H_2} = 7.5$ and 0 ata.

Table 3 gives for the considered in Figures 6, 7 variants 1-4 the respective initial data on microstructure and local values of hydrogen concentration $[H]_{loc}$ (P_{out}) in points 1, 2 and results of calculation by (5)-(7), demonstrating the degree of the possible in-

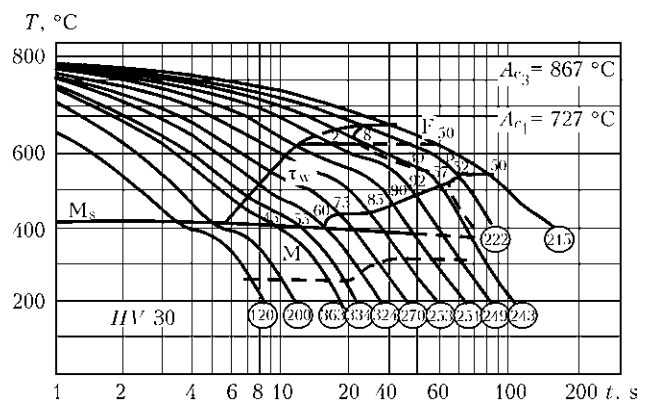


Figure 5. APA diagram for steel of 17G1S type

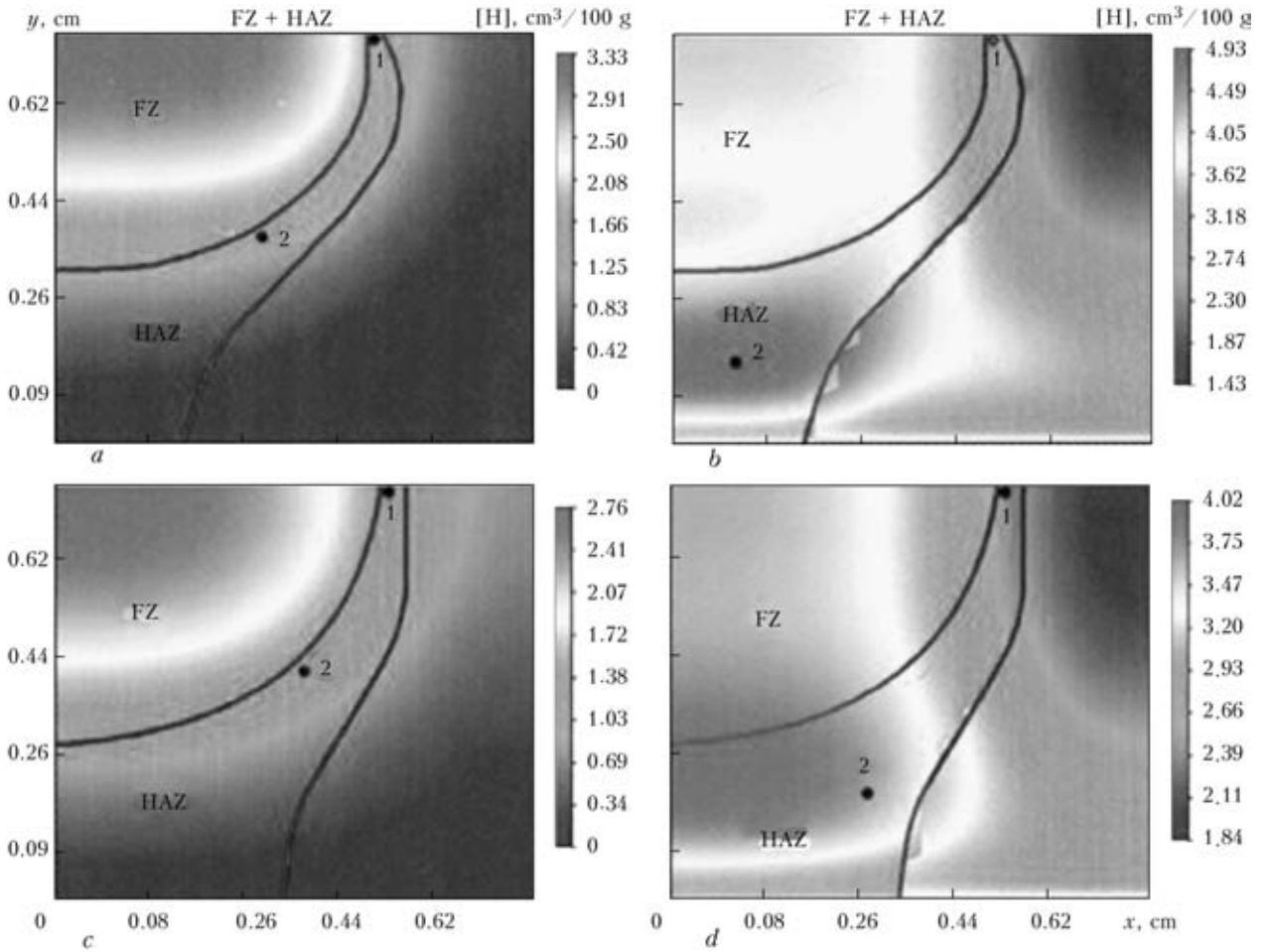


Figure 6. Distribution of diffusion hydrogen in the cross-section of the first pass at $\Delta_{\min} = 5$ mm at the moment of time $t = 98$ s at $P_{H_2} = 0$ (a, c) and 7.5 (b, d) at $T_0 = 20$ (a, b) and 150 (c, d) °C in FZ and HAZ

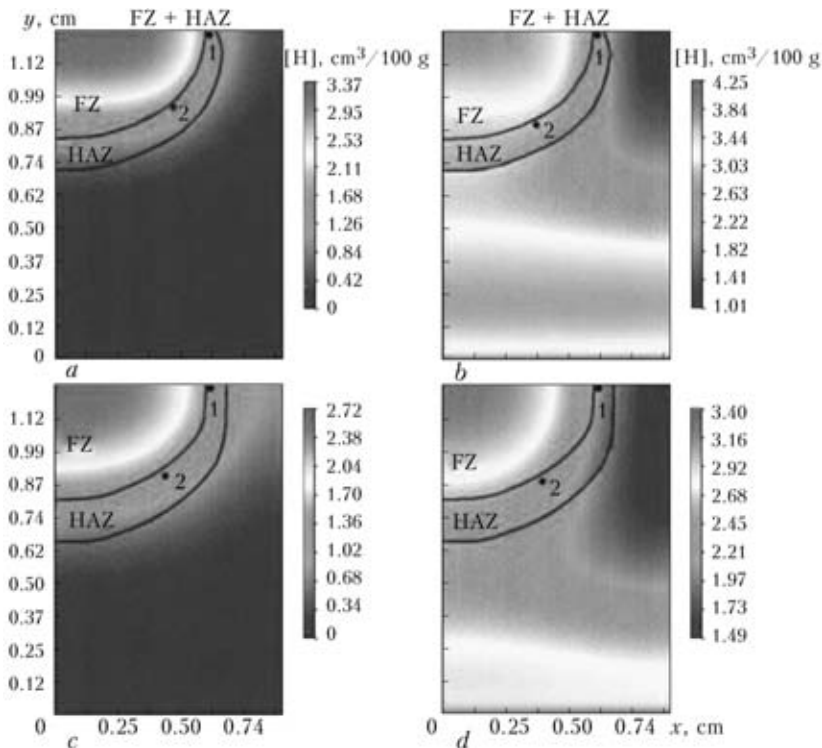


Figure 7. Same as in Figure 6, but at $\delta_{\min} = 10$ mm

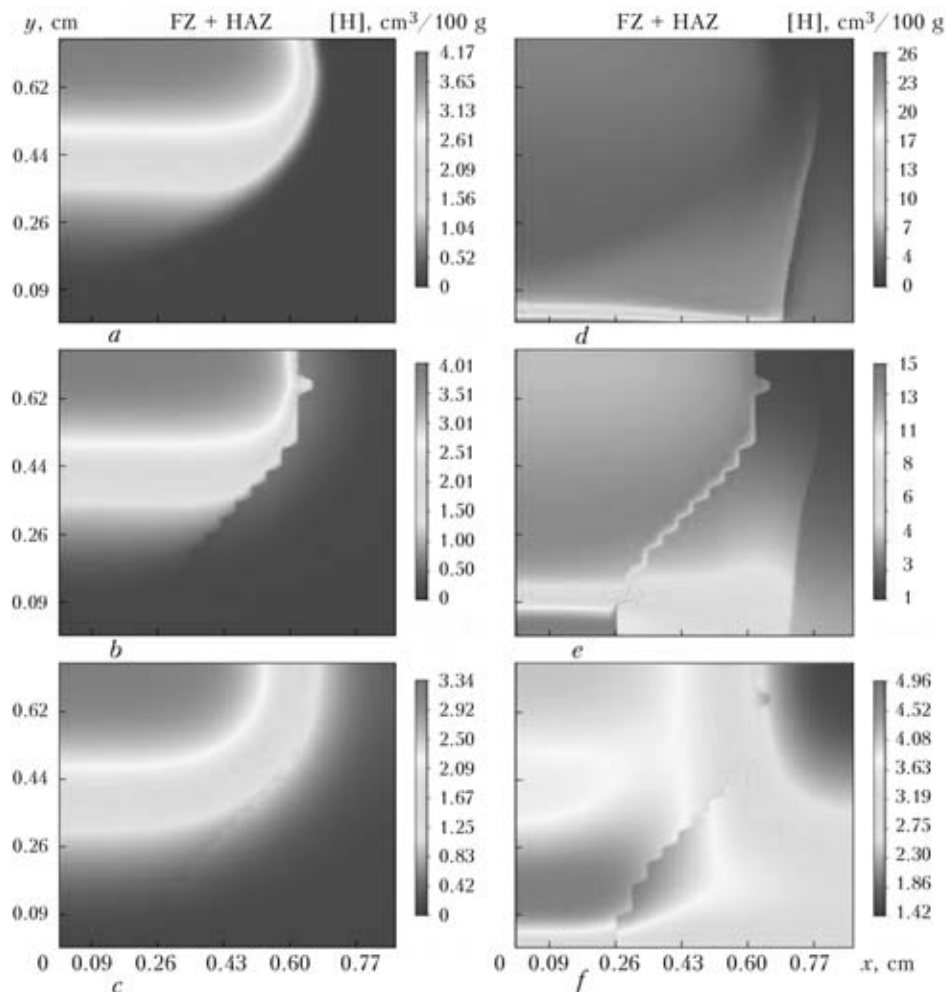


Figure 8. Concentration of diffusion hydrogen at $\delta_{\min} = 5$ mm and $T_0 = 20$ °C in different moments of time $t = 2$ (a, d), 10 (b, d) and 58 (c, f) s since the moment of welding heat source passing through this section at $P_{H_2} = 0$ (a-c) and 7.5 (d-f) ata in the FZ and HAZ

fluence of diffusion hydrogen entering the HAZ metal on the risk of formation of cold (hydrogen) cracks.

The given data lead to the conclusion that the additional source of diffusion hydrogen, related to natural gas transported through the pipeline, in repair pressure welding can lead at small δ_{\min} to an essential saturation of welding heating zone by diffusion hydrogen in the high temperature range. However, during cooling of the pipe walls diffusion hydrogen concentration is equalized, both in the wall metal and between the wall and hydrogen containing layer in the near-wall region with partial pressure P_{H_2} . As a result, at temperatures below 150 °C and $P_{H_2} < 7.5$ ata (≈ 0.75 MPa) the influence of additional diffusion hydrogen source on cold crack formation is low and can be quite well compensated by low hydrogen content in the filler metal. At higher partial pressures of diffusion hydrogen, however, $P_{H_2} > 7.5$ ata the risk of cold cracking rises considerably.

Determination of real P_{H_2} values or its level in the operating main gas pipelines is a quite urgent task. With this purpose the paper authors organized experimental measurements in the operating gas pipelines:

- in the area of CU «Boyarka» ($P_{op} = 4.8$ MPa, $D \times \delta = 700 \times 16$ mm, $T = 8$ °C);
- CU «Kremenchug» ($P_{op} = 7.5$ MPa, $D \times \delta = 700 \times 16$ mm; $T = 48$ °C);
- in the area of GDS of TEP 5 ($P_{op} = 4.5$ MPa, $D \times \delta = 350 \times 11$ mm; $T = 13$ °C).

The essence of measurements consisted in application of a layer of glycerin 3–5 mm thick on the section of pipeline outer surface, having first cleaned it to remove paint and rust to metal luster.

It was assumed that bubbles of diffusion hydrogen going out through the pipe wall, will be fixed in the glycerin layer (standard procedure of glycerin test [8]). Observations in the above facilities were made for 7–10 days. As a result, not a single bubble was found in the glycerin sample, leading to the conclusion that the magnitude of hydrogen flow through the pipeline wall is below the resolution of the used method.

Thus, as a result of the conducted rather extensive experimental measurements using the glycerin test to determine the actual hydrogen flow through the wall of the main pipelines in Ukraine, allowing for the resolution of about $1 \text{ mm}^3 / (\text{cm}^3 \cdot \text{h})$, it was found that the real sought flow is below the resolution of the

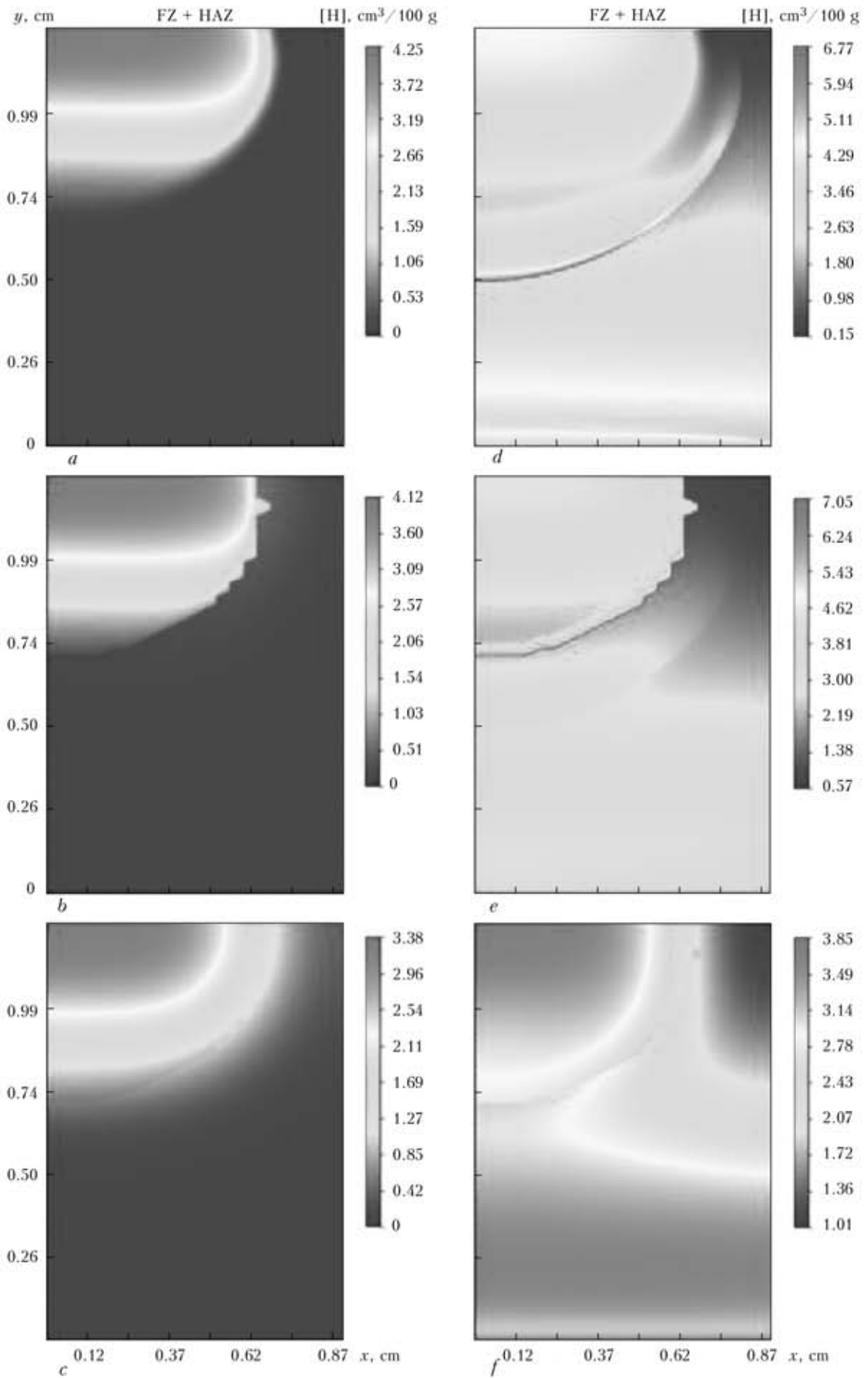


Figure 9. Same as in Figure 8, but at $\delta_{\min} = 10$ mm

**Table 3.** Results of calculation of the parameter of cold cracking risk for variants 1–4

Variant number	T_0 , °C	Points	V_M , %	P_{H_2} , ata	$[H]_{loc}$, cm ³ /100 g	ϕ	$\frac{\phi}{4.264}$
1 (Figure 6, a, b)	20	1	95	0	2.0	4.264	1.0
				7.5	3.0	4.440	1.03
		2	50	0	1.5	4.264	1.0
				7.5	4.9	4.750	1.11
2 (Figure 6, c, d)	150	1	30	0	1.5	4.264	1.0
				7.5	2.5	4.490	1.05
		2	20	0	1.7	4.264	1.0
				7.5	3.0	4.510	1.06
3 (Figure 7, a, b)	20	1	100	0	1.5	4.264	1.0
				7.5	2.5	4.490	1.05
		2	55	0	1.5	4.264	1.0
				7.5	2.5	4.490	1.05
4 (Figure 7, c, d)	150	1	50	0	1.5	4.264	1.0
				7.5	2.0	4.390	1.03
		2	45	0	1.5	4.264	1.0
				7.5	2.5	4.490	1.05

used method, i.e. according to Table 1 partial pressure of diffusion hydrogen in the main pipelines is much lower than 1 ata (0.1 MPa), which allows regarding the influence of diffusion hydrogen from hydrocarbon gas transported through the pipeline, on hydrogen cracking to be quite negligible in repair welding on pipeline wall.

- Makhnenko, V.I., Korolova, T.V., Lavrynets, I.G. (2002) Numerical study of the effect of microstructural transformation on hydrogen redistribution in fusion welding of structural steels. In: *Mathematical modelling of weld phenomena 6*. Ed. by H. Cerjak. London: Maney Publ., 903–923.
- Katz, D.L. (1965) *Guideline on recovery, transport and processing of natural gas*. Moscow: Nedra.
- Makhnenko, V.I., Korolyova, T.V., Lavrinets, I.G. (2002) Effect of microstructural transformations on redistribution of hydrogen in fusion welding of structural steels. *The Paton Welding J.*, **2**, 6–13.
- Nechaev, Yu.S. (2008) Physical complex problems of ageing, embrittlement and fracture of metallic materials of hydrogen power engineering and main gas pipelines. *Uspekhi Fizich. Nauk*, **178(7)**, 709–726.
- Makhnenko, V.I. (2006) *Safe service life of welded joints and assemblies of current structures*. Kiev: Naukova Dumka.
- Seyffarth, P., Meyer, B., Scharff, A. (1992) *Grosser Atlas Schweiss-ZTU-Schaubilder*. Duesseldorf: DVS.
- (1998) *Welding Handbook*. Vol. 4: Materials and application. Pt 2. 8th ed. Miami: AWS.
- Petrov, G.L., Million, A. (1964) Processes of hydrogen redistribution in welded joints of carbon and low-alloy steels. *Svarochm. Proizvodstvo*, **10**, 1–6.



DEVELOPMENT OF THE TECHNOLOGY AND EQUIPMENT FOR LASER AND LASER-ARC WELDING OF ALUMINIUM ALLOYS*

G.A. TURICHIN, I.A. TSYBULSKY, E.V. ZEMLYAKOV, E.A. VALDAJTSEVA and M.V. KUZNETSOV
St.-Petersburg State Polytechnic University, St.-Petersburg, Russian Federation

Results of computer modelling of the process of hybrid welding of Al–Mg system aluminium alloys up to 10 mm thick by using a dynamic model are considered. Examples of computation of the welding process parameters and their experimental validation are given. The developed technological laser-arc system for implementation of the hybrid welding process is described.

Keywords: *laser and laser-arc welding, aluminium-magnesium alloys, process modelling, computations, geometric characteristics of the weld, thermal cycles, distribution of alloying elements, package of equipment, monitoring of the welding process*

High energy concentration of laser radiation pre-determines considerable intensification of the processes of treatment of materials. The concentrated energy input allows materials to be treated at higher speeds and lower residual thermal distortions. Recent achievements in the field of physics and engineering have made it possible to develop new laser radiation sources with much higher energy efficiency.

In welding of alloys, especially light ones based on aluminium, computation of parameters of a welded joint and prediction of its chemical composition and mechanical properties present a difficult problem because of the necessity to allow for removal of volatile additions, such as magnesium, lithium or zinc, which are crucial for the entire set of mechanical properties. Part of these additions is evaporated during welding. As a result, chemical composition and mechanical properties of the weld metal may differ from those of the base metal.

The Al–Mg system is one of the most promising in terms of development of alloys to be welded. Mechanical properties of the welded joints, as well as properties of the base metal, depend mostly on the magnesium content of an alloy, as strength of the alloy grows with increase of the magnesium content. Lithium also exerts a significant effect on properties of aluminium alloys, as variations in the lithium concentration influence both mechanical properties of the alloys and their sensitivity to cracking.

Computer model of laser-arc welding (LAW) based on technologically applicable descriptions of the processes taking place during LAW was used to increase efficiency of development of the LAW technology and equipment [1].

One of the results of many years' efforts is software LaserCad developed by the Institute of Laser and Welding Technologies of the St.-Petersburg State Polytechnic University for modelling of laser, arc and hybrid welding. The software allows computation of geometric characteristics of the weld, thermal cycles in the weld metal and HAZ, and content of alloying elements in the weld metal.

Mathematical modelling of hybrid welding based on the physically adequate model, allowing investigation of relationship between various physical phenomena responsible for development of instabilities in the weld pool, is the most expedient method to analyse causes of the humping effect occurring in the welding process and choose the ways of its elimination. The processes of hybrid LAW with deep penetration, as well as the related processes of laser welding, are often accompanied by formation of porosity and root peaks in the welds [2]. According to current notions about a physical nature of the laser welding processes, this is caused by development of self-oscillations of the keyhole and weld pool in welding with deep penetration [3].

Numerous experimental results confirm that the welding process with deep penetration is not stationary even in the case of stabilisation of all external factors affecting the weld pool [4]. In particular, high-speed filming of laser welding of composite specimens made from metals and optically transparent materials [5] showed a continual variation in shape of the keyhole, quasiperiodic motion of the zone with a maximal intensity in depth of the keyhole, as well as presence of such zones on the rear wall of the keyhole. Filming of the plasma plume also showed the presence of its periodic fluctuations [6].

Comparative investigations of motion of molten metal on the weld pool surface and process of formation of the root peaks confirm correlation between

* Based on the paper presented at the 5th International Conference «Laser Technologies in Welding and Materials Processing (Katsiveli, Ukraine, 24–27 May 2011).



Figure 1. Optical unit of the «Registrator» system (a), high-speed digital camera CENTURIO C100 (b) and lens spectrograph SL100M (c)

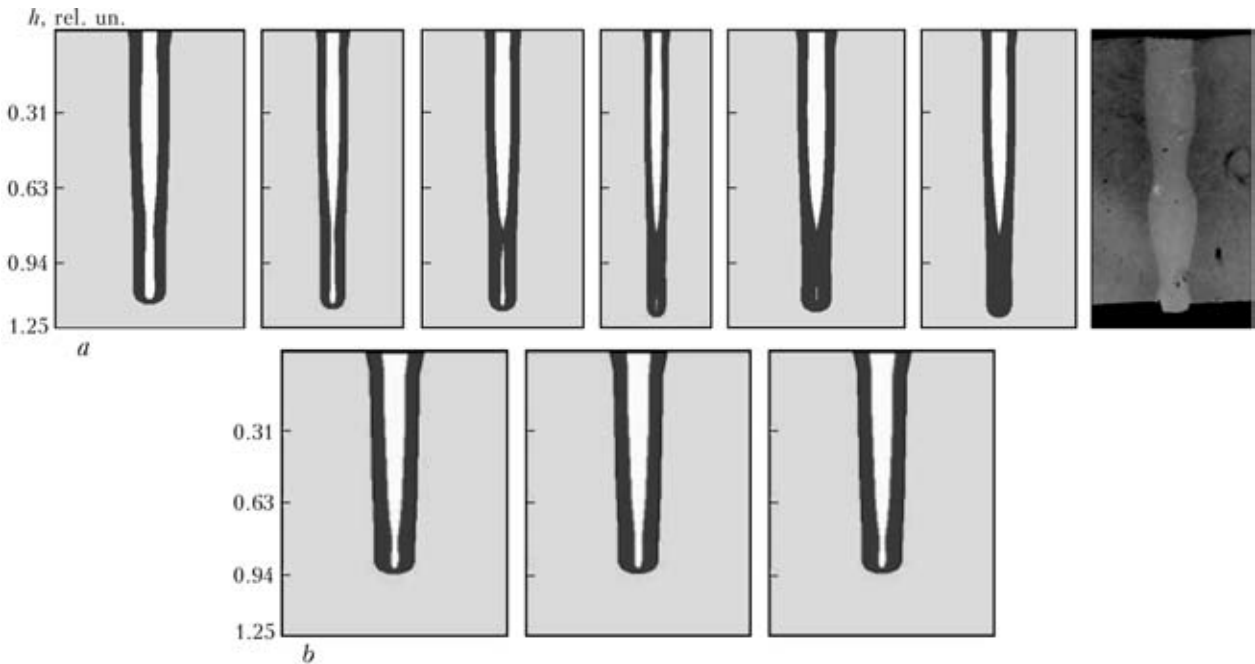


Figure 2. Calculated penetration shapes at $v_w = 10$ cm/s: a – every 1 ms, $N = 15$ kW; b – every 3 ms, $N = 12$ kW

formation of the peaks and splashing of the molten metal from the weld pool. The same results were obtained later in X-ray filming [7].

The experiments were carried out by using the hybrid LAW system developed and assembled by the Institute of Laser and Welding Technologies of the St.-Petersburg State Polytechnic University. Ytterbium fibre laser LC-15 with a maximal output power of 15 kW was used as a laser radiation source. Radiation was transported via the fibre cable to an optical welding head of the laser-arc module. The «Precitec» welding head YW50 ZK with a focal distance of 400 mm and focal diameter of 0.4 mm, equipped with one-coordinate DC-Scanner having a maximal frequency of 600 Hz and amplitude of up to 10 mm, was used to focus the radiation. Also, the experimental system was fitted with arc power supplies VDU-1500DS and EWM Phoenix 520 RC PULS. Filler metal was fed by using wire feed mechanisms PDGO-511 and Phoenix Drive 4 ROB 2.

Flat specimens measuring 100×50 mm, made from alloy AMg6 10 mm thick, and alloy 1424 (Al + 4.5 % Mg + 1.7 % Li + 0.6 % Zn) 4 mm thick, were penetrated and butt welded during the experiments.

Welding was performed with the straight-line welds in flat position. Argon and a mixture of argon with helium were employed to shield the weld pool and weld metal, and wire AlMg6Zr was used as a filler metal.

Quality of all the welds was assessed visually from their appearance and on the base of metallographic examinations of transverse sections. Penetration depth

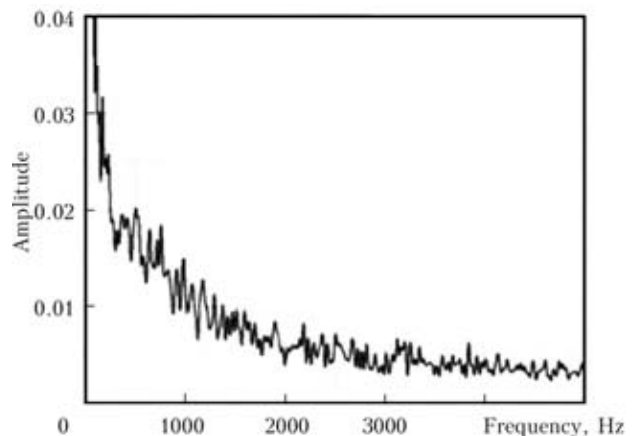


Figure 3. Frequency spectrum of oscillations of the melt

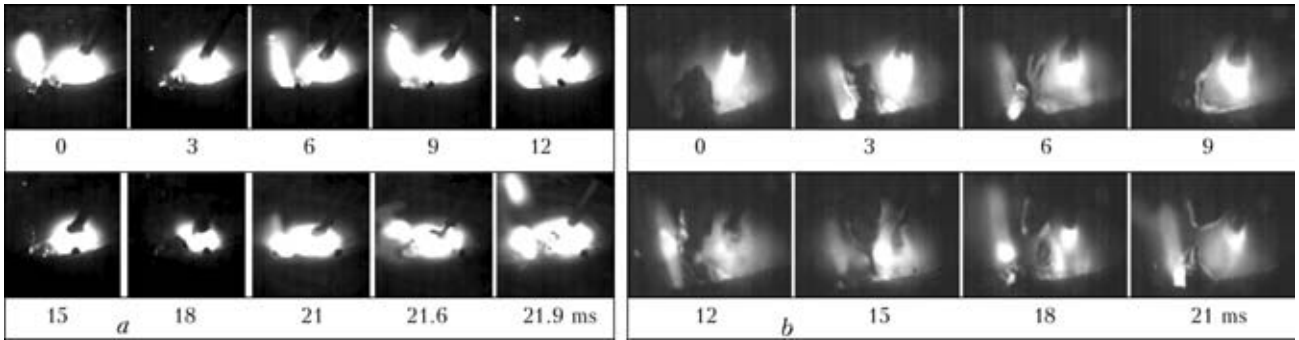


Figure 4. Frames of video filming of the process of formation and detachment of a droplet during hybrid welding using arc power supplies EWM Phoenix 520 RC PULS (a) and VDU-1500DC (b) at $N = 15$ kW, $v_w = 6$ m/min and $I_w = 120$ A

and other parameters of the weld geometry were determined.

Time characteristics of the dynamic processes occurring in the zone of a hybrid discharge over the workpiece surface were determined by using the

plasma plume registration system (Figure 1), which consisted of an optical registration unit with an objective lens, holder for light filter and CCD matrix for registration of signals, and video camera CENTURIO C100 allowing filming at a speed of up to Mg, %

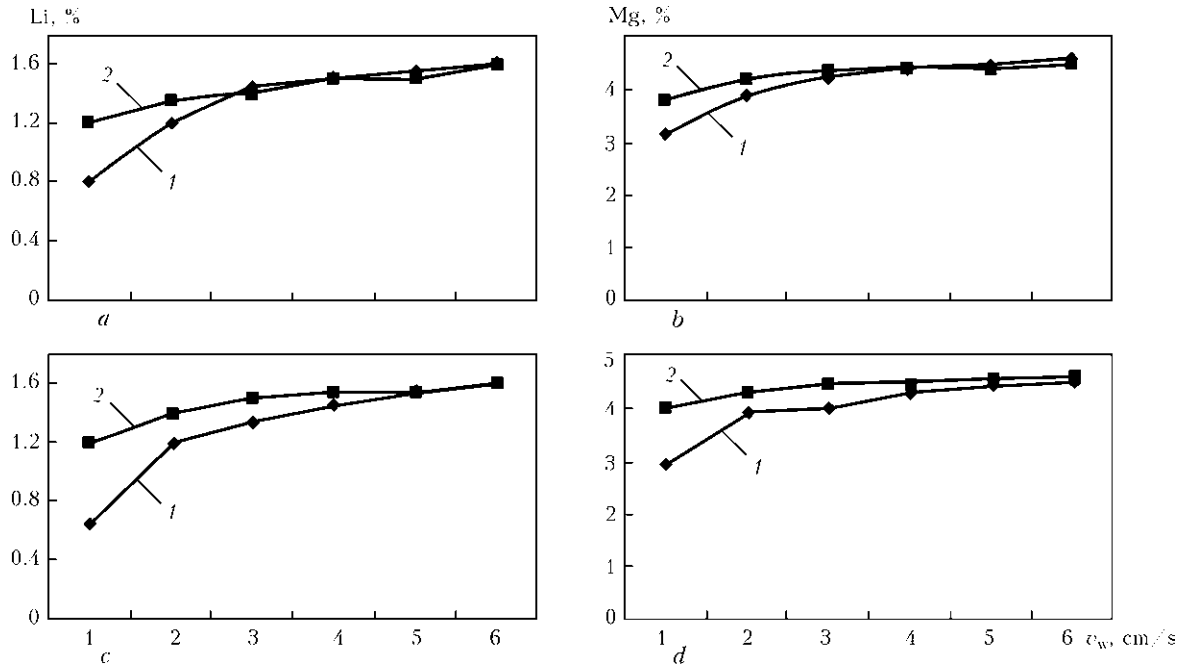


Figure 5. Computed content of lithium (a, c) and magnesium (b, d) in the weld metal on a specimen surface in laser welding of alloy 1424 at $N = 3500$ (a, b, d) and 3000 (c) W, $d = 0.3$ mm and thicknesses of 4 (1) and 10 (2) mm

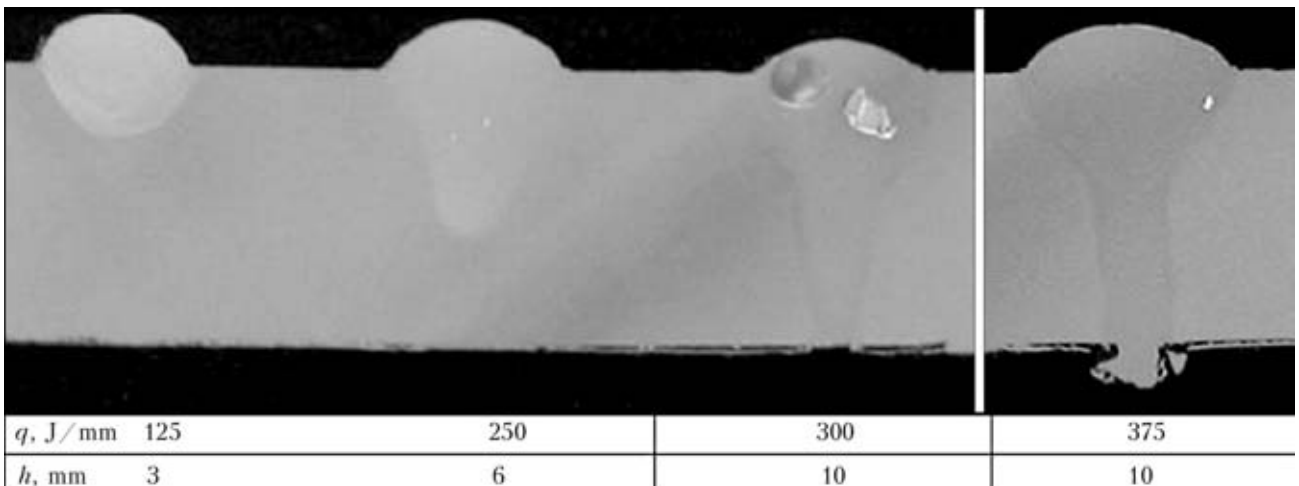


Figure 6. Results of laser penetration of the AMg6 plate by using filler wire with $v_{f.w} = 19$ m/min



100,000 frame/s. Lens spectrograph SL100M with astigmatism correction was applied to investigate the optical emission spectrum of the plasma plume.

The computer modelling results obtained with the help of the dynamic model (Figure 2) show that, despite stabilisation of all technological parameters, the

process of high-speed welding of thick metals is substantially non-stationary, the root part of the keyhole and penetration channel being most unstable. Characteristic narrowing of the weld, which may lead to formation of a defect, can be seen in Figure 2, *a*, which shows cross sections of the laser weld made at the

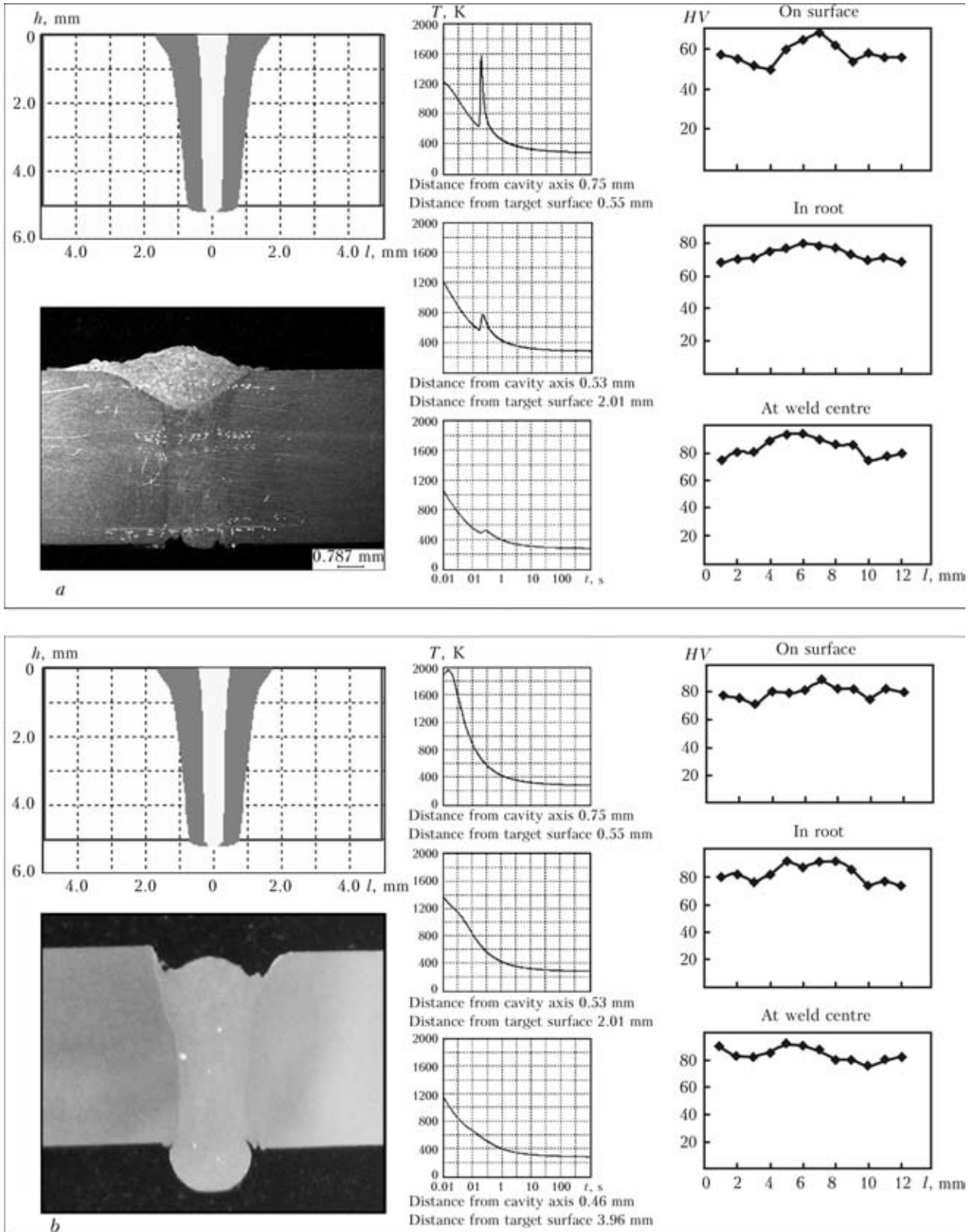


Figure 7. Computation data on shape of cross section, thermal cycles of the weld and microhardness after laser-arc welding of aluminium alloy ($q = 100 \text{ J/mm}^2$): *a*, *b* – distance between laser beam and electrode equal to 15 and 2 mm, respectively

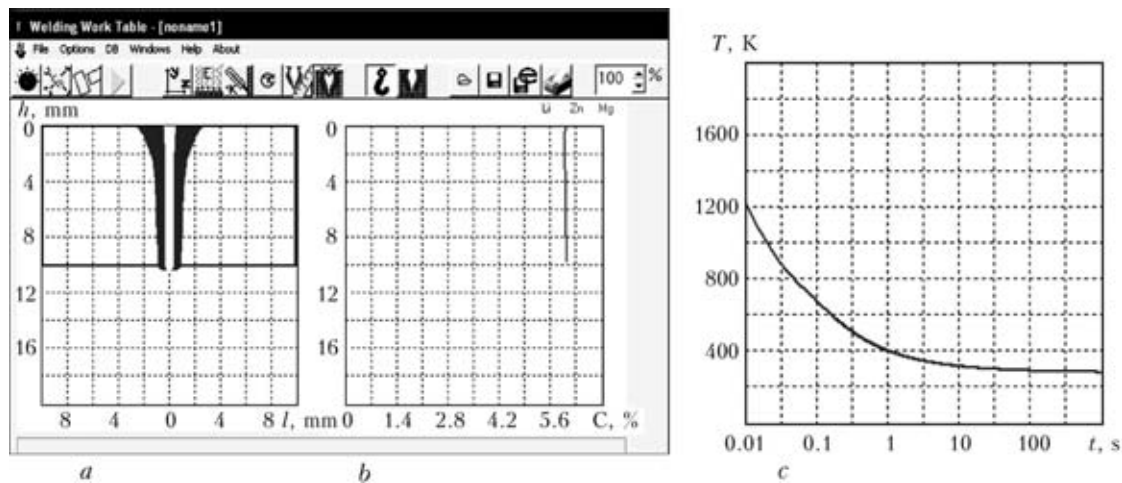


Figure 8. Computed cross section of the penetration zone (a), distribution of magnesium in depth of the weld (b), and thermal cycle in hybrid welding of alloy AMg6 (c)

same process parameters with an interval of 1 ms. A more stable weld pool can be provided by using circular scanning of the laser beam with small (up to 0.5 mm) radii and high (above 300 Hz) frequency of scanning (Figure 2, b). The absence of this stabilisation may lead to formation of large-diameter pores and root peaks, resulting from collapse of the keyhole.

The experiments showed that dynamic behaviour of brightness of radiation of the melt is characterised by the presence of low-frequency oscillations. These frequencies were determined by means of computer modelling using the dynamic model, as well as experimentally by means of photodiodes directed to the weld pool. Figure 3 shows the characteristic frequency spectrum of signals from the photodiodes.

The speed of video filming is determined by the frequency of oscillations of the melt. Analysis of dynamic behaviour of the melt pool showed the absence of oscillations with frequencies of over 500 Hz in the melt. Therefore, to examine the surface of the weld pool the speed of filming should be not less than 1000 frame/s (Figure 4).

Analysis of the high-speed filming frames allowed determination of position of an electrode relative to the laser beam.

Results of computation of the amount of alloying elements made with software LaserCAD at different

thicknesses and process parameters for alloy 1424 are shown in Figure 5. Decrease in the welding speed leads to increase in losses of volatile alloying elements that provide high service properties of alloys, this leading to weakening of the weld.

Due to evaporation, the content of impurities in the weld metal in welding at decreased speeds is substantially different from that in the base metal, especially in the upper part of the molten zone, where radius of the keyhole is maximal. As the upper part of the keyhole is of a decisive character for the process of multiple re-reflections in this keyhole, evaporation of impurities considerably changes the shape and size of the penetration zone. An example of such broadening is shown in Figure 6. Increase of heat input in laser welding using filler metal led to a substantial growth of the penetration zone.

In addition to the high-speed video filming, thermal cycles were computed and microhardness in the laser-affected zone (Figure 7) was measured to determine position of the electrode relative to the laser beam.

Structure of the weld metal across its section in hybrid welding is homogeneous, consisting of fine dendrites. In case of an increased distance between the heat sources, the time of dwelling of the weld metal at increased temperatures is longer and, as a result,

	LW	LAW + MIG	LW + MIG
Investigation object			
On surface	5.298	6.485	3.135
In root	4.624	5.871	3.274
At centre	5.710	5.510	3.279
Base metal		6.442	2.648
Welding wire		6.25	

Figure 9. Distribution of the amount of magnesium in depth of the weld in different method of welding of aluminium alloy

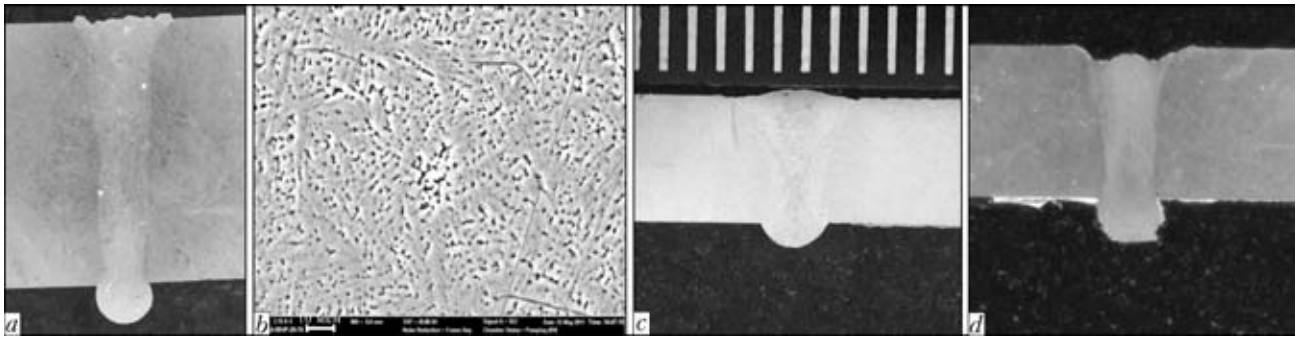


Figure 10. Cross sections of the welds in LAW of alloys AMg6 (a), 1424 (c) and Al-Mg3 (d), and microstructure of the weld metal on alloy AMg6 (b)

the dendrites in the upper part of the weld increase in size. In the hybrid process, microhardness of the weld metal is close to that of the base metal, this being caused both by its fine-dendritic structure and higher magnesium content.

Further experiments were carried out at the maximal welding speed and a distance between the laser beam and electrode equal to 2 mm.

An example of modelling of hybrid welding of alloy AMg6 is shown in Figure 8.

The X-ray spectrum microanalysis results shown in Figure 9 confirmed the computed values. As seen from this Figure, the use of filler metal allows compensation for the losses of alloying elements.

Figure 10 shows a cross section and microstructure of metal of the butt weld with through penetration of the 10 mm thick plates of alloy AMg6 ($q = 175 \text{ J/mm}$) and, as examples of welding of other alloys, cross sections of the welds on the 5 mm thick plates of alloys 1424 and Al-Mg ($q = 100 \text{ J/mm}$).

The laser-arc technological system (LATS) was developed and manufactured in the course of the work. It consists (Figure 11) of a laser unit (fibre laser), arc equipment package, laser-arc module (work tool), manipulator, gas preparation and distribution unit, seam monitoring subsystem (seam guidance), process monitoring subsystem, and automatic control system. LATS is equipped with a system for guiding the laser-arc module to the joint welded, which is based on a triangulation laser sensor. This system provides monitoring of geometric parameters of a welded joint and tracking the coordinates of the joints at a welding speed of up to 6 m/min with the following parameters: $\pm 0.5 \text{ mm}$ in a transverse direction relative to the joint, and $\pm 0.2 \text{ mm}$ in the vertical direction.

The investigation results on dynamics of behaviour of the weld pool and vapour-plasma plume allowed the development of equipment for control of the technological process integrated into the welding process monitoring system.

CONCLUSIONS

1. The possibility was shown of using scanning to improve the quality of the welds.



Figure 11. General view of LATS

2. The required frequencies of scanning corresponding to fluctuations of the weld pool were determined.

3. It was shown that the character of penetration and properties of the weld metal depend on the laser beam-arc distance.

4. It was shown that the content of alloying elements in the weld metal decreases with increase of the welding speed.

5. It was confirmed that filler metal compensates for the losses of alloying elements in LAW.

6. Welded joints characterised by a high depth to width ratio, high quality and low distortions were produced on aluminium-base alloys.

1. Turichin, G. (1997) Model of laser welding for technology application. In: *Proc. of the Academy of Sci., Physics Series*, 61(8), 1613–1618.
2. Matsunawa, A., Mizutani, M., Katayama, S. et al. (2003) Porosity formation mechanism and its prevention in laser welding. *Welding Int.*, 17(6), 431–437.
3. Lopota, V., Turichin, G., Tzibulsky, I. et al. (1999) Theoretical description of the dynamic phenomena in laser welding with deep penetration. In: *Proc. of SPIE, Series 3688*, 98–107.
4. Forsman, T., Powell, J., Magnusson, C. (2001) Process instability in laser welding of aluminium alloys at the boundary of complete penetration. *J. Laser Appl.*, 13(10), 193–198.
5. Bashenko, V.V., Mitkevich, E.A., Lopota, V.A. (1983) Peculiarities of heat and mass transfer in welding using high energy density power sources. In: *Proc. of 3rd Int. Coll. on EBW* (Lion, 1983), 61–70.
6. Lopota, V.A., Smirnov, V.S. (1989) Structure of material and its parameters in beam-affected zone in laser welding with deep penetration. *Fizika i Khimiya Obrab. Materialov*, 2, 104–115.
7. Matsunawa, A., Kim, J.-D., Seto, N. et al. (1998) Dynamics of the keyhole and molten pool in laser welding. *J. Laser Appl.*, 10(12), 247–254.



EXPERIMENTAL INVESTIGATION OF HOT CRACKING SUSCEPTIBILITY OF WROUGHT ALUMINUM ALLOYS

P. KAH, E. HILTUNEN and J. MARTIKAINEN

Lappeenranta University of Technology, Lappeenranta, Finland

The process of gas tungsten arc (GTA) and gas metal arc (GMA) welding of heat treatable wrought aluminum alloys 6005-T6 and 6082-T6, filler metal composition and preheating temperature as the main factors affecting the formation of hot cracking are considered. It has been shown in experiments that specimens welded with 5356 filler wire are more prone to hot cracking than those welded with 4043 wire, and GMAW demonstrates less cracks than GTAW due to its lower heat input. The effect of preheating proves to have little or no consequence.

Keywords: hot cracking, GMAW, GTAW, filler alloys, preheating, alloy 6005, alloy 6082, heat input

Outstanding in their unique combination of light weight, high strength, high toughness, extreme temperature capability, excellent corrosion resistance and versatility of extruding and recycling capabilities, aluminum alloys have applications in almost every manufacturing sector such as in transportation, construction and building. A typical application of 6005-T6 and 6082-T6 heat-treatable wrought aluminum alloys is structural and architectural. Aluminum-based alloys can be successfully arc welded without any cracking related problems or with only minor ones. There are three areas that can significantly influence the probability of hot cracking in an aluminum welded structure. These are the susceptible base alloy chemistry, selection and use of the most appropriate filler alloy, and choosing the most appropriate joint design. The 6xxx series alloys are very sensitive to cracking if the base metal composition remains close to the filler metal composition. During arc welding, the cracking tendency of these alloys is adjusted to acceptable levels by the dilution of the base material with excess magnesium (by the use of the 5xxx series Al-Mg filler alloys) or excess silicon (by the use of the 4xxx series Al-Si filler alloys).

The most appropriate and successful method used to prevent cracking in the 6xxx series base materials is to ensure that an adequate filler alloy is added during the welding operation [1–10].

Much research has been conducted fully understand the main causes of hot cracking with Al-Mg-Si alloys during welding [4–13]. To avoid or minimize the cracking effect it is recommended to use appropriate filler alloys [5–10]. Filler alloys 5356 with 5 % Mg and 4043 and with 5 % Si have been used to compare the effect of filler metal composition on hot cracking. It was concluded that a weld with filler 4043 is less prone to hot cracking than that with filler 5356 due to the narrow solidification temperature range and the lower eutectic temperature of the weld metal which enable the base metal to solidify first (Figure 1). The problem with 4043 filler is that it is easily anodized after welding, producing dark weld metal and a highly visible weld result. This is due to the amount of silicon in the composition. Thus, there is no significant difference in hardness when using either of the two filler alloys. In fact the specimens welded with filler 4043 showed a HAZ that was on average 2 mm wider than those welded with filler 5356 in both GTA (GTAW) and GMA welding (GMAW).

GTAW and GMAW were employed to compare different heat inputs, where the heat input in pulsed GTAW was about 4 times higher than that in pulsed GMAW. Some of the test specimens were also preheated to reduce tensile stresses and the cooling rate so as to decrease the liquation cracking effect. Liquation cracking occurs in the partially melted zone (PMZ) of a weld, i.e. just next to the fusion zone. Liquation can occur along the grain boundary as well as in the grain interior. Grain boundary liquation makes the PMZ susceptible to liquation cracking [14, 15]. Hot cracking is a high-temperature cracking mechanism and mainly a function of how metal alloy systems solidify.

The degree of restraint also significantly affects liquation cracking. The more restraint the material shows, the higher is the probability of liquation crack-

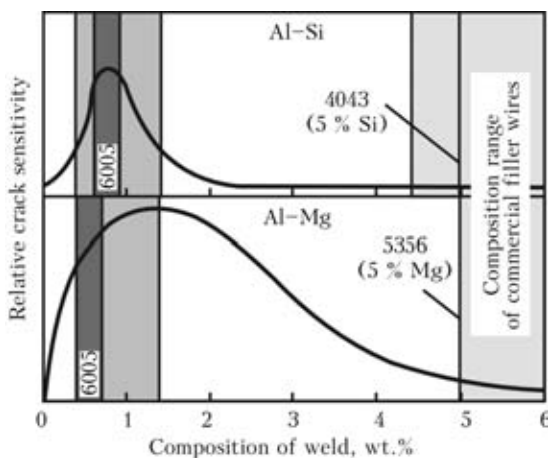


Figure 1. Effect of composition on crack sensitivity of binary Al-Si and Al-Mg alloys [17]



Chemical composition of the base aluminum alloys and filler wires, wt.%

Alloy	Si	Fe	Cu	Mn	Mg	Cr	Zn	Others	Al
6005	0.6	0.21	0.12	0.15	0.54	0.028	0.01	0.15	Bal.
6082	1.2	0.33	0.08	0.50	0.78	0.14	0.05	0.15	Bal.
Wire								B	
4043	5.0	0.8	0.3	0.05	0.05	0.20	0.10	0.0008	Bal.
5356	0.25	0.4	0.1	0.05–0.20	5.0	0.10	0.14	0.0008	Bal.

ing. Because aluminum alloys have high thermal contraction and, if they are not relaxed to solidify, they develop high tensile stress that tends to tear or open the liquated grains. Selecting a base metal which is fine-grained and less susceptible to liquation cracking, such as a material that does not contain low melting impurities or segregates, can also help to reduce this problem if it is feasible [9, 16].

Experimental procedures. 10 mm thick 6005-T6 and 6082-T6 wrought aluminum alloy specimens have been tested for cracking based on different criteria. First, filler alloys were used to understand their effect on cracking. The actual chemical compositions of the base and nominal composition of filler metals are shown in the Table. The influence of different welding processes, preheating temperatures and the base alloys were examined on hot cracking. Mechanized 90 Hz pulsed GTAW and GMAW with short circuiting droplet transfer were used for all the experiments for good repeatability.

The welding parameters used were as follows:

- ambient temperature of approximately 20 °C, and some of the samples were heated to about 120 °C before welding to examine the effect of preheating;
- welding currents of 172, 210 and 352 A for both base alloys with and without preheating;
- voltages of 17, 22 and 26 V, respectively;
- welding speed of 2.8–10.0 mm/s;
- filler wire feed rate of 0.34–13.50 m/min;
- pure argon (Ar + 0.03 % NO) was used as a shielding gas in both cases, and flow rates were 14 and 10 l/min for GMAW and GTAW, respectively;
- filler wire electrode diameter of 1.2 and 2.4 mm in GMAW and GTAW, respectively;
- stick-out of 15 mm in GMAW;
- bead-on-plate technique was used in all cases.

Sufficient cleaning of the surface was done using a stainless wire brush prior to welding, with the goal of removing all oxides, oils and loose particles from the surface to be welded. This is especially important because of the susceptibility of the aluminum weld to porosity due to hydrogen and the dross due to oxygen. The materials to be welded should be rigid enough in order to prevent them from contracting without restraint during welding. This allowed hot cracking to be occurred during welding and the crack susceptibility to be evaluated [18–20].

For the GTAW tests, the new Fronius Majicwave 5000 Job G/F GTAW machine was used. The pulsed AC from this machine could be adjusted and measured. The ESAB CWF1 wire feeder was used for the wire feeding purpose. In the case of GMAW, the Kemppi Pro GMA 530 welding machine with pulsed AC was used in all the experiments. The resultant welds were cut, polished and etched with a solution of 8 % HF and 12 % HCl in water for microstructural examination by optical microscopy. The transverse cross-sectional area of each weld was determined with a digital camera and a computer using commercial software.

Results and discussion. Macro and micro photos of the weld cross-sections and Vickers hardness tests (3 kg) were performed so as to investigate the cracks and the resultant loss of mechanical properties, i.e. hardness due to welding. Each hardness graph shows the hardness across the weld. The results of experiment that demonstrate the effect on crack sensitivity are shown in Figure 2. The material used was 6005-T6 alloy GTA-welded at $I = 300A$ and $v_w = 2.5 \text{ mm/s}$, and no filler metal nor preheating (20 °C) was applied. As can be seen, in welding without filler metal, hot cracks are located in the weld and HAZ.

Effect of filler alloys. Qualitative evaluation was used to present hot cracking test susceptibility; thus, the extent of cracks due to the filler alloys was simply assessed by an observation of the intensity of cracks in the weld cross-section using high magnification of

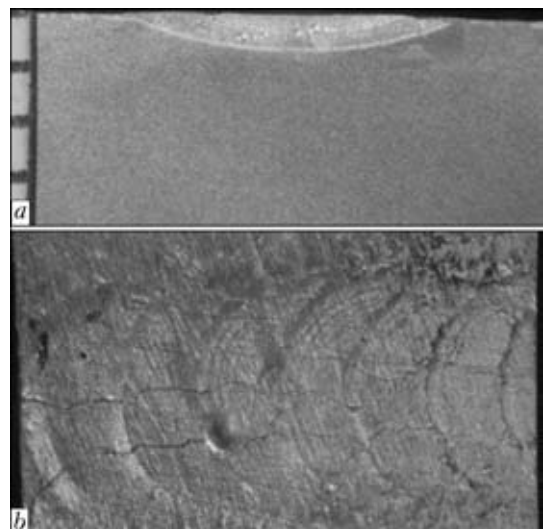


Figure 2. Example of hot cracking: a – weld cross-section; b – from top view

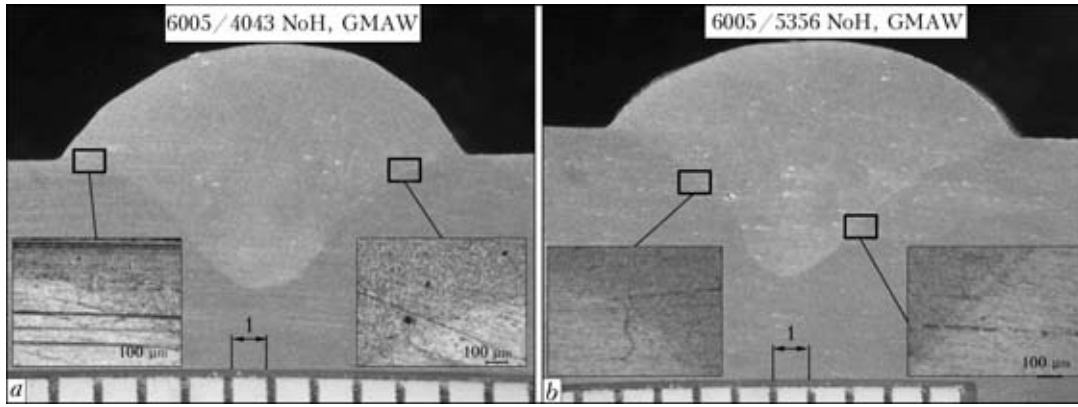


Figure 3. Macro- and microsections demonstrated the effect of filler metal on liquation cracking (here and in Figures below NoH – not preheated sample)

X100. Figure 3, *a* and *b*, show the macrographs of the weld obtained at heat input $Q = 440$ and 426 J/mm on alloy 6005 with fillers 5356 and 4043, respectively. Open liquation cracks are evident along the outer edge and the root of the weld. The effect of these filler wires on the reduction of cracks can be seen from the macrophotos (see Figure 3), and their influence on hardness can be observed from the graphs of hardness tests (Figure 4).

As can be seen from Figure 4, on the whole the hardness distributions are similar in the weld, HAZ and base metal. Figure 4, *a* and *b*, respectively present the hardness distributions for alloy 6005 specimens GTA- and GMA-welded without preheating. The minimum values in both GTA and GMAW for those welds using filler 4043 are less than $HV3-60$. If 6082 alloy is welded with the same filler wires, the situation is different. The hardness distribution goes below $HV3-60$ and slightly above $HV3-80$. Thus, there is no significant difference in hardness when using either of the two filler alloys. In fact the specimens welded with filler 4043 showed a HAZ that was on average 2 mm wider than those welded with filler 5356 in both GTA and GMAW. Fewer and smaller cracks

can be observed in the joint that was GMA-welded with 4043 filler wire (see Figure 4, *a*). Hence, it can be concluded that 4043 filler wire is preferable to 5356 from the viewpoint of liquation cracking susceptibility in the GTA and GMAW of the 6005 alloy.

Effect of welding process. The dependence of the intensity of cracks on GTA and GMAW processes can be found by comparing Figure 5, *a* and *b*. There are cracks and few smaller cracks in Figure 5, *a*, but only one large crack and fewer small cracks in Figure 5, *b*. But there can be more cracks, including invisible cracks. Accordingly there are more cracks in the GTA-welded specimens than in the corresponding GMA-welded ones. Thus, the GMA-welded samples demonstrate less cracks and higher or similar hardness values with a narrower HAZ than those in GTA-welded ones (Figure 6). The difference in the hardness values of the GTA- and GMA-welded specimens is significant especially (of about $HV3-9$ on average) for 6082 alloy (Figure 6, *c* and *d*). The smallest (of about $HV3-1.5$) difference in hardness values can be observed in the 6005 alloy (Figure 6, *a* and *b*). The width of the HAZ in GTA-welded joint is 4–5 mm greater than that in GMA-welded joint due to the higher heat input.

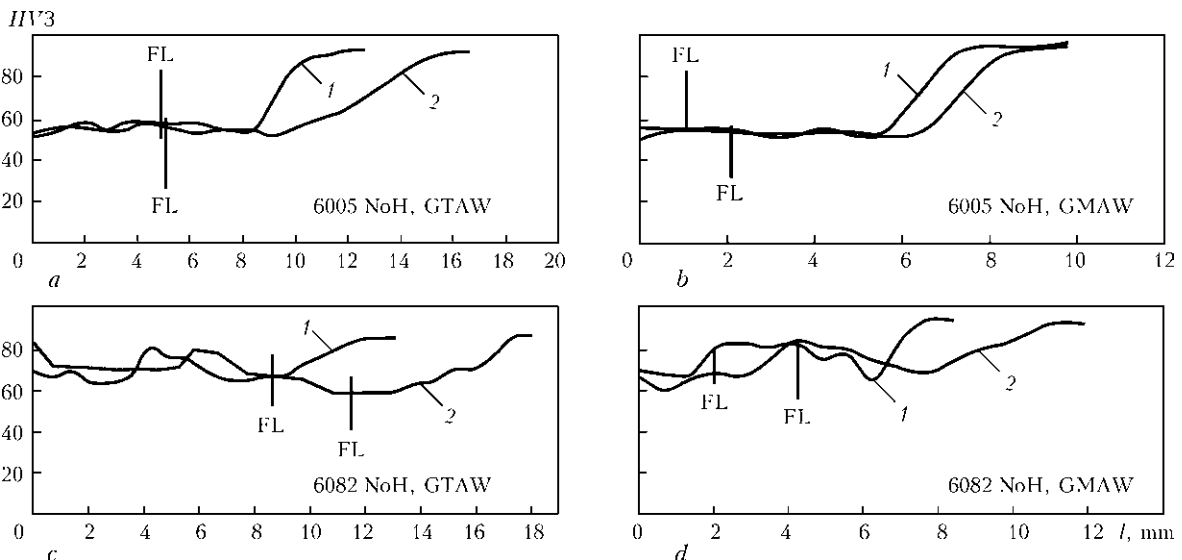


Figure 4. Distribution of hardness in cross-section of the joints of 6005 (*a*, *b*) and 6082 (*c*, *d*) alloys GTA- (*a*, *c*) and GMA-welded (*b*, *d*) with filler wire 5356 (*1*) and 4043 (*2*) (here and in Figures below *l* – distance from the weld centerline; FL – fusion line)

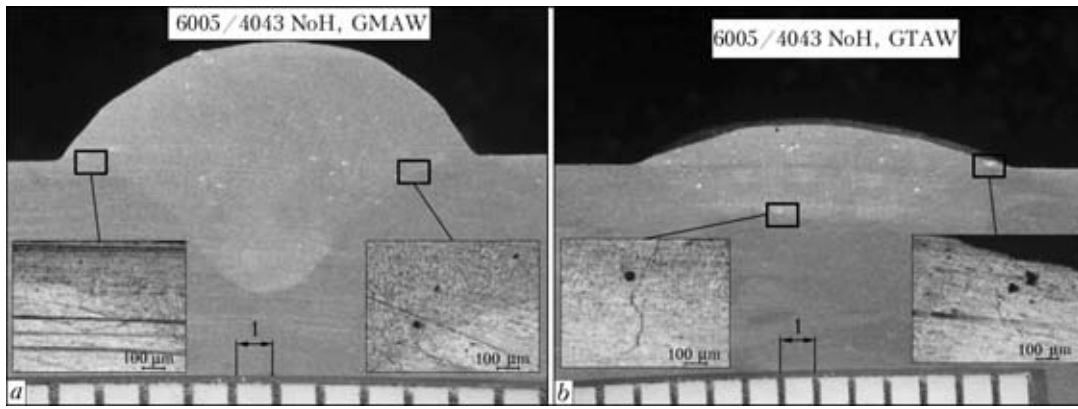


Figure 5. Macro- and microsections of the 6005 alloy joints GMA- (*a*) and GTA-welded (*b*) with 4043 filler at heat input of 440 (*a*) and 1290 (*b*) J/mm

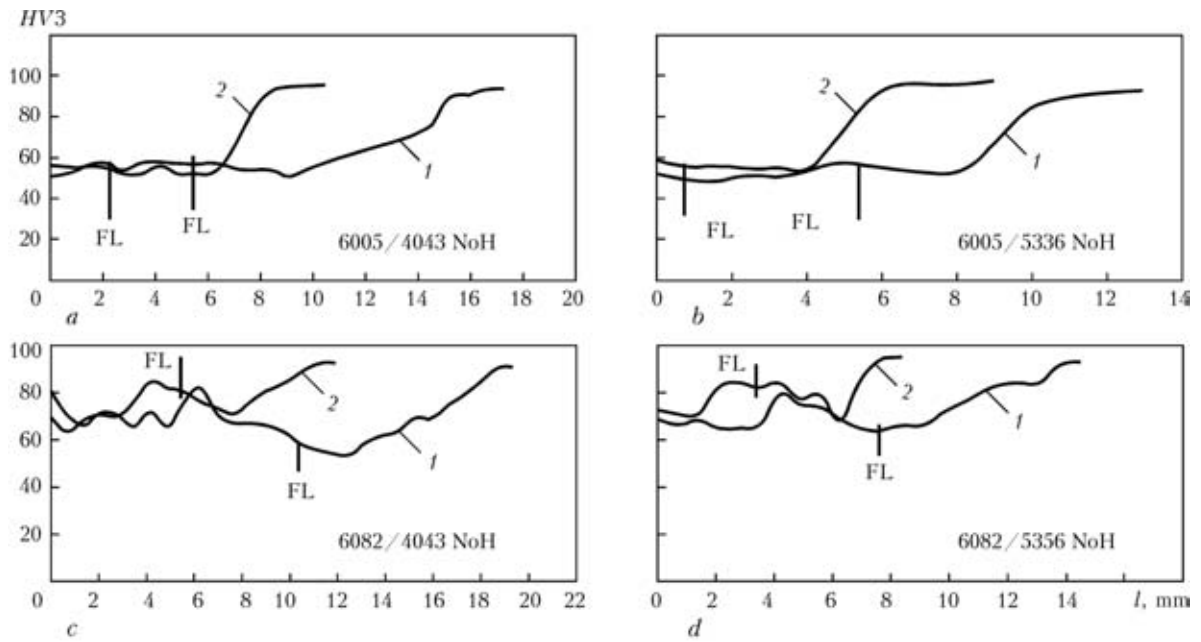


Figure 6. Distribution of hardness in cross-section of the joints of 6005 (*a, b*) and 6082 (*c, d*) alloys GTA- (*1*) and GMA-welded (*2*) with filler wire 4043 (*a, c*) and 5356 (*b, d*)

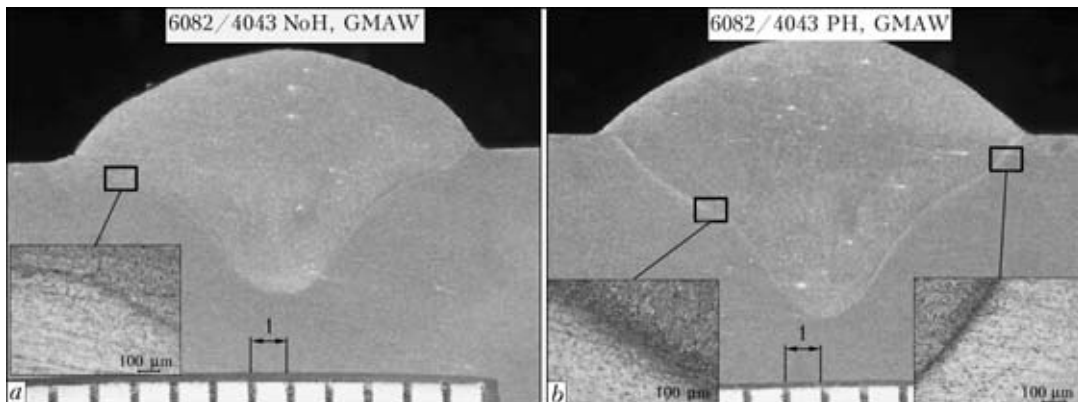


Figure 7. Macro- and microsections of the 6082 alloy joints GMA-welded using 4043 filler without (*a*) and with (*b*) preheating at heat input of 440 J/mm

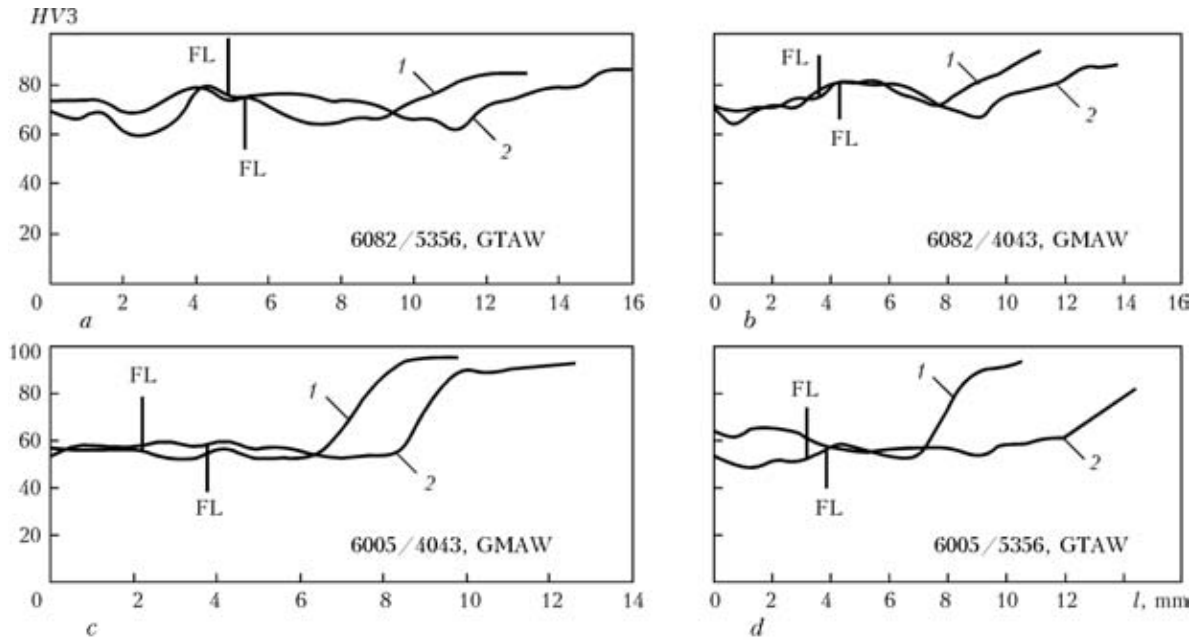


Figure 8. Distribution of hardness in cross-section of the joints of 6082 (a, b) and 6005 (c, d) alloys GTA- (a, d) and GMA-welded (b, c) using filler wire 5356 (a, d) and 4043 (b, c) without (1) and with (2) preheating

Effect of preheating. Preheating helps in minimizing hot cracking by reduces stresses during cooling. Thus, lower heat input can also be used. Preheating is heating the whole base metal or part of it up to a desired temperature before welding, if it is recommended. This preheating temperature is mostly found in the welding specification procedure for the alloy at hand, but generally it can range from 110–140 °C for most commercial aluminum alloys. Preheating can be done in a furnace if the structure is small, and a bank of heating torches, electrical strip heaters or induction heaters can be required if the structure is larger. The major benefit of preheating is the lower cooling rate for weld and base metal, which leads to better ductility and more resistance to cracking. Especially for highly restrained structures and joints it minimizes the shrinkage stresses in the weld and the adjacent base metal, besides slow cooling enables hydrogen to diffuse before it makes a problem after solidification [21–23]. Al–Mg–Si alloys are sensitive to overheating which can form liquation cracking in the HAZ, so proper care has to be taken when preheating [12].

Figure 7 shows macro and micro photos of the samples GMA-welded with 4043 filler with and without preheating. It was noticed that with preheating, the penetration tends to be slightly deeper than without preheating. The reduction of cracks due to preheating is not remarkable, as can be seen when comparing Figure 7, a and b. Even though in the case of the 6005 specimen preheated and GTA-welded with filler 5356, the size of the cracks decreases somewhat, but there is still approximately the same number of cracks.

The hardness profiles in Figure 8 demonstrate that there is not more than the HV3-1.5 difference in the hardness at preheating and without it, and there is the 1–2 mm wider HAZ in the preheated specimens. When preheating, the softened area enlarges due to the rise in the temperature.

In all three cases, when we combined both the loss of hardness and number of cracks formed, without considerable hardness differences, the intensity of cracks is less when using the 4043 filler than the 5356 one, as well as with the GMA-welded specimen as

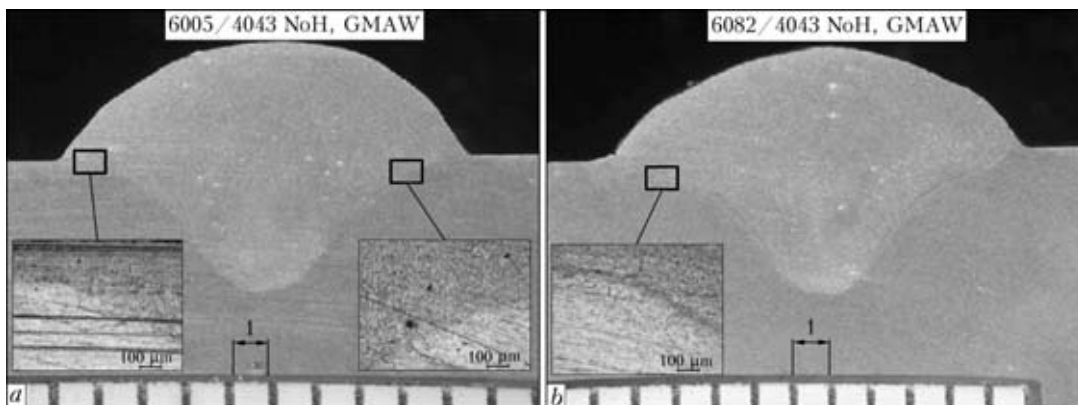


Figure 9. Macro- and microsections of the 6005 (a) and 6082 alloy joints (b) GMA-welded with 4043 filler without preheating



with the GTA-welded ones. However, the effect of preheating does not show any reduction in the number of cracks.

Effect of base metal. Thus, it follows that according to this experiment the 6082 base alloy is less susceptible to liquation cracking than the 6005 one (Figure 9) at equal heat input $Q = 440 \text{ J/mm}$ in both cases.

CONCLUSIONS

1. The 6082 alloy base metal is less susceptible to liquation cracking than the 6005 alloy.

2. When assessing the liquation cracking susceptibility in GTAW and GMAW of 6005 and 6082 base alloys, GMAW results in fewer liquation cracks and higher or similar hardness with a narrower HAZ than GTAW.

3. The 4043 and 5356 filler metals are immune to solidification cracking, even though liquation cracking can occur.

4. Preheating has little significant effect on avoiding liquation cracks.

Acknowledgements. *This work was supported by the Finnish Funding Agency for Technology and Innovation (TEKES) under Grant (MODUVA). The authors are grateful to Antti Kahkonen and Antti Heikkinen for providing the test materials.*

- Adamowski, J., Szkodo, M. (2007) Friction stir welds of aluminum alloy AW6082-T6. *J. Achievements in Materials and Manufact. Eng.*, **20**, 403–406.
- Cross, C.E., Bollinghaus, T. (2006) The effect of restraint on weld solidification cracking in aluminum. *Welding in the World*, **50**, 51–54.
- Mazzolani, F.M. (1995) *Aluminium alloy structures*. 2nd ed. London: Chapman & Hall.
- Gittos, N.F., Scott, M.H. (1981) Heat affected zone cracking of Al–Mg–Si alloys. *Welding J.*, **60**(6), 95–103.
- Kou, S. (2003) Solidification and liquation cracking issues in welding. *Welding J. Minerals, Metals and Materials*, **55**(6), 37–41.
- Huang, C., Kou, S. (2000) Partially melted zone in aluminum welds – liquation mechanism and directional solidification. *Suppl. to Welding J.*, May, 113–120.
- Huang, C., Kou, S. (2002) Liquation mechanisms in multi-component aluminum alloys during welding. *Welding J.*, Oct., 211–222.
- Huang, C., Kou, S. (2003) Liquation cracking in partial-penetration Al–Mg–Si welds. *Ibid.*, July, 184–193.
- Huang, C., Kou, S. (2004) Liquation cracking in full penetration Al–Mg–Si welds. *Ibid.*, April, 111–121.
- Cao, G., Kou, S. (2006) Predicting and reducing liquation-cracking susceptibility based on temperature vs fraction solid. *Ibid.*, Jan., 9–18.
- Hunziker, O., Dye, D., Reed, R.C. (2000) On formation of a centerline grain boundary during fusion welding. *Acta Mater.*, **48**(17), 4191–4201.
- Messler, R.W. Jr. (2004) *Principle of welding*. Weinheim: Wiley.
- Davis, J.R. Jr. (1994) *Aluminum and aluminum alloys*: ASM specialty handbook.
- Kou, S. (2003) *Welding metallurgy*. 2nd ed. New York: John Wiley.
- Ma, T., Den Ouden, G. (1999) *Int. J. Joining of Materials Denmark*, **11**(3), 61–67.
- Yeomans, S.R. (1990) Successful welding of aluminium and its alloys. *Australian Welding J.*, 4th quart.
- Grong, O. (1994) *Metallurgical modeling of welding*. 2nd ed. (1994) *Lincoln Electric procedure handbook of arc welding*. Cleveland: Lincoln Electric.
- Rao, K.P., Ramanaiah, N., Viswanathan, N. (2008) Partially melted zone cracking in AA6061 welds. *Materials and Design*, **29**, 179–186.
- Schenk, T., Richardson, I.M., Kraska, M. et al. (2009) A study on the influence of clamping on welding distortion. *Comput. Materials Sci.*, **45**, 999–1005.
- Akahter, R., Ivanchev, L., Burger, H.P. (2007) Effect of pre/post T6 heat treatment on the mechanical properties of laser welded SSM cast A356 aluminum alloy. *Materials Sci. and Eng. A*, **447**, 192–196.
- Funderburk, S. (1998) *What is preheat?* Cleveland: Lincoln Electric.
- Lyndon, B.J. (2006) *Process specification for the heat treatment of aluminum alloys space center*. Houston, Texas: NASA.



OPTIMIZATION OF CONDITIONS OF REDUCTION HEAT TREATMENT OF BLADES OF ALLOY KhN65VMTYu AFTER LONG-TERM SERVICE

Yu.P. TARASENKO, O.B. BERDNIK and I.N. TSARYOVA

A.A. Blagonravov Institute of Engineering Science, RAS, Novgorod, Russian Federation

Condition of the material of gas turbine engine blades after long-term service was studied and their repairability was determined. Parameters were developed for high-temperature heat treatment of alloy KhN65VMTYu (EI893) to extend the service life of product.

Keywords: blades, reduction heat treatment, microstructure, physical-mechanical properties, extension of service life

The blades of the first stage of turbine rotor, manufactured of alloy KhN65VMTYu (EI893) using method of hot stamping, were taken as objects of investigation at operating time of 53,000, 60,142 and 62,449 h. The blades can be in service for a long time (tens of thousands of hours) at high temperature of about 700–750 °C [1]. However, it inevitably results in structure-phase transformations affecting their serviceability. In the process of service the corrosion, erosion, static, thermal-fatigue and fatigue damages are accumulated.

The purpose of this work is to study the post service state of material of gas-turbine engine blades, passed long service period, to determine their repairability and possibility of restoration.

To recover the structure and properties of material of pilot blades the billets cut out of them were heat treated using different conditions [2, 3]:

- heating up to 1160 °C, holding for 2 h, air cooling + heating up to 1000 °C, holding for 4 h, air cooling + heating up to 900 °C, holding for 8 h + heating up to 820 °C, holding for 15 h, air cooling;
- heating up to 1160 °C, holding for 2 h, air cooling + heating up to 950 °C, holding for 6 h, air cooling + ageing at 820 °C for 12 h, air cooling;
- heating up to 1160 °C, holding for 2 h, air cooling + ageing at 800 °C for 12 h, air cooling;
- heating up to 1050 °C, holding for 3 h, air cooling + ageing at 850 °C for 12 h, air cooling;
- heating up to 1030 °C, holding for 2 h, air cooling + ageing at 850 °C for 12 h, air cooling;
- ageing at 750 °C for 24 h, air cooling.

To analyze the state of material the methods of optical metallography (microscope «Neophot-32») and scanning electron microscopy (VEGA/ TESCAN) were used. The tensile tests of mechanical properties of flat specimens at room temperature were carried out in the rupture machine U10T. Microdeformations were determined using method of X-ray diffraction

analysis in the diffractometer «Dron-3M» (applying Cu- K_{α} radiations in traditional geometry of Bregg–Brentano).

Using analysis of a sample the chemical composition of alloy was determined, wt. %: 16 Cr; 1.5 Al; 4 Mo; 1.45 Ti; 9 W; 0.5 Mn; 0.01 B; 3 Fe; 0.05 C. The chemical composition of material of blades was in compliance with standards established by TU 14-1-322–72 for the alloy KhN65VMTYu.

The microstructures of alloy KhN65VMTYu after different operating time are presented in Figures 1–3. It follows from the analysis of structure of metal of all blades that as a result of long-term service at operating temperatures the structure-phase state of material changes considerably and is deteriorated. Trans- and intercrystalline microcracks in the structure were not revealed, but microstructure of alloy is characterized by difference in grains. It is known that at the boundaries of different-grain metal in the process of service the cracks can appear as the volumes of coarse and fine grain deform in different way. Metal in the root part has more homogeneous microstructure. In the metal with lower operating time (53,000 h) the strengthening intermetallic γ' -phase (Ni_3Al , Ti) is almost completely dissolved in the solid solution and its remnants have chaotic distribution in the volume of grains. The grain boundaries are linear, filled with fine-dispersed carbide and intermetallic phases (see Figure 1).

With increase of service time up to 60,142 h, the precipitation of large carbides (up to 3 μm), forming in chains along the grain boundaries, is observed in microstructure of specimens (see Figure 2). The redistribution of strengthening intermetallic phase was occurred, the larger part of which was precipitated near grain boundaries which depletes the body of a grain. With increase of service time of material up to 62,449 h (see Figure 3) the additional precipitation and coarsening of carbides of the type MeC , MeC_6 , MeC_{23} of dispersion from 0.5 to 6.0 μm and precipitation of a large amount of fine-dispersed γ' -phase (Ni_3Al , Ti) occur. According to the instruction on prolongation of service period of metal of base ele-



Table 1. Mechanical properties of alloy KhN65VMTYu

State of material	σ_t , MPa	$\sigma_{0.2}$, MPa	δ , %	ψ , %
TU 108.02.005–76	≥ 850	490–660	≥ 20	≥ 25
After service during 53,000 h	990	340	19	22
	1030	445	26	23
After service during 60,142 h	1090	430	22	28
After service during 62,449 h	1000	350	21	26
RHT modes:				
1. Hardening from 1160 °C for 2 h, air cooling + ageing at 1000 °C for 4 h, air cooling + ageing at 900 °C for 8 h, air cooling + ageing up to 820 °C for 15 h, air cooling	770	350	44	41
2. Hardening from 1160 °C for 2 h, air cooling + ageing at 950 °C for 6 h, air cooling + ageing up to 820 °C for 12 h, air cooling	680	410	22	22
3. Hardening from 1160 °C for 2 h, air cooling + ageing at 800 °C for 12 h, air cooling	790	415	42	39
4. Hardening from 1050 °C for 3 h, air cooling + ageing at 850 °C for 12 h, air cooling	920	490	36	25
5. Hardening from 1150 °C for 3 h, air cooling + ageing at 850 °C for 12 h, air cooling + ageing at 750 °C for 24 h, air cooling	980	460	30	26
Service for 60,142 h + RHT	990	555	28	43
Service for 62,449 h + RHT	940	485	20	24

ments of turbines SO 153-34.17.448–2003 the conglomerates of chromium carbides of the size of more than 5 μm are not admitted in microstructure of alloy KhN65VMTYu. The alloy with operating time of more than 62,000 h cannot be more under the service.

As a result of microspectral analysis of carbide inclusions located at the boundary and inside the grains of metal, the spectrograms were obtained which allow us to state that the investigated carbide inclusion, presented in Figure 4, *a*, was formed on the basis of tungsten, molybdenum and chromium and corresponds to complex carbide of group II of the type (W, Mo, Cr)C, while in Figure 4, *b* – to carbide of molybdenum Mo_2C , which is also carbide of the group II (interstitial phase). Due to a low carbon content in the alloy KhN65VMTYu ($\leq 0.07\%$) the amount of carbide phase in it is negligible and it is located mostly along the boundaries of austenite grains.

The results of mechanical tensile tests of specimens at room temperature showed that the material in post-service state does not correspond to the requirements of TU 108.02.005–76 as to yield strength and ductility

properties independently of the period of operating time. It is seen from Table 1 that in the process of long service the increase of strength and decrease of ductile properties occurred in material of blade airfoil as a result of additional formation of disperse particles of γ' -phase. Tensile strength of material increased up to 1000–1090 MPa at 850 MPa admissible according to TU 108.02.005–76, and yield strength decreased down to 340–430 MPa at the standard of 490–660 MPa.

The testing of alloy KhN65VMTYu on the material with the lowest operating time (53,000 h) of experimental conditions of reduction heat treatment (RHT) resulted in the decrease of level of strength and considerable increase of ductile properties (elongation and reduction in area). The optimal result was obtained after application of the conditions 4 and 5 of RHT (see Table 1). It follows from the analysis of microphotos in Figure 5 that microstructure of alloy KhN65VMTYu becomes more homogeneous, the decrease in grain difference occurs. RHT results in some stabilization of microstructure, increase of amount of

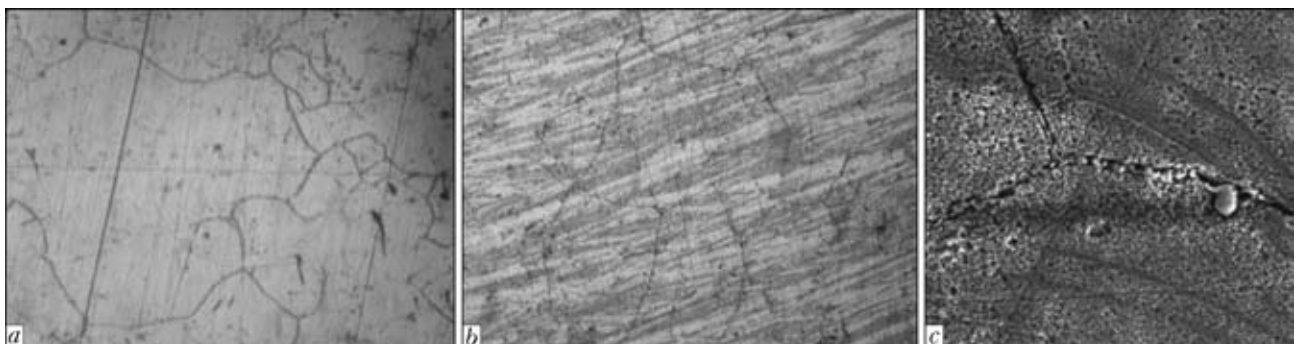


Figure 1. Microstructure of alloy the KhN65VMTYu specimens after service during 53000 h cut from the first (*a*, *b* – $\times 250$) and root part of blade (*c* – $\times 10000$)

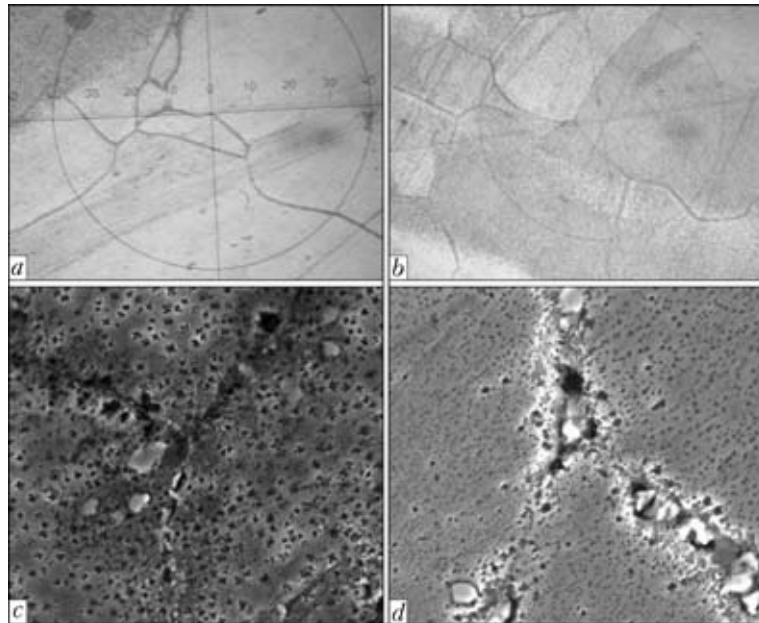


Figure 2. Microstructures of the alloy KhN65VMTYu specimens after service during 60,142 h cut from the first (a, c) and root part of blade (b, d) (a, b – $\times 250$; c, d – $\times 10000$)

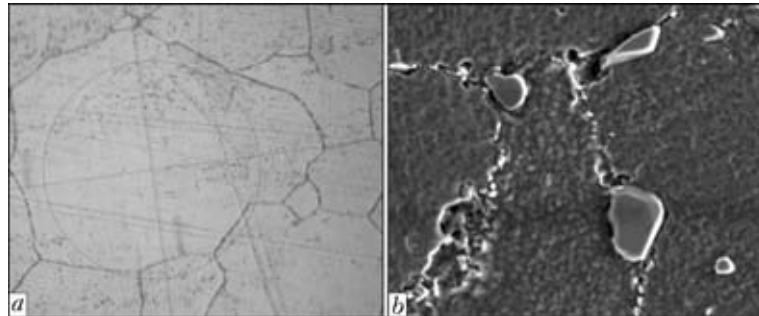


Figure 3. Microstructure of alloy KhN65VMTYu after service during 62,449 h (a – $\times 250$; b – $\times 1000$)

γ' -phase: in use of step conditions of RHT the content of γ' -phase is increased up to 3–4 %, during one-step ageing at 820 or 850 °C the amount of γ' -phase is increased up to 10 %, which is the admissible content for this alloy. In RHT of specimens using the condition 5 during 30 h, the complete regeneration of degrade structure of blade metal occurs. In this case the excessive intermetallic γ' -phase is observed in a form of fine-disperse precipitates. The content of γ' -phase after RHT is increased up to 12 %, however at long-time ageing the precipitation of coarse carbides at the grain boundary occurs which are the concentrators of stresses.

For the alloys with operating time of 60,142 and 62,449 h, the condition 4 of RHT was applied (see Table 1), which showed optimal values of structural

and mechanical values on the specimens of alloy with operating time of 53,000 h.

In RHT on the alloys with operating time of 60,142 and 62,449 h (Figure 6) the satisfactory result was obtained: the dissolution and redistribution of intermetallic phase and refining of carbides occurred. The changes in microstructure were positively reflected on mechanical characteristics of material presented in Table 1. RHT resulted in decrease of tensile strength to 990–940 MPa and increase of yield strength up to 555–485 MPa which corresponds to the standardized values of mechanical properties.

To restore geometric sizes of blades the welding-surfacing works were applied using wire on nickel bases of grade 04KhN50VMTYuB-VI (EP648-VI) of the following chemical composition, %: 0.04 C; 0.14 Mn; 0.25 Si; 22.2 Cr; 66.3 Ni; 1.26 Nb; 2.4 Mo; 1.6 Ti; 0.4 Al; 0.95 Fe; 4.4 W. The values of strength characteristics of selected surfacing wire are close to the values of base metal of blades (as to tensile strength $\sigma_t = 800$ MPa $K = 0.94\sigma_t^{BM}$, as to yield strength $\sigma_{0.2} = 470$ MPa $K = 0.95\sigma_y^{BM}$) which satisfies the requirements for the deposited material. To relieve residual stresses after welding, the tempering at 700 °C

Table 2. Data of X-ray diffraction analysis of materials

State of material	D , nm	ϵ	r_L , cm^{-2}	ρ_e , cm^{-2}
After service	270	0.0004	$4.1 \cdot 10^9$	$8 \cdot 10^9$
Surfacing using wire 04KhN50VMTYuB-VI	57	0.00011	$9.2 \cdot 10^{10}$	$6.1 \cdot 10^8$
After surfacing and tempering	~ 500	0.00046	$\sim 10^9$	10^{10}

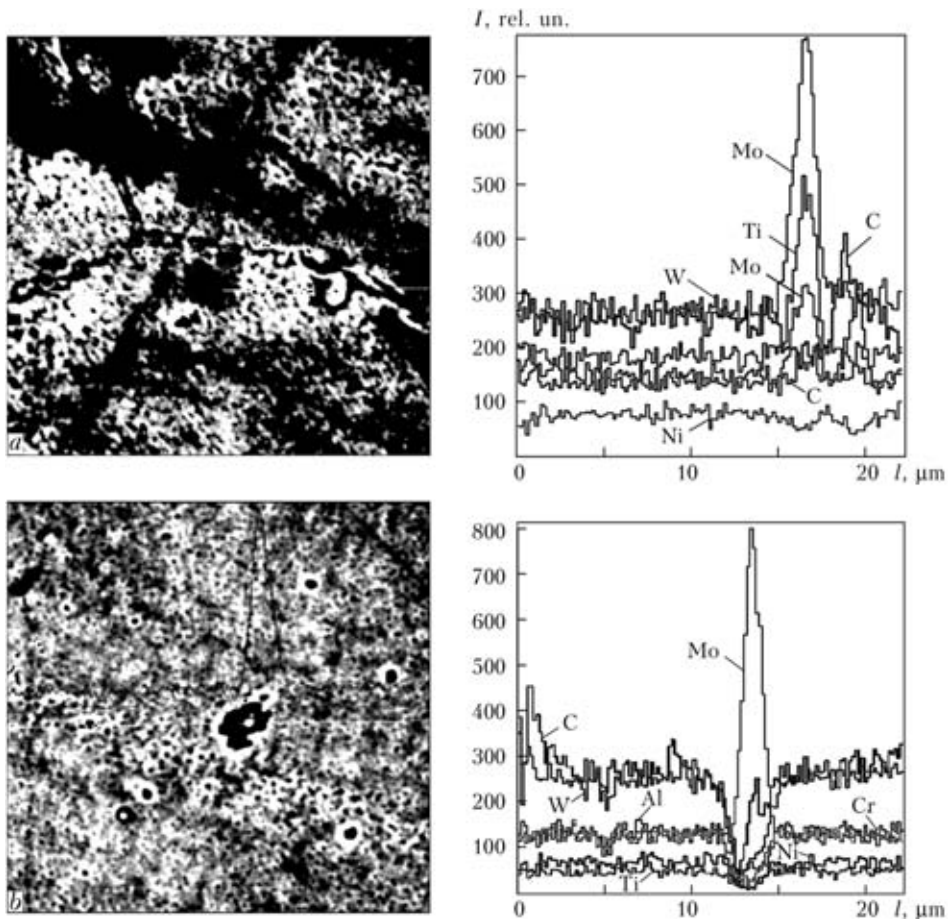


Figure 4. Microstructures and spectrograms of carbide inclusions detected at the surface of cross sections: *a* – after service; *b* – after RHT using mode 4 (see Table 1)

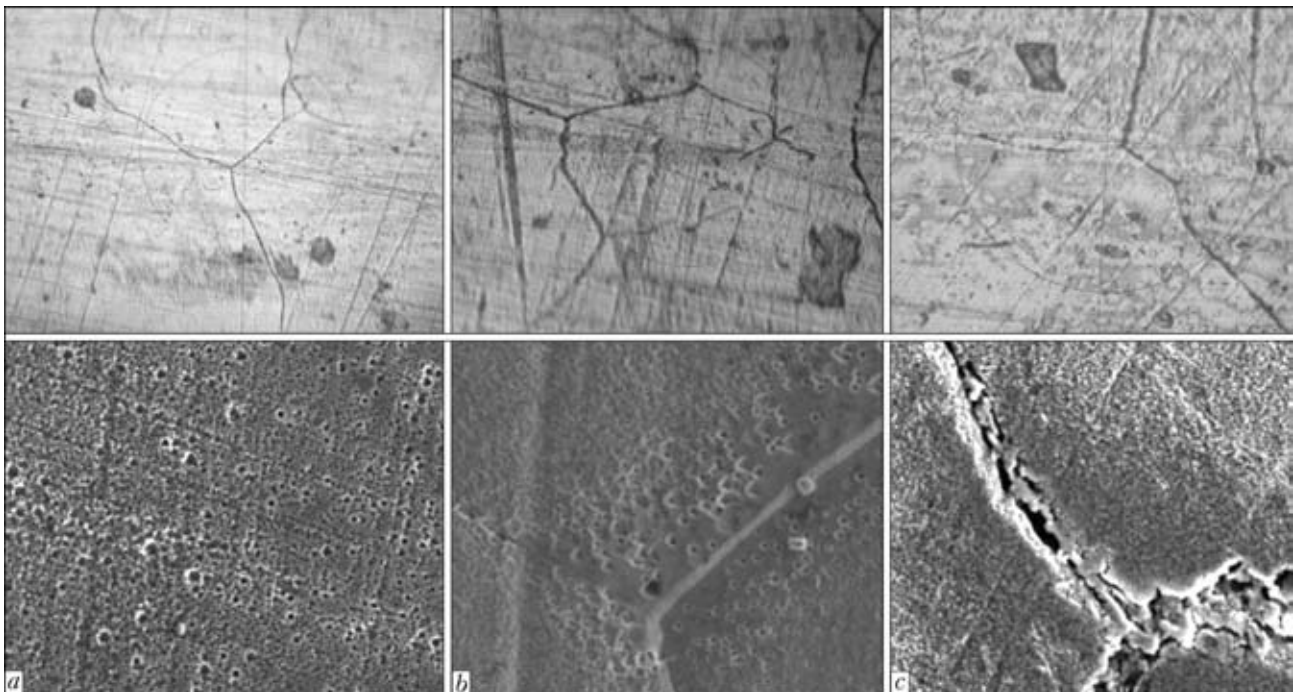


Figure 5. Microstructure of alloy KhN65VMTYu with operating time of 53,000 h after different variants of RHT: *a* – mode 1; *b* – mode 2; *c* – mode 5 (see Table 1)

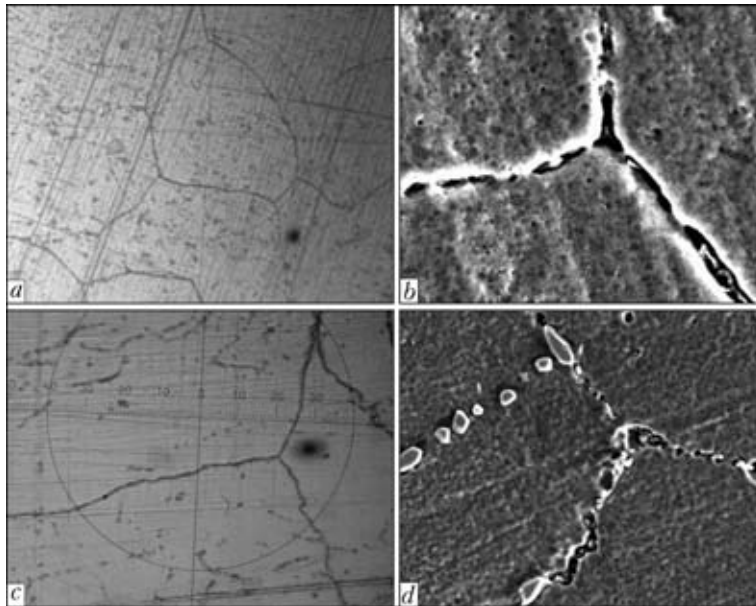


Figure 6. Microstructure of alloy KhN65VMTYu after RHT: *a, b* – mode 4 at operating time of 60,142 h; *c, d* – the same at operating time of 62,449 h (*a, c* – $\times 500$; *b, d* – $\times 10000$)

for 8 h was done. Table 2 gives results of X-ray diffraction analysis of specimens.

In the post service state the average level of microdeformations and homogeneous distribution of density of dislocations inside and at the boundaries of subgrain blocks were recorded in the blade material. The surfacing considerably refines subgrains and abruptly increases the density of boundary dislocations (almost by 2 orders), that in its turn can embrittle the boundaries. RHT facilitates the coarsening of blocks of mosaics and decreasing the density of dislocation defects at the boundary.

On the basis of carried out research works one can conclude that material of blades with different operating time from 53,000 to 62,449 h has a degrade microstructure and needs RHT. The operation of blades of alloy KhN65VMTYu for more than 62,000 h without restoration repair is not desirable as the negative changes in microstructure (formation of coarse carbides at the boundaries of grains) can result in fracture of blades. All the blades investigated in this work are maintainable and have passed the complete restoration cycle including heat treatment for reduction of structure and physical-mechanical properties, surfacing works for restoration of geometric sizes of

a workpiece and deposition of protective heat-resistant coating using gas-plasma method. At the present time the blades are installed into the units and are in service. Thus, technological cycle of reduction treatment can be presented in a form of scheme:

100 % incoming control + RHT (hardening + ageing) + machining (defects preparation) + surfacing works (restoration of geometry), control + heat treatment (tempering for stress relieving) + preparation of surface for coating + deposition of protective heat-resistant coatings using gas-plasma method (Ni-Al + ZrO_2) + 100 % outgoing control.

From the editorial board. In the opinion of the reviewer of this work, the performance of heat treatment of as-serviced blades in air at 1050 °C can result in oxidation of surface of a root, and further cleaning or grinding does not eliminate thinning of the root part and not air-tight joining of blades.

1. Getsov, L.B. (2010) *Materials and strength of gas turbine parts*. Book 1. Rybinsk: Gazoturb. Tekhnologii.
2. Rybnikov, A.I., Getsov, L.B. (1995) Heat treatment of coated blades. *Metallovedenie i Termich. Obrab. Metallov*, **9**, 21–25.
3. Filatov, M.A., Sudakov, V.S. (1995) Effect of heat treatment on structure and properties of heat-resistant nickel alloys. *Ibid.*, **6**, 12–15.



PROPERTIES OF IRON-BASE ALLOYS FOR PLASMA POWDER HARD-FACING OF SEALING SURFACES OF FITTINGS

E.F. PEREPLYOTCHIKOV and I.A. RYABTSEV

E.O. Paton Electric Welding Institute, NASU, Kiev, Ukraine

The paper gives investigation results on properties of iron-base alloys designed for plasma powder hard-facing of sealing surfaces of various-purpose fittings. It is shown that deposited metal 15Kh19N9M4S5G3D features the best combination of corrosion resistance, hot hardness, score and heat resistance.

Keywords: *plasma powder hard-facing, hard-facing consumables, properties of deposited metal, hard-facing of fittings, corrosion resistance, hot hardness*

Iron-base alloys are widely applied for hard-facing of sealing surfaces of fittings used in power, petrochemical, marine and general engineering. Many CIS enterprises use manual or mechanised electric arc welding for these purposes. Depending on the service conditions of fittings, manual electric arc welding is performed by using electrodes UONI-13/NZh-2, TsN-6L, TsN-12M and TsN-24, and mechanised submerged arc welding — by using solid wires Np-20Kh14, Sv-20Kh13, Sv-10Kh17T and Sv-13Kh25T, as well as flux-cored wires PP-AN106, PP-AN133, PP-AN157 and flux-cored strip PL-AN150.

Compared to manual arc welding using stick electrodes, mechanised electric arc welding using flux-cored wires provides better quality of the deposited metal. However, it is performed at least in three layers, this leading to excessive utilisation of welding consumables and increase in time of the hard-facing process [1]. In addition, mechanised electric arc welding of small-diameter parts (≤ 200 mm) involves difficulties related to removal of slag crust from the previous deposited layer. In this case, when welding is performed on seats, it is necessary to use forming devices.

As proved by experience, plasma powder hard-facing provides deposited metal of a preset chemical composition even in the first layer, and is free from many drawbacks characteristic of arc hard-facing [2].

The task of this study was to investigate properties of iron-base alloys as applied to plasma powder hard-facing of sealing surfaces of different-purpose fittings.

Based on the available experience, the following materials were chosen for the investigations: chromium steel 22Kh16N2M, chrome-nickel-silicon steel 08Kh17N8S6G (corresponds to metal deposited with electrodes TsN-6L), steel 13Kh16N8M5S5G4B (corresponds to metal deposited with electrodes TsN-12M, foreign-made powders of the DS ZN12, Hogas X-FeSP573 and C1111 grades, and flux-cored wire of

the SK AF Antinit Dur500 grade [3]), experimental chrome-nickel-silicon steels 04Kh19N10M4S5GFA and 15Kh19N9M4S5G3D differing in the contents of carbon, vanadium, nitrogen and copper, and nickel alloy N77Kh16S3R3 (used as a reference).

The experimental chrome-nickel-silicon steels were alloyed with nitrogen to increase their ductility, and with copper — to improve their antifriction properties. Molybdenum in steel 22Kh16N2M provides increase in its heat resistance and hardness in the deposited state.

All of the above hard-facing consumables were used in the form of powders with a particle size of 80–200 μm . They were made by nitrogen atomisation of molten metal under industrial conditions.

Plasma powder hard-facing for the investigations was carried out by using standard equipment fitted with the plasmatron with a local lateral introduction of powder into the arc, which provides stability of the hard-facing process when using ferromagnetic powders [4].

Measuring of hardness at working temperatures was performed by using the «Pomp Celtic» Instrument «Pomea» under a load of 108 N on the indenter, holding for 1 min and air pressure of 1.33 MPa in the working chamber. Hardness was measured on the hard-faced samples with a diameter of 37 mm and height of 5 mm.

Tests to general corrosion resistance were carried out in water vapour and in air at a temperature of 700 °C for 500 h, as well as in distilled water at a temperature of 300 °C and pressure of 20 MPa for 1000 h. Test specimens measuring 40 × 10 × 3.5 mm were cut out from the deposited metal after tempering at 600 °C for 2 h.

Resistance of the deposited metal to intercrystalline corrosion (ICC) was investigated by the standard AMU methods (GOST 6032–2003) [5] and electrochemical method [6]. For the latter, the test specimens measuring 30 × 10 × 50 mm were held in the $\text{NClO}_4 + \text{NaCl}$ solution after provoking tempering at temperatures of 650, 730 and 850 °C for 2 h. The sensitivity to ICC was evaluated from growth of anode



Figure 1. Appearance of rings with deposited layer for heat resistance tests

dissolution current i at a direct potential of +0.3 V within the activation region.

Tests to score resistance were conducted by using a special test rig in the vapour environment under the following conditions: $T = 300\text{ }^\circ\text{C}$ and $P = 12\text{ MPa}$, $T = 540\text{ }^\circ\text{C}$ and $P = 16\text{ MPa}$, and $T = 545\text{ }^\circ\text{C}$ and $P = 25.5\text{ MPa}$. Real components of the DN150 valve gates, the sealing surfaces of which operate under conditions of the highest specific pressure, were used as test specimens. The accepted maximal quantity of openings and closings in the tests was equal to 100. The path of relative movement of the gate components under the pressure was about 32 mm per cycle. The state of the gates during the tests was monitored on a base of vapour leaks. The permissible vapour leak was about 55 g/min. The value of a specific score, i.e. the ratio of a maximal depth of scratches (in micrometres) to a total friction path (in metres) was used as an indicator of score resistance.

Tests to crack resistance under thermal cycling (heat resistance) were conducted on rings of steel 20. The rings were 130 mm in outside diameter, 18 mm wide and 25 mm high. They were subjected to one-sided hard-facing on their end surfaces (Figure 1). Thickness of the deposited layer was 3.8–4.0 mm. Hard-facing was followed by tempering at a temperature of 600 °C for 2 h. The tests provided for heating of the rings in electric furnace to 300 °C and cooling in running water to room temperature. Heat resistance of the alloys investigated was evaluated from the quan-

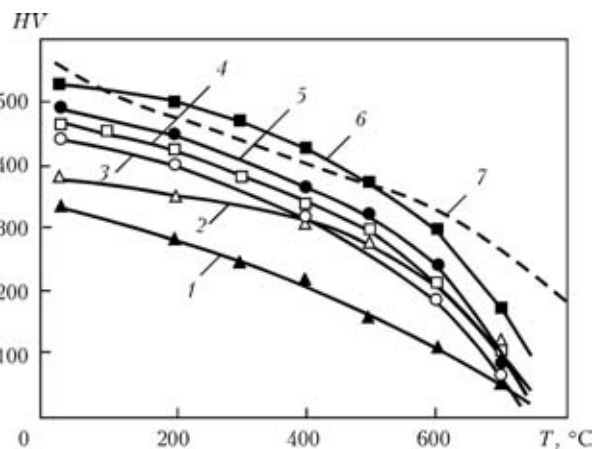


Figure 2. Temperature dependence of hardness HV of the deposited metal for hardening of sealing surfaces [6]: 1 – 08Kh17N8S6G; 2 – 04Kh19N10M4S5GFA; 3 – 22Kh16N2M; 4 – 13Kh16N8M5S5G4B; 5 – 15Kh19N9M4S5G3D; 6 – N77Kh16S3R3; 7 – Stellite No.6

tity of thermal cycles to formation of cracks in the deposited layer. The presence of cracks was detected by the fluorescent method.

Dependence of hardness of the investigated alloys on temperature is shown in Figure 2. To compare, the Figure shows hot hardness of nickel and cobalt alloys, which are characterised by the excellent performance. All types of the iron-base deposited metal, except for 08Kh17N8S6G, preserve a sufficiently high level of hardness at $T = 400\text{--}600\text{ }^\circ\text{C}$. The highest value of hot hardness was exhibited by standard alloy 13Kh16N8M5S5G4B and experimental deposited metal 15Kh19N9M4S5G3D. However, their hot hardness was lower than that of the nickel and cobalt alloys.

All iron-base materials oxidise in water vapour and in air much less intensively than the nickel-base alloy. All types of the investigated deposited metals are classed as «highly resistant» to corrosion in distilled water (GOST 13819–68).

As seen from potentiometric direct anode curves (Figure 3), deposited metals 22Kh16N2M and 08Kh17N8S6G are characterised by increased current i at a potential of +0.3 V, this being indicative of their sensitivity to ICC. The rest of the deposited metals feature resistance to ICC, as they have no activation region at a potential of +0.3 V.

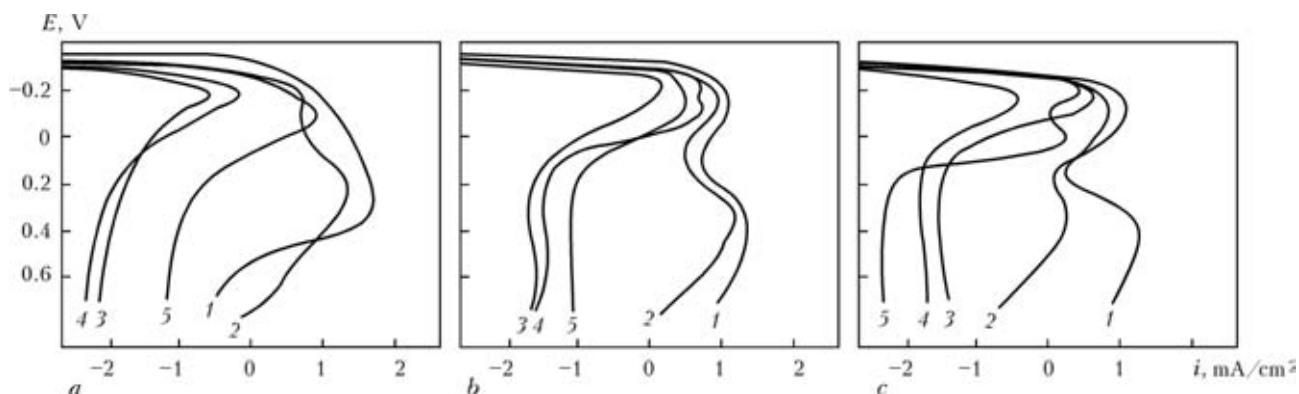


Figure 3. Potentiometric direct anode curves of deposited metals in tempering at different temperatures of 650 (a), 730 (b) and 850 (c) °C for 2 h: 1 – 22Kh16N2M; 2 – 08Kh17N8S6G; 3 – 13Kh16N8M5S5G4B; 4 – 04Kh19N10M4S5GFA; 5 – 15Kh19N9M4S5G3D



Score and corrosion resistance test results [9]

Type of deposited metal	Hardness of deposited metal <i>HRC</i>	Specific score, $\mu\text{m}/\text{m}$	Test time, h		
			500		1000
			Water vapour	Air	Distilled water
08Kh17N8S6G	31–34	9.3	0.0135	0.0186	0.0097
13Kh16N8M5S5G4B	45–49	4.6	0.0093	0.0145	0.0061
22Kh16N2M	42–45	14.5	0.0087	0.0137	0.0081
15Kh19N9M4S5G3D	48–51	1.8	0.0075	0.0132	0.0051
04Kh19N10M4S5GFA	37–42	2.8	0.0061	0.0121	0.0041
N77Kh16S3R3	51–53	1.3	0.0991	0.0250	0.0038

When tested to ICC resistance by the AMU method, all specimens after boiling in a solution containing $160 \text{ g}/\text{dm}^3 \text{ CuSO}_4$ and $100 \text{ g}/\text{dm}^3 \text{ H}_2\text{SO}_4$ for 24 h fractured in bending to 90° . The integrated tests show that ICC develops deep into the hard-faced layer in deposited metals 22Kh16N2M and 08Kh17N8S6G as a result of depletion of the boundary regions of grains in chromium.

Normally, score and heat resistance of materials of the sealing surfaces is evaluated by procedures that provide for testing of small specimens cut out from the deposited metal, or 45 mm diameter hard-faced disks using special laboratory rigs simulating service conditions [7, 8].

In contrast to testing of small specimens, our experiments on real components make it possible to allow for a number of factors that may cause or accelerate formation of thermal fatigue cracks and scores, i.e. the state of structure of the deposited layer and presence of substantial stresses in it (working, welding, thermal, etc.), as well as technological defects (pores, lacks of fusion, non-metallic inclusions, etc.).

The tests show that the deposited metal of the type of chromium steel 22Kh16N2M features a good score resistance at a vapour temperature of 300°C and pressure of 12 MPa. However, under conditions of high parameters of the working environment (545°C and 25.5 MPa, respectively), its resistance decreases to a considerable extent (Table), although hot hardness in this case remains at a sufficiently high level (see Figure 2).

Among the chrome-nickel-silicon materials, the best score resistance was exhibited by deposited metal 15Kh19N9M4S5G3D. Both in manual welding with electrodes TsN-6L and in plasma welding by using powder as a filler, deposited metal of the 08Kh17N8S6G type was inferior in score resistance to 13Kh16N8M5S5G4B [9, 10]. As seen from the Table, all types of the iron-base deposited metals are much inferior in score resistance to nickel alloys.

Deposited metal 13Kh16N8M5S5G4B is characterised by a low heat resistance, independently of the welding method and type of a welding consumable (Figure 4). It should be noted that heat resistance of

the materials under consideration decreases as a rule with increase in their hardness and score resistance, which is usually accompanied by a dramatic decrease in ductility. At the same time, the optimal level of these characteristics of the Fe–Cr–Ni–Si–Mo system deposited metals can be provided owing to rational complex alloying and modification. As seen from Figure 3, deposited metal 15Kh19N9M4S5G3D featured the optimal heat resistance. Having approximately the same hardness as nickel-base alloy of the N77Kh16S3R3 type (*HRC* 50–51), it provides approximately identical heat resistance.

Deposited metal 15Kh19N9M4S5G3D in the initial state has an austenitic-ferritic structure, the volume content of the ferrite phase being 40%. Depending on the type of the base metal and its thermal-physical characteristics determining solidification conditions of the deposited metal, structure of the said type of the deposited metal markedly changes (Figure 5).

After welding, this metal has a comparatively high hardness (*HRC* 42–44), this indicating to the probable presence of the carbide-silicide phase in its structure. The concentration of ferritising elements (chromium, silicon, molybdenum, etc.) in the ferrite phase is known to be higher than in the austenite phase. Diffusion mobility of these elements in it is higher as well, this leading to a more intensive hardening of the ferrite component due to its ordering and decomposition processes occurring during holding within the appropriate temperature range. Tempering in a 650–

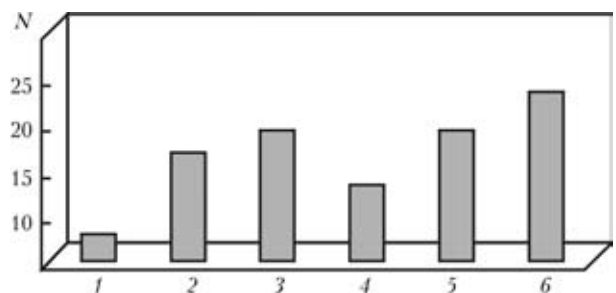


Figure 4. Heat resistance of deposited metal [9]: 1 – 13Kh16N8M5S5G4B; 2 – 22Kh16N2M; 3 – 15Kh19N9M4S5G3D; 4 – 04Kh20N10M4S5GFA; 5 – N77Kh16S3R3; 6 – 08Kh17N8S6G; N – quantity of thermal cycles to formation of the first crack

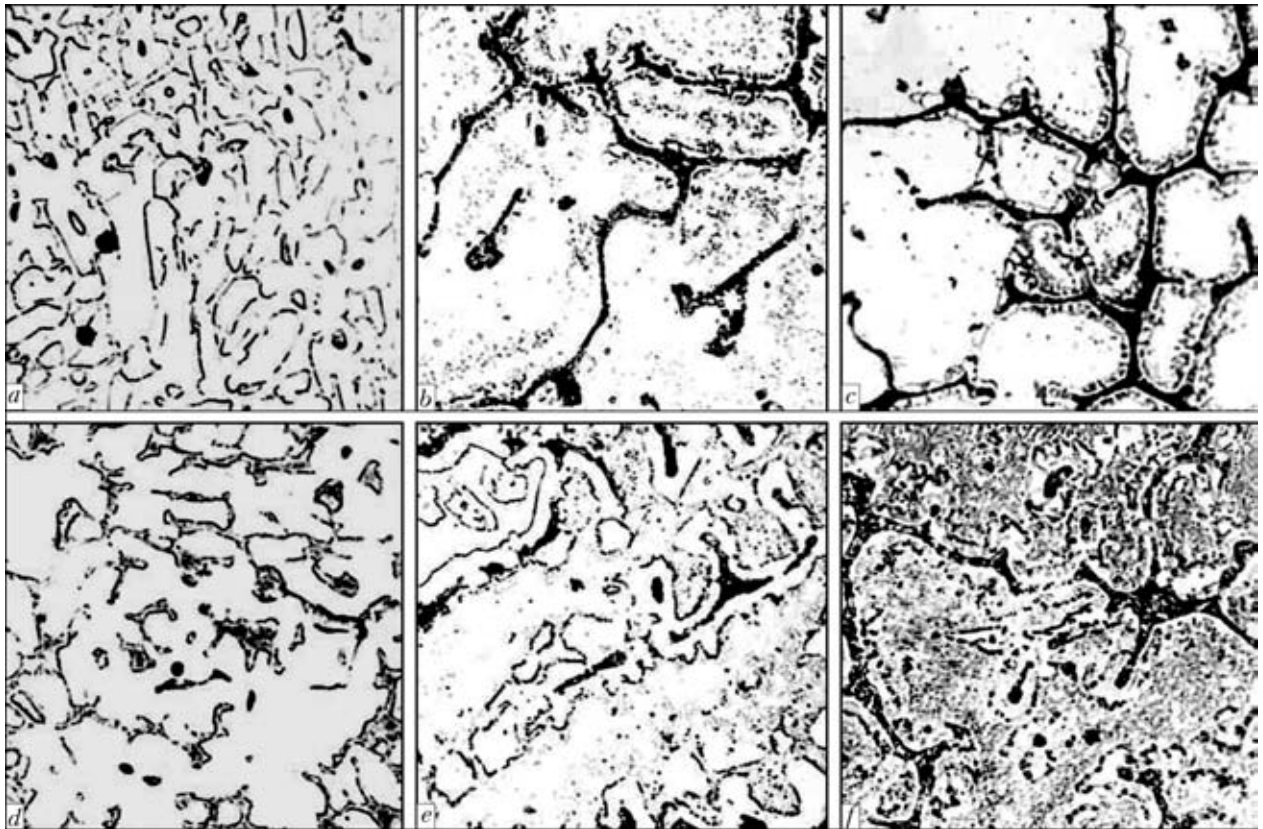


Figure 5. Microstructures ($\times 500$) of metal deposited with powder 15Kh19N9M4S5G3D on steel 20 (*a, d*), 12Kh1MF (*b, e*) and 08Kh18N10T (*c, f*) in the initial state (*a-c*) and after tempering at 650 °C for 2 h (*d-f*)

850 °C range leads to increase in hardness of this type of the deposited metal to HRC 46–51 and is accompanied, according to the magnetic measurement data, by a marked decrease in the amount of ferrite — the higher the ferrite content of the initial structure, the more substantial is the said decrease (see Figure 5). Probably, decomposition of ferrite under such conditions occurs by the following scheme: $\alpha \rightarrow \gamma'' + \text{Me}_6\text{C}$ type carbides + intermetallics of the σ -phase type + silicides of the $\text{Cr}_3\text{Ni}_5\text{Si}_2$ type (where α is the ferrite phase, and γ'' is the secondary austenite).

As seen from Figure 6, owing to a low penetration of the base metal, which is characteristic of plasma welding, the required hardness and preset chemical

composition of the deposited metal are achieved already at a distance of 0.3–0.5 mm from the fusion surface. As a result of ageing at 600 °C for 500 and 1000 h, the ferrite decomposition processes become more completed. No substantial changes in hardness of the deposited layer take place, and no hard and brittle components form in the fusion zone, which should have a favourable effect on performance and reliability of the hard-faced fittings.

As proved by the tests conducted on iron-base alloys under the conditions that are as close as possible to the service conditions of power fittings, the best combination of corrosion resistance, hot hardness, score and heat resistance was exhibited by deposited

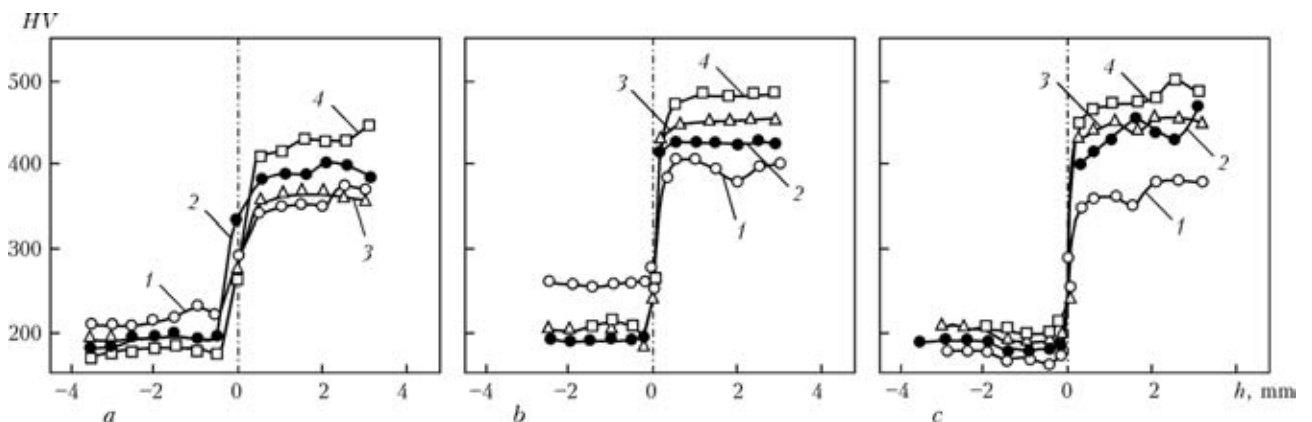


Figure 6. Distribution of hardness in height of deposited layer 15Kh19N9M4S5G3D: *a* — base metal steel 20; *b* — base metal steel 12Kh1MF; *c* — base metal steel 08Kh18N10T in the initial state (*1*), after tempering (*2*), and after tempering and ageing at $T = 600$ °C for 500 (*3*) and 1000 (*4*) h, respectively



metal 15Kh19N9M4S5G3D. This material is not inferior in heat resistance at dramatic thermal cycles and in score resistance to known chrome-nickel alloys containing boron and silicon, and is much superior to metal 13Kh16N8M5S5G4B (hard-facing with electrodes TsN-12M and their analogues). As to a number of service properties and price, chromium steel 22Kh16N2M is fully acceptable for hard-facing of sealing surfaces of components of general-engineering fittings, which are used at a temperature of up to 400 °C and pressure of 16 MPa.

1. Ereemeev, V.B., Strelyany, Yu.V., Korbut, V.A. et al. (1979) Chemical microheterogeneity of metal deposited with different electrode materials. In: *Properties and tests of deposited metal: Theoretical and technological principles of surfacing*. Kiev: PWI.
2. Pereplyotchikov, E.F. (2004) Plasma-powder cladding of wear- and corrosion-resistant alloys in valve manufacturing. *The Paton Welding J.*, **10**, 31–37.
3. Stepin, V.S., Starchenko, E.G. (2010) Application of dispersion-hardening Cr–Ni–Si steels for valve elements and cladding of sealing surfaces of fittings of thermal power and nuclear plants. *Armaturostroenie*, **3**, 66–69.
4. Gladky, P.V., Pereplyotchikov, E.F., Ryabtsev, I.A. (2007) *Plasma cladding*. Kiev: Ekotekhnologiya.
5. GOST 6023–2003 (Instead of GOST 6032–89): Corrosion-resistant steels and alloys. Methods for testing to intercrystalline corrosion resistance. Minsk: Standart.
6. Medvedeva, L.L., Knyazheva, V.M., Kolotyркиn, Ya.M. et al. (1975) Electrochemical method for quantitative evaluation of susceptibility of steels to intercrystalline corrosion. *Zashchita Metallov*, **11(6)**, 699–705.
7. Ratner, A.V. (1965) *Fittings for supercritical-parameters vapour*. Moscow; Leningrad: Energiya.
8. Ivniysky, B.Ya., Galanov, V.A., Chernyshova, V.V. et al. (1975) Evaluation of resistance to thermal cycles of materials of sealing surfaces of fittings. *Energomashinostroenie*, **7**, 27–29.
9. Gladky, P.V., Pereplyotchikov, E.V., Rabinovich, V.I. (1970) *Plasma cladding in power valve manufacturing*. Moscow: NIInformTyazhmash.
10. Blagov, E.E., Ivniysky, B.Ya. (1974) *Throttle control valves in power engineering*. Moscow: Energiya.

PARTICLE DISPERSITY AND MANGANESE VALENCE IN WELDING AEROSOL

I.K. POKHODNYA¹, V.I. KARMANOV¹, I.R. YAVDOSHCIN¹, I.P. GUBENYA¹, O.Yu. KHIZHUN² and I.V. KHOBTA²

¹E.O. Paton Electric Welding Institute, NASU, Kiev, Ukraine

²I.M. Frantsevich Institute of Problems of Materials Science, NASU, Kiev, Ukraine

Method of X-ray photoelectron spectroscopy was used to establish the valent state of manganese compounds in the welding aerosol. Valent state of manganese compounds (Mn⁺⁴) was found in welding with basic electrodes. Analysis of dispersity of welding aerosol solid compound was performed using the method of laser granulometry.

Keywords: arc welding, coated electrodes, solid component of welding aerosol, particle dispersity, bimodal distribution, agglomerates, manganese valence

In welding of carbon low-alloyed steels, manganese compounds are the most hazardous components of the solid component of welding aerosol (SCWA) [1, 2]. Toxicity of these compounds, in its turn, depends on manganese valence and increases with the increase of its oxidation level. Threshold limit values (TLV) of manganese and its compounds in the welding aerosol (WA) in the working zone air are equal to 0.6/0.2 and 0.3/0.1 mg/m³ (numerator shows the maximum one time, and the denominator – shift average TLV) at its content in WA below 20 % and from 20 up to 30 %, respectively [3]. Modern norms of manganese TLV in WA and recommendations do not separate manganese compounds by valence and establish one TLV norm equal to 0.2 mg/m³ [4, 5]. Manganese in WA belongs to the second hazard class [3].

A number of investigations devoted to study of SCWA composition [1, 6–9] showed that the most probable manganese state is Mn²⁺, Mn³⁺.

Staff members of the E.O. Paton Electric Welding Institute and I.M. Frantsevich Institute of Problems of Materials Science studied the valent state of man-

gane in aerosols formed in welding with electrodes with coating of rutile and basic types. Investigations were performed using X-ray photoelectronic spectrometer ES-2401.

Investigations were performed using SCWA forming in welding with test electrodes with coating of rutile (electrode index E4) and basic types (electrode index PSh4 and PSh5). Here, SCWA for analysis were selected by deposition on a filter, mechanical removal from the filter and placing into a brass weighing bottle with subsequent filling of the latter by argon to prevent final oxidation of samples at contact with ambient oxygen. Spectra were excited by non-monochromatized radiation of MgK_α-lines. SCWA were rubbed into the copper plate surface, which was first ground and etched by nitric acid. Studied samples completely covered the copper plate, so that lines corresponding to copper atoms were not observed in the plain spectra. Mn2*p*- and Mn3*p*-spectra were filmed in the plain mode and optimum mode of Mn2*p*-spectra measurement was selected for investigations. By the results of obtained Mn3*p*-spectra (Figure 1, *a*) it was established that manganese in SCWA of electrodes with basic type coating (PSh4, PSh5) is present in valent state +4 (peak *I*), and in SCWA of electrodes with a

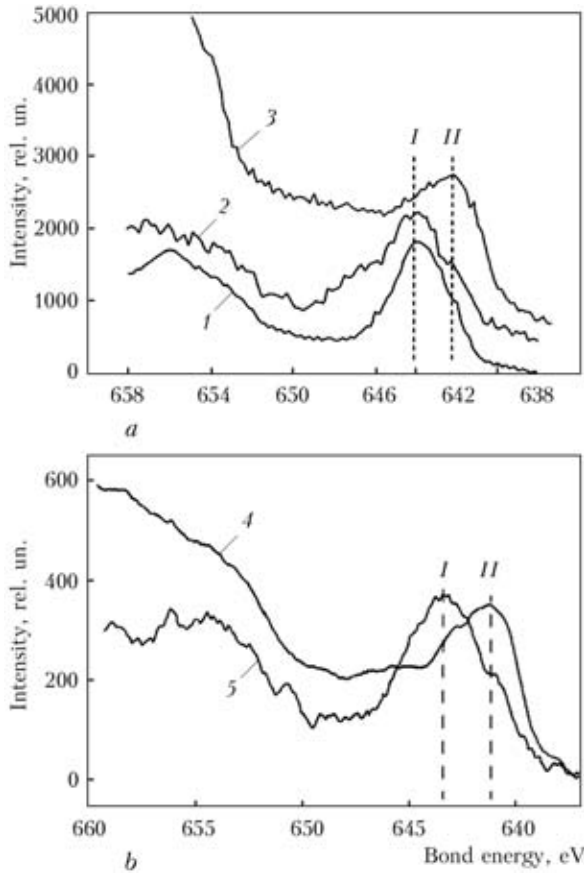


Figure 1. Comparison of XPS spectra of SCWA of electrodes with coatings of basic PSh4 (1), PSh5 (2) and rutile E4 (3) types (a) and commercial electrode grades MR-3 (4) and UONI-13/55 (5) (b) (for I, II designations see the text)

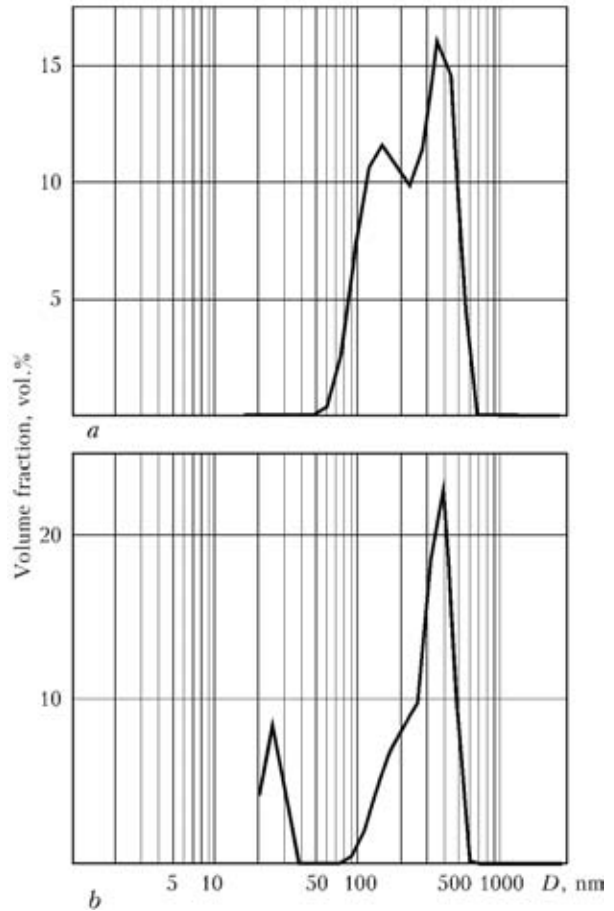


Figure 3. Volume distribution of SCWA dispersity of electrodes with coating of rutile MR-3 (a) and basic UONI-13/55 (b) type

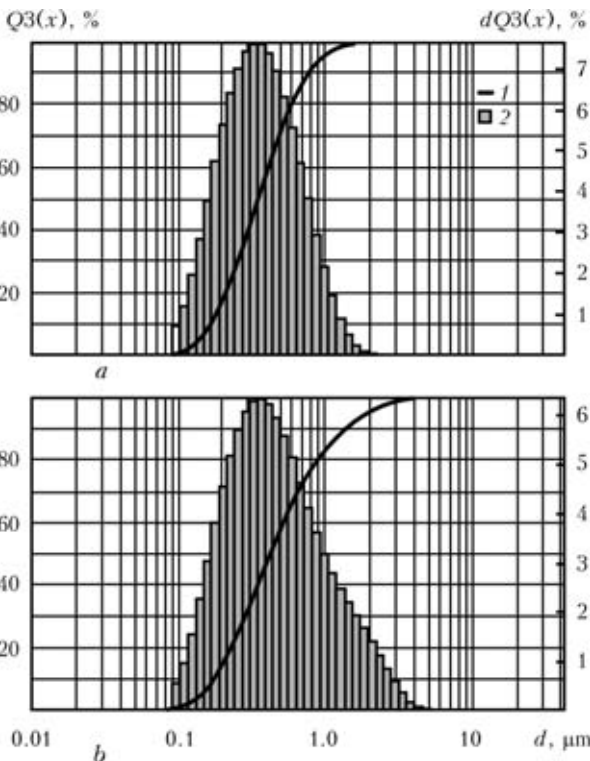


Figure 2. Volume distribution $Q3(x)$ (1) and distribution density $dQ3(x)$ (2) of dispersity of SCWA of electrodes with coating of basic UONI-13/55 (a) and rutile MR-3 (b) types

rutile-type coatings (E4) it is present in valent state +3 (peak II).

Experimental data obtained on test electrodes were confirmed at X-ray photoelectronic spectrometric (XPS) investigations of valent state of manganese in SCWA of commercial grade electrodes UONI-13/55 and MR-3 (Figure 1, b). The given data are indicative of the presence of four-valent manganese in SCWA formed in welding with basic electrodes.

An important factor determining SCWA toxicity is dispersity of WA particles. Particles of less than 20 μm diameter can remain suspended in the air. 100 % of particles of less than 1 μm diameter penetrate into the body through the respiratory tract [10]. About 30 % of particles of 0.1–1.0 μm size precipitate in the lungs. Particles of less than 0.1 μm size (100 nm) are also inhaled and precipitate in the lungs. Penetration of nano-sized particles through the skin [11], as well as their penetration into the brain through the nerves in the nasal sinuses is possible [12, 13].

Most of the recent research was conducted using cascade impactors, operating by the method of aerodynamic separation [7, 9, 14–16].

In this work SCWA dispersity was assessed by the method of laser granulometry with Analysette 22 MicroTec Plus analyzer of «Fritsch» Company (measurement range of 0.08–42 μm). Studied were SCWA generated in welding with basic and rutile electrodes. WA extracted from the filter, were stored in a glass weighting bottle. In preparation for analysis the sam-



ple was mixed with a spatula, which was followed by placing it into a beaker, where distilled water with SAS (0.1 % solution of sodium pyrophosphate) was added. The suspension was mixed for three minutes in an ultrasonic dispenser Ultrasonic Bath LABORETTE 17. Before suspension analysis it was checked for stability.

Each sample was analyzed three times. Figure 2 gives the results of measurements and calculations. Volume distribution of particles was calculated using Fraunhofer theory. Results of investigation of SCWA dispersity were as follows. In UONI-13/55 electrodes the volume of particles of less than 10 μm diameter is equal to 0.2 %; those of less than 50 μm diameter – 0.4 %, and those of less than 90 μm diameter – 0.8 %. In MR-3 electrodes particles smaller than 10 μm amount to 0.2 %, those smaller than 50 μm – 0.4 %; those smaller than 90 μm – 1.4 % in the first two measurements, and 1.3 % in the third measurement, respectively. From the above data it is seen that the average diameter of aerosol particles in electrodes of both basic and rutile type is in the range of 0.3–0.4 μm (peak of histograms of distribution density $dQ3(x)$ in Figure 2). SCWA of MR-3 electrodes also have a higher percentage of coarser particles.

Presented results give a general idea of SCWA dispersity. For a more detailed analysis of the nano-range of particles, which present a particular hazard because of a higher ability of penetration into the welder's body, analysis was performed in Zetasizer 1000HS instrument (measurement range of 0.002–3 μm) at the I.M. Frantsevich Institute of Problems of Materials Science.

Studied were SCWA generated in welding with electrodes with coating of basic (UONI-13/55) and rutile (MR-3) types. WA extracted from the filter were mechanically crushed and poured into a plastic container filled with distilled water with SAS (1 % solution of sodium hexametaphosphate). The suspension was stirred for 10 min in ultrasonic dispenser UZDN-A. Several drops of the obtained suspension were added to the cuvette filled with dispersion medium for 2/3. The cuvette was placed into the instrument, where the degree of saturation of the analyzed solution was determined during initial analysis.

During analysis of each sample PC was used to perform three calculations, each of which was conducted proceeding from the results of ten measurements with determination of an average value. Results of measurements and calculations are given in Figure 3 and in the Table. Average time of analysis of one sample was equal to 25 min. Volume distribution of particles was calculated using Mie theory.

Obtained data indicate that SCWA of both electrode types have a bimodal particle distribution by dimensions. Average diameter of WA particles for MR-3 and UONI-13/55 electrodes is equal to 209.8 and 236.1 nm.

Particles of WA of MR-3 electrodes form agglomerates with average size of 150±60 and 370±120 nm, and primary particles are not clearly defined. Primary WA particles of UONI-13/55 electrodes have a narrow distribution, their average size is about 25±6 nm.

Results of analysis of SCWA dispersity

Peak	Area, arb. un.	Average, nm	Width, nm
Peak analyses by intensity			
I	100.0	236.2	243.4
	99.9	259.9	220.6
Peak analyses by volume			
I	48.0	156.5	96.5
	16.8	25.6	6.0
II	52.0	370.1	243.1
	83.2	318.2	212.1
Peak analyses by quantity			
I	100.0	129.8	85.0
	99.4	25.6	6.0
<i>Note.</i> Numerator gives data for MR-3 electrodes, denominator – for UONI-13/55.			

A susceptibility to formation of agglomerates of 320±100 nm size was observed.

CONCLUSIONS

1. Mn⁺⁴ compounds were found in aerosols formed in welding with basic electrodes.
2. SCWA, formed in welding with electrodes with coatings of basic and rutile types, have a bimodal distribution by dimensions.
3. WA particles of both types form agglomerates at cooling.

1. Voitkevich, V. (1995) *Welding fumes: formation, properties and biological effects*. Cambridge: Abington Publ.
2. (2006) *ISO 15011-4*: Health and safety in welding and allied processes – laboratory method for sampling fume and gases generated by arc welding. Pt 4: Fume data sheets.
3. *GN 2.2.5.1313-03*: Maximum allowable concentration of harmful substances in working zone air. Introd. 15.06.03.
4. (2005) *TLVs and BEIs*. Threshold limit values for chemical substances and biological exposure indices. ACGIH.
5. (2009) The JSOH Recommendation of occupational exposure limits (2009–2010). *J. Occupational Health*, **51**, 454–470.
6. Jenkins, N.T., Eager, T.W. (2005) Chemical analysis of welding fume particle. *Welding J.*, **6**, 87–93.
7. Sowards, J.W., Lippold, J.C., Dickinson, D.W. et al. (2008) Characterization procedure for the analysis of arc welding fume. *Ibid.*, **87(4)**, 76–83.
8. Gonser, M.J., Lippold, J.C., Dickinson, D.W. et al. (2010) Characterization of welding fume generated by high-Mn consumables. *Ibid.*, **89(2)**, 25–33.
9. Sowards, J.W., Lippold, J.C., Dickinson, D.W. et al. (2010) Characterization of welding fume from SMAW electrodes. Pt 2. *Ibid.*, **89(4)**, 82–89.
10. Sterjovski, Z., Norrish, J., Monaghan, B.J. (2008) The effect of voltage and metal-transfer mode on particulate-fume size during the GMAW of plain-carbon steel. *IIW Doc. VIII-2092-08*.
11. Hoet, P.H.M., Bruske-Hohlfeld, I., Salata, O.V. (2004) Nanoparticles – known and unknown health risks. *J. Nanobiotechnology*, **12(2)**.
12. Raloff, J. (2010) Destination brain. *Sci. News*, **177(11)**.
13. Glushkova, A.V., Radilov, A.S., Rembovsky, V.R. (2007) Nanotechnologies and nanotoxicology – view of the problem. *Toksikologich. Vestnik*, **6**, 4–8.
14. Jenkins, N.T., Pierce, W.M.G., Eagar, T.W. (2005) Particle size distribution of gas metal and flux cored arc welding fumes. *Welding J.*, **84**, 156–163.
15. Sowards, J.W., Lippold, J.C., Dickinson, D.W. et al. (2008) Characterization of welding fume from SMAW electrodes. Pt 1. *Ibid.*, **87(4)**, 106–112.
16. Berlinger, B., Benker, N., Weinbruch, S. et al. (2010) Physicochemical characterization of different welding aerosols. *Analyt. and Bioanal Chemistry*, **10**, 1773–1789.

WELDED ELECTRIC CONTACTS OF DISSIMILAR CONDUCTORS

B.E. PATON¹, V.I. LAKOMSKY¹ and V.I. BRAGINETS²

¹E.O. Paton Electric Welding Institute, NASU, Kiev, Ukraine

²PTZ SRC of E.O. Paton Electric Welding Institute, Zaporozhie, Ukraine

High energy effectiveness of application of welded electric contacts of metals with different carbon materials and welded electric contacts of cathode units and burnt anodes developed at PWI is substituted. Designs of electric contact plugs (ECP) as well as arcotrons, i.e. nozzle-free torches using an oxide cathode, were developed. Examples of effective application of contact assemblies with ECP in synthesis and Acheson furnaces are given.

Keywords: *energy consumption, loss of energy, electric contact, transient electric resistance, oxide cathode, arcotron, wetting, metal to carbon material welding, electric contact plugs, welded contact assembly, electrolytic cell, Acheson furnace*

Cost of electricity constantly rises, according to the data of world market of electrical energy, and apparently such a tendency remains for a long time unless forever. Therefore, prime task of the industrial engineers should lie in searching of new ways of minimization of energy consumption in the technological processes and constant control of energy loss. What is a level of effectiveness of this task solving in production?

Let us show by example of aluminum production how prodigally electricity is consumed in this sub-branch of non-ferrous metallurgy.

Transfer of electricity from a power station to aluminum plant depends on distance and loss can make up to 13 %, therefore, the powerman make a number of efforts for energy-saving, increasing, for example, voltage in the electric main. But after electricity has been supplied to the plant attitude to it changes. One of the authors saw how welding of the main aluminum bus bars was carried out by open carbon arc of large power without any gas or slag shielding in a shop of magnesium production at one of Ural industrial enterprises. Such an operation performance was only used in N.N. Benardos time when the arc welding in Russia began and steel but not aluminum was welded in such a way. Strictly speaking this technological process is difficult to be termed welding. At the moment we can just imagine a number of oxide films being involved in a weld at that and amount of electricity that was lost then on this joint.

Recently, complex «aluminum plant–electric power station» is considered as a whole in designing of new aluminum plants, and all necessary measures for energy saving are to be taken.

It is known from statistical data, obtained as far back as soviet time, that an aluminum industry was the most energy consuming among all consumers of electricity in the national economy of the Soviet Un-

ion. Considering the next example we can imagine an amount of electricity necessary for a current aluminum production. Production of 36 mln t of aluminum (recently obtained annual production of metal all over the world) requires the amount of electricity that can be generated in two and a half year period by such a giant as Krasnoyarsk hydropower plant.

Such a huge consumption of energy during aluminum production by high-temperature electrolysis is explained, first of all, by strong bond between aluminum and oxygen in Al₂O₃ alumina, i.e. a raw for this metal production. Around 7000 kW·h counting on each tone of obtained metal are necessary, on different data, for breaking a bond between elements in the compaund with the purpose of aluminum release. At the same time, specific consumption of electricity in the industry makes at average 14000 kW·h. The rest 7000 kW·h is the loss. So, only half of all electricity being supplied to the electrolytic cell is used effectively. This is too prodigally, isn't it?

Yu.V. Bajmakov, serious and conscientious scientist, standing at the beginnings of aluminum metallurgy of USSR, thoroughly analyzed energy consumption in the production of light metals back in prewar years and wrote small but very important book [1] during the Leningrad blockade. He showed that the clamping electric contacts between steel contact jaws and electrodes from graphitized carbon material are the most wasteful elements in the structure of aluminum electrolytic cell if they are produced using cast iron pouring. Only these contacts lose up to 30 % from the whole being observed in multiple electric contacts of the electrolytic cell. This is the Moloch consuming electricity so difficultly obtained by humanity. Followers of Yu.V. Bajmakov scorned his advices and even invented the title to these parasitic contact resistances, i.e. «heating resistances». Thus, they have rehabilitated these losses, adjusted to them and, therefore, the same structure of contacts that have been used more than hundred years ago in first industrial devices is preserved today even in the electrolytic cells of the XXI century.

All aluminum engineers know that the electric contacts in a hearth of electrolytic cell are manufactured by means of liquid cast iron pouring in a technological gap formed between steel current jaw and channel in carbon hearth block. The liquid cast iron gives good wetting to solid steel, therefore, a good electric contact is provided. At the same time the liquid cast iron makes no wetting to carbon material of the hearth block, thus, transfer of electric charges through this interface is provided with large energy loss and the interface itself is available for penetration of different fusible materials in it. Separate elements of electrolyte pool leak out on this surface through a cathode unit and, in particular, along the seams between the blocks in a process of electrolytic cell running. In time this interface loses significant part of still small electrical conductance. This is one more reason of heavy losses of electricity and example of that how large electricity losses are tolerated then in the process of five-four years operation of the electrolytic cell for the sake of simplicity of technology for assembly of the cathode units.

Further, the analysis shows that the most electric contacts in electrometallurgy units operate under elevated temperatures up to 250–300 °C as well as 850–900 °C (hearth blocks). But, electric heavy-current contacts are still manufacture as clamping ones regardless heavy operating conditions that promotes great electricity loss due to high transient electric resistance, increasing during unit operation that is in particular important. For example, each microhm of resistance in the current electrolytic cell for 175 kA leads to $1 \cdot 10^{-6} (175)^2 \cdot 10^6 \cdot 24 \cdot 365 = 268000$ kW·h annual loss that can illustrate amount of loss of electricity on the heavy-current contacts. Note that this is only for one contact!

A lot of electrolytic cells with self-baking anodes (Soderberg anodes) are still used in the aluminum industry. Electricity to them is fed from main bus bar of the shop with the help of aluminum-copper-steel chutes. Workers often have to dress contact surfaces manually under uncomfortable operating conditions (temperature up to 150–200 °C) if clamping contacts are used in them. In our opinion it is violent to ask workers to perform these tasks at heights and under such temperatures. Apparently, industrial engineers at aluminum plants forgot that the task of engineers according to the history of technologies development was facilitation of labor of workers, mechanization of their work, development of such structures which would save workers from activity under difficult conditions.

We gave these two examples for showing that the aluminum engineers use out-of-date structures of powerful contact assemblies in the electrolytic cells, regardless that advanced welding technologies have existed already for more than 20 years.

Method for production of the welded electric contacts of metals with different carbon materials [2] was

developed and thoroughly examined under industrial conditions by the E.O. Paton Electric Welding Institute of the NAS of Ukraine back in 1980s due to creation of the oxide cathodes of welding arcs [2, 3].

The E.O. Paton Electric Welding Institute developed technologies of assembly using welded electric contacts of cathode units and burnt anodes. Energy-saving contact having not need in dressing of contact surfaces during the whole life time of the electrolytic cell was designed in the Institute based on new welding technology with respect to «aluminum-copper» hanging contact. This contact was termed «PWI hanger» since being located in the hanged condition.

Formerly all electric contacts in the aluminum shops were clamping ones, but after the Great Patriotic War all the plants were obliged to change them in the welded electric contacts by order of Ministry of Non-Ferrous Metals of USSR. Methods of welding of dissimilar materials were unknown at that time and transfer to the welded contacts allowed saving 7 % of electricity, consumed by «Soyuzalyuminprom», only in metal conductors. This had obvious economic effect along the country on the whole.

Today the developments of the E.O. Paton Electric Welding Institute in area of welding of dissimilar current-conducting materials are well-known but the aluminum plants avoid them for some reasons. They, wasting large amount of electricity, include these losses in a cost price of the metal and do not want to turn to new methods of assembly of the electric contacts. Thus, electricity makes a half of the cost price of aluminum. No ministry could make the plants to master new welding technology! Obviously, that a decision of the government is necessary in this case, since electricity loss, for example, in Russia producing 5–6 mln t of aluminum per year, is evaluated on a national scale. In our opinion, the government should not agree with requests from aluminum engineers for reduction of rate of electricity, generated by state electric power station. They have own internal reserves which allow them reducing specific consumption of electricity and, thus, decreasing metal cost price that will raise competitiveness of aluminum in the external market.

It should be recognized that performance of erection works using cathode units and burnt anodes, certainly, more laborious process than pouring of the blocks by liquid cast iron. However, transfer to new technology allows the plant saving electricity, the price of which overlaps the costs for wages of more qualified workers-welders than pourers of liquid cast iron. It should be remembered that the plant makes contribution to solution of one of the social tasks paying larger salaries to the workers. Besides, the plant removes the cupola-furnaces being the sources of harmful gases, dust and slag, unusual for aluminum production, and, thus, improving ecological conditions on the plant.

Now examine the contact again. It is known from the theory of contacts of the solid bodies [5] that no matter how thoroughly the surface of metal contacts is prepared, it, however, remains rough and real contact of two contact jaws is performed only over the micropeaks on this surface and not along the whole visible area. For example, an actual area on copper-aluminum contacts makes only 5 % of the visible area. In this connection the contact surfaces are pressed to each other with force trying to deform micropeaks and, thus, increasing the actual area of clamping contact. However, increase of the area of real indicated contact more than to 30 % is physically impossible.

Hyperbolic dependence of contact electric resistance on pressing force of the contacting pair explains this effect. Initial pressing forces are highly effective, and, further forces vice versa have very small effect on resistance of contact.

The same character of dependence between contact electric resistance and, as it may be strange at first sight, current intensity is observed at normal (room) temperature in «carbon material–cast iron» contact: the higher intensity of current, passing through the contact, the lower is its resistance. This effect (fitting effect) is explained by electric breakdown of a narrow air gap between contacting materials. At that, so-called additional microbridges from cast iron are formed in the area of large currents and current is passing along them. It should be noted that this effect is observed only at normal temperature. If elevation of temperature and oxidation of cast iron surface are made at that, then the fitting effect, unfortunately, is not observed.

In contrast, the actual contact surface equals observable surface in the welded contacts. This is the main advantage of welded metal electric contacts. It is natural that contact electric resistance of the welded contacts is significantly lower than that of the clamping ones and has no increase during contact operation, what is very important.

Welded electric contacts of metals with carbon materials take separate position at that. The matter is that all hard carbon materials are porous. Total porosity varies from 20 to 30 %. There are special graphitized materials with 50 % porosity.

Materials specified have pores of two types: closed, isolated and channel, transporting pores. It should be

noted that the latter makes 3/4 of total volume of pores.

This their peculiarity is used in welding of metals with carbon materials. Liquid copper or aluminum provides no wetting of carbon materials under normal conditions. If intensive carbide-forming elements, the best of which are silicon and manganese in this case, are added to them, then an angle of wetting of carbon materials decreases up to 5–15°, and liquid overheated alloy penetrates to 10–15 mm deep inside the graphitized materials through their transporting pores. At that, the area of actual contact tens and even hundred times exceeds observable area. This is an unprecedented case in the practice of electric contacts and man should use this gift of the nature. Carbon materials are wetted by liquid iron, however, some carbide-forming chemical elements are also added to electric iron-based contacts.

Structural element of different welded contact assemblies is so-called electric contact plug (ECP). Three variants of structure of this plug are shown in Figure 1. ECP is a plug of 30 mm diameter and not more than 40 mm depth, welded in a body of carbon block whenever this is cathode unit of the electrolytic cell or its burnt anode. The ECP is a common element for all three variants of electric contact assemblies. They differ by method of electric contact joint with flat metal contact jaw. Variant *A* is recommended for the use in contact assemblies if distance between end plugs does not exceed 200 mm, and variant *B* is applied at distances depending on diameter of a tip-compensator up to 500 mm. Finally, variant *C* can be used without inter-plug distance limitations. Figure shows that the compensator, whether it being single bar or bunch of bars, is welded to current jaw using manual or semiautomatic welding.

Basis of electric contact alloy of the plug and material of the compensators must be the same as a metal of contact jaw. The compensators are necessary for smoothing a great difference in the values of thermal coefficient of linear expansion (TCLE) of carbon material ($4 \cdot 10^{-6} \text{ K}^{-1}$) and, for example, aluminum ($28 \cdot 10^{-6} \text{ K}^{-1}$). If compensators are abandoned then the welded joint can failure under effect of thermal stresses during temperature change. ECP contact resistance, measured at room temperature, varies from 50–70 for copper electric contact alloy to

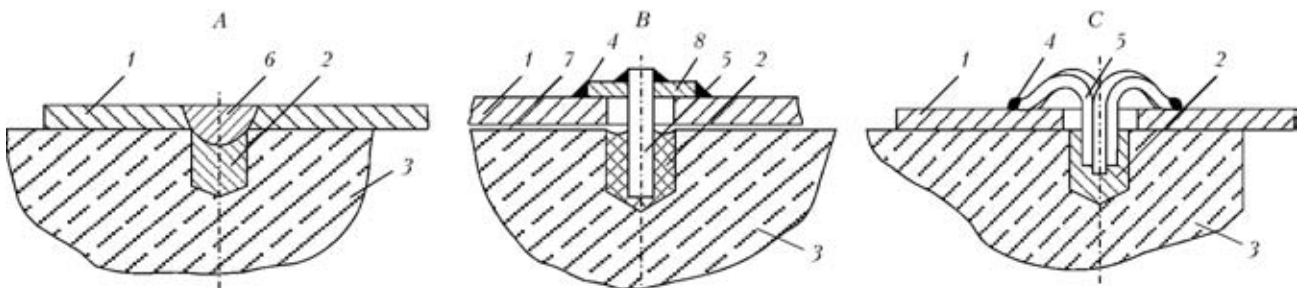


Figure 1. Scheme of the metal to carbon material welded joints of different variants A–C: 1 – metal plate; 2 – ECP; 3 – carbon block; 4 – weld; 5 – compensator; 6 – plug weld; 7 – gap between plate and carbon block; 8 – washer

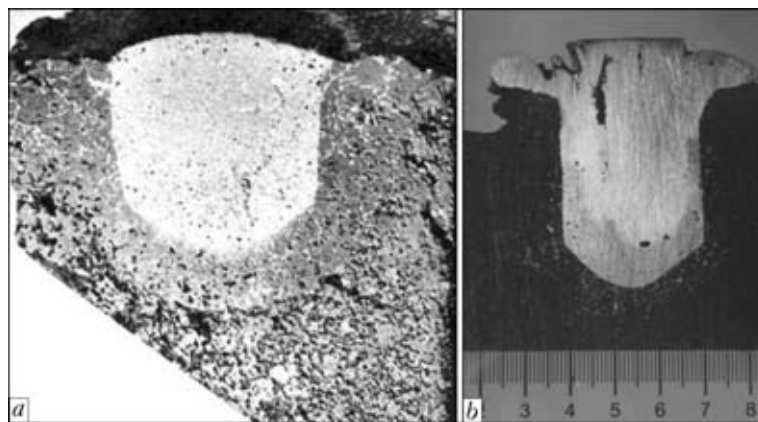


Figure 2. Macrosections of ECP welded in carbon material: *a, b* – iron- and aluminum-based alloy, respectively

100–120 μOhm for iron alloy depending on alloy material. Limit value of the current load of ECP varies from 400 (for iron alloy) to 750 A (for aluminum and copper alloys).

Development of ECP was a complex task. Dimensions of the plug are determined by comparison of the adhesion forces of alloy to carbon material with forces caused by casting shrinkage of ECP liquid alloy at its solidification and thermal shrinkage of metal at its further cooling.

Constant values of contact resistance of the plug in a course of long-term operation are specific and very important property. Note that its resistance reduces on 20–30 % at ECP heating.

It is strange from point of view of metallurgy that content of oxygen, for example in the metal of iron-based alloy, does not exceed 0.005 % after welding on open air. The same content of oxygen is observed in a simple gray cast iron. We believe that the low local partial pressure of oxygen in gas atmosphere inside the deepening of carbon material during plug welding-in, short-time plug performance and presence of electric contact alloy in the metal among additions of strong deoxidizers can explain this phenomenon.

Longitudinal sections in Figure 2 show normal microstructure of ECP. Dense well-formed plug-carbon material interface and fine distributed shrinkage porosity in the plug volume can be observed in Figure 2, *a*. It is seen from Figure 2, *b* that the layers of carbon material attached to the plug are deeply saturated by electric contact alloy.

Contact electric resistance as well as mechanical force of plug tear-out from carbon body control the technology of plug welding-in. The tear-out force depending on plug alloy makes from 600 to 1000 kg. Figure 3 shows two torn-out plugs. Cone shape of torn plug indicates maintenance of welding technology. Alloy in this case penetrated deep into metal by transporting capillary channels. Such a plug can be torn out applying 1000 kg force, its contact resistance is minimum. Other plug being cylindrical on shape with «bold» surface, has been torn out at minimum forces below 600 kg and has increased value of contact resistance. This plug is made with technology violation.

Technology and procedure of welding in of plugs in the carbon material block is our know-how and can be transmitted to a client after license purchasing. ECP is produced using an arcotron, i.e. special nozzle-free plasma torch operating on oxide cathode.

The oxide cathodes (Figure 4) are a development of the E.O. Paton Electric Welding Institute. They belong to the category of non-consumable electric-arc electrodes as tungsten and carbon ones. But the oxide cathodes in contrast to them can operate in all oxygen-containing gases up to pure oxygen. Their life time is $2-4 \cdot 10^{-8}$ g/K like in tungsten electrodes in argon atmosphere. Cathode spot reaches 2 mm in diameter on liquid oxide alloy at large arc currents and current density makes 300 A/mm^2 on it. It is recommended that welding current on the arc does not exceed 750–800 A. Diameter of the anode spot on carbon material reaches 20 mm. The parameters indicated for welding arcs are unique.

Lower by an order voltage stress in the arc column, high self-stabilizing, noiseless as well as flat maximum of temperature in a cross-section of arc column and



Figure 3. Appearance of the plugs after tear-out test: upper is performed with technology compliance, and lower – with violation



Figure 4. Oxide cathodes of welding arc for different technologies

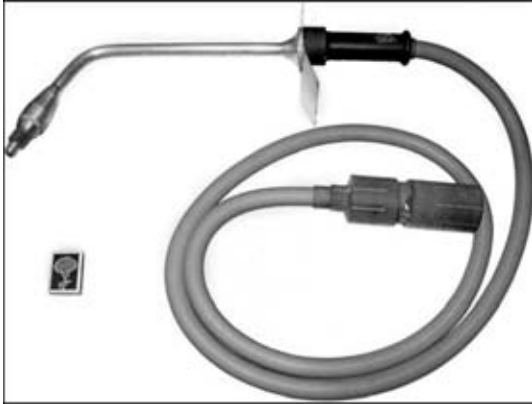


Figure 5. Special arcotron D-4A

anode spot make an electric arc of oxide cathode differ from free arcing.

A series of torches for different currents, beginning from 50 A, having commercial name «arcotron», were developed for oxide cathode application in welding. It is nozzle-free plasmatron with heat efficiency 95 % from point of view of design. Works on ECP welding

in the carbon body are performed with the help of D-4A arcotron (Figure 5).

Numerous experiments, carried out in laboratory and industrial scales, showed that application of ECP for assembly of cathode units of electrolyte cell allows achieving additionally 50–200 kg of metal per each tone of aluminum at the same electricity consumption. This is achieved due to reduction of loss of electricity in the contacts during its transfer from steel contact jaws to cathode carbon units as well as virtually complete elimination of such an effect as secondary oxidation of aluminum in the pool. The fact is that sufficiently inhomogeneous current density is observed on working surface of the hearth blocks at side supply of electricity to the hearth. It is 16 times higher in the place of current supply than in remote areas of the block. This, naturally, promotes formation of parasitic horizontal currents in the metal pool. Interaction of these currents with magnetic field of the electrolytic cell provokes formation of macrocurrents of metal and electrolyte. Fine drops of aluminum suspended in the electrolyte are carried out to the interface with air and being oxidized. This is secondary metal oxidation.

If ECP is used for energy supply to the block than excellent current homogeneity is achieved. Current density varies in 3 % range along the whole working surface of the block of 550 × 1800 mm. At that, of course, the parasitic horizontal currents come to negligibly small values and secondary oxidation of metal is, virtually, eliminated.

It should be added to mentioned above that interaction of the parasitic horizontal currents with the main magnetic field promotes formation of standing wave of liquid metal pool. The latter makes technologists increasing thickness of electrolyte layer that results in over-expenditure of energy for electrolysis performance.

Besides, change of clamping electric contacts of the cathode units for ECP allows saving 1/3 of cathode carbon materials since simple parallelepiped is used (Figure 6) instead of archaic shape in this case.

Economy of steel rolled metal for current jaws (up to 20 %) is also take place due to uniform density of current in the current jaws of long and short cathode units and as a result of elimination of sodium barrier since in this case its function is performed by flat current jaws to cathode units.

In turn, the electrode plants should reduce price for the cathode units since their production is simpli-

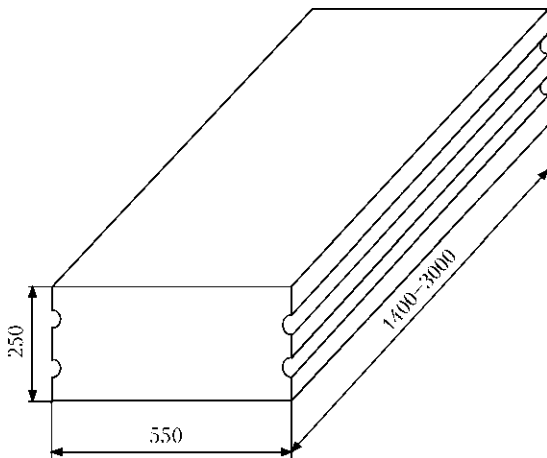


Figure 6. Scheme of typical hearth block of new design



Figure 7. Fragments of two contact assemblies for hearth of aluminum electrolytic cell

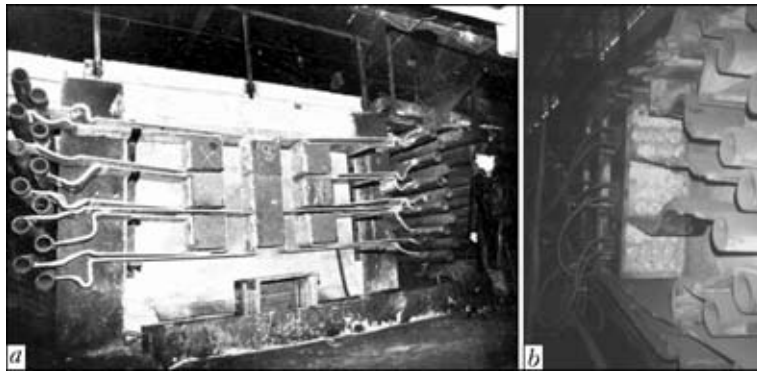


Figure 8. Back ends of graphitization furnaces performed using ECP with free (a) and forced (b) cooling



Figure 9. Contact assembly of furnace for carbide silicon synthesis made with ECP application

fied. There is no necessity in extrusion of units on extremely expensive powerful presses.

There are several examples of ECP application in aluminum (Figure 7) and magnesium electrolytic cells, in Acheson furnaces for graphitization of carbon materials (Figure 8) and synthesis of silicon carbide (Figure 9).

Figure 8 shows a back end of Acheson furnace for 100 kA, in which all electric contacts between metallic current jaws and graphitized electrodes, are welded and copper lead is changed for aluminum one.

Contact assembly with air cooling of 20 kA Acheson furnace for silicon carbide synthesis, also made from aluminum, is shown in Figure 9. Figure 10 shows one of the elements of contact assembly of this furnace prepared for manual erection welding.



Figure 10. Element of contact assembly of Acheson furnace prepared for erection welding

Characteristic of both examples referring to Acheson furnaces is that they are cheaper than the contacts with copper lead on costs for materials and servicing of contacts for the plant.

Therefore, application of solutions described in the paper, found by the specialists of the E.O. Paton Electric Welding Institute, allows the plants of non-ferrous metallurgy, electrode and tool industry saving electricity and improving work environment.

1. Bajmakov, Yu.V. (1944) *Electrolysis in metallurgy*. Vol. 3: Electric energy consumption in production of light metals. Moscow: Metallurgizdat.
2. Lakomsky, V.I., Fridman, M.A. (2004) *Plasma-arc welding of carbon materials with metals*. Kiev: Ekotekhnologiya.
3. Lakomsky, V.I. (1997) *Oxide cathodes of welding arc*. Zaporozhie: Internal.
4. Lakomsky, V.J. (2000) *Oxide cathodes for electric arc*. Harwood Acad. Publ.
5. Holm, R. (1961) *Electric contacts*. Moscow: Inostr. Literatura.

ELECTRON BEAM WELDING OF BODIES OF DRILL BITS WITH MODIFYING OF WELD METAL BY ZIRCONIUM

V.M. NESTERENKOV, A.A. BONDAREV, Yu.A. ARKHANGELSKY and V.I. ZAGORNIKOV
E.O. Paton Electric Welding Institute, NASU, Kiev, Ukraine

The influence of weld metal modifying in EBW of new designs of drill bits was studied. It is known that application of zirconium inserts-modifiers allows preventing cracks in welded joints of 40KhN and 14Kh3MNA steels.

Keywords: electron beam welding, drill bit, zirconium, weld modifying, cracks, microstructure, hardness

It is commonly known that the only effective method for search and exploration of oil and gas fields is a deep drilling. The principal difference of deep drilling for oil and gas from other kinds of drilling consists in depth of wells. The updating equipment and technology for deep drilling, sufficient increase of efficiency of drill bits and decrease of their cost price are the tasks put before many leading companies-manufacturers of drilling equipment. In the complex structure of drilling system the bits are the component on which efficiency of the whole drilling process greatly depends. Therefore much attention is paid both to modernization of existing designs of bits and also to the development of new ones. The result of this work is the increase of average drifting for one modern bit by 122 % as compared to the similar value for bits of design of 1984.

As far as drill bits are operated under very rigid conditions, the selection of steels for their manufacture should be strictly differentiated for each single element of a bit, i.e. from bodies of slide rolling and materials of bearings to bodies of legs and bits.

The steel used for manufacturing of a bit leg should provide high strength and ductility combined with a good wear resistance. Many leading companies-manufacturers of drill bits abroad use steel AISI 4815H (analogue of the steel 15Kh3MA) or AISI 9315H (analogue of the steel 19KhGNMA) to manufacture legs.

At the same time, for new designs of drill bits the manufacture of their body part is planned of steel 40KhN (Figure 1), and joining with the steel 14Kh3MNA of nipple part should be performed by a

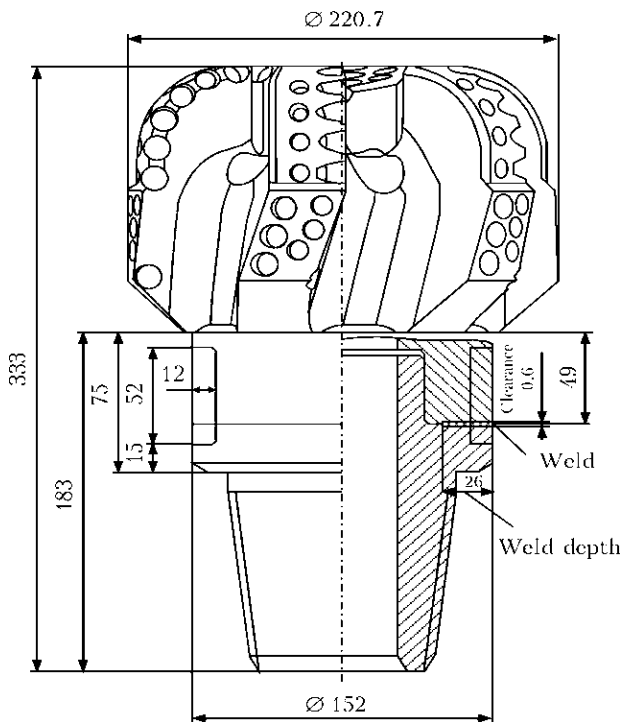


Figure 1. Scheme of general view of bit manufactured of steels 40KhN and 14Kh3MNA

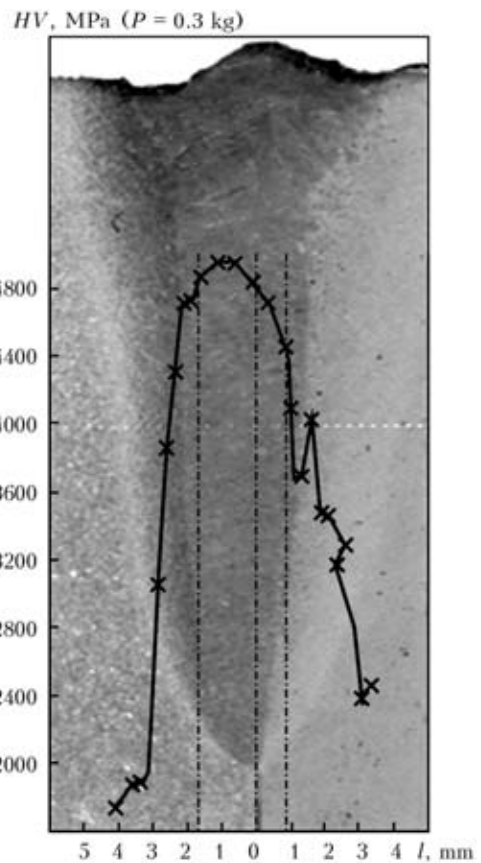


Figure 2. Cross section and distribution of microhardness in welded joint of steels 40KhN and 14Kh3MNA

circular weld. Selection of steel 40KhN is predetermined by need in increase of structural strength of a bit to increase speed of drilling. From the practice of arc welding of steels with increased carbon content the tendency of their welded joints towards crack formation is well known. The steels of the type 40KhN have tendency to reversible temper brittleness [1]. The prevention of cracks in arc welding of these steels is achieved by preliminary and postweld heat treatment which allows increasing ductility of welded joints. For the same purpose the welding methods of steel 40KhN with high concentration of energy are more challenging which provides less weakening of welds.

It is known that frequency of rotation of bits is a key factor in achieving the high speeds of drilling. At the modern market the bits demonstrating reliable operation at the frequency of rotation of up to 500 rpm and more are already available. The production of these bits should provide minimal design deviations

in geometry of ready-made products from the drawings. Applying arc welding during joining of composite parts of a bit into single one, the residual deformations result in deviations of sizes which does not allow using them at high frequency of rotation. Thus, this problem also urgently requires highly concentrated sources of heating in welding production of drill bits.

The purpose of this work was the investigation of weldability of steels 40KhN and 14Kh3MNA and development of principal technology for EBW in production of new designs of drill bits.

The nature of brittle fracture of welded joint is predetermined by effect of two main factors: heat and load influence of welding. The local fracture affects base metal in direct vicinity of a weld, at the distance of one or several grains from it, i.e. in those places where steel was overheated to the temperatures exceeding 1200–1300 °C. To minimize overheat, i.e. to decrease the time of duration of area of near-weld zone

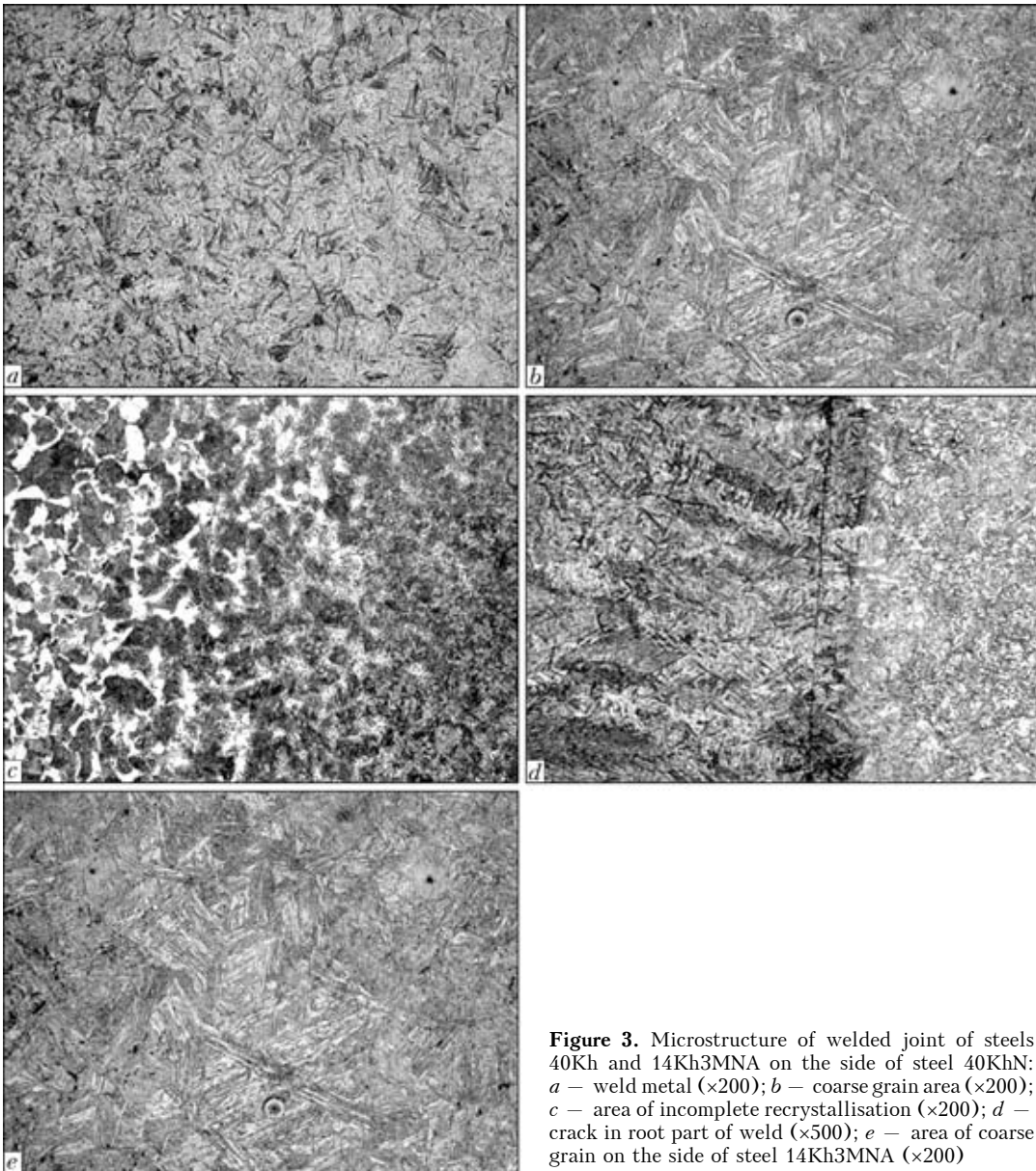


Figure 3. Microstructure of welded joint of steels 40Kh and 14Kh3MNA on the side of steel 40KhN: *a* – weld metal ($\times 200$); *b* – coarse grain area ($\times 200$); *c* – area of incomplete recrystallisation ($\times 200$); *d* – crack in root part of weld ($\times 500$); *e* – area of coarse grain on the side of steel 14Kh3MNA ($\times 200$)

adjacent to the weld at the temperatures of more than 1200–1300 °C, such concentrated heat source as electron beam is required.

The investigations carried out earlier [2] clearly showed that application of EBW allows sharp reducing of overheat in near-weld zone, delaying growth of austenite grains, preventing propagation of macrocracks from one areas of welded joint to other due to «tempering» of defects of physical character (dislocations, secondary boundaries) and eliminating possibility of their ordering into the boundary. Taking this into consideration, one can expect positive results as for quality of welded joints of dissimilar steels, one of which is 40KhN.

The principal technology of EBW was practiced on the flat models of welded joints of steels 40KhN and 14Kh3MNA of 30 mm thickness. Depending on the sizes of bits the required penetration depth should be 15–26 mm. The optimal shape of a weld is characterized by practically parallel walls with small convergence to the root in combination with a design penetration depth (Figure 2). It was provided by a certain heat input of welding which, for example, was 970 kJ/m for 16 mm depth. Directly before EBW

the cleaning of a butt using electron beam was performed under the following conditions: speed of movement of electron beam $v = 6$ mm/s, welding current $I_w = 12$ mA, current of focusing lense $I_f = 563$ mA, circular scan of a beam $A = 10$ mm diameter. After welding and mechanical cutting of welds the structures of welded joints were investigated. The microstructure of weld metal is martensite one. It is characterized by ageing with acicular orientation at 60° angle. The hardness is rather high, i.e. of HV0.1-4810–5050 MPa (Figure 3, a).

The microstructure of base 40KhN metal is ferrite-pearlite with not high hardness HV0.1-1680–2180 MPa. The fusion line on the side of 40KhN is distinct, cracks and other defects along the fusion line are not observed. In the zone of overheat (on the area of coarse grain) the martensite structure with hardness HV0.1-4810 MPa (Figure 3, b) is observed. The microstructure of fine grain area is also martensite with somewhat lower hardness than that of coarse grain area — HV0.1-4410 MPa. In the area of partial recrystallisation (Figure 3, c) ferrite and pearlite are observed in the structure. Hardness drops smoothly with increase of ferrite and pearlite content in structure.

The width of HAZ on the side of 40KhN is from 0.3 mm in the root part up to 2 mm in the upper part of a weld. In a number of cases the cracks were observed in welded joints (Figure 3, d).

In the coarse grain area on the side of the steel 14Kh3MNA the structure of mostly lower bainite is observed which preserved orientation at the angle of 60° (Figure 3, e). The hardness of this structure is lower than martensite one and is HV0.1-3790–4180 MPa. At some distance from the fusion line the areas of ferrite component appear in the structure and the hardness respectively falls down to HV0.1-2470 MPa. The width of HAZ on the side of steel 14Kh3MNA is somewhat wider than HAZ on the side of 40KhN and amounts 0.5 mm in the root part, and in the upper part of a weld it is up to 3 mm.

Lamellar-acicular structure of welded joint of steels being investigated with large drop of hardness predetermines low ductility of joints with formation of cracks in them. To transform lamellar-acicular structure and improve strength properties of joints, the weld modification was applied using inserts to the butt in a form of a foil 0.1–0.2 mm thick of steel Kh18N9T, titanium and zirconium. The efficiency of this method was proved earlier in the development of technology of EBW of large-size drill bits.

In this case the best results from the point of view of preventing cracks formation in welded joints were obtained using inserts of zirconium. Inserts in a shape of rectangles of foil 4 × 10 mm in size and 0.1 mm thick were located along the whole length of a butt with a 30 mm gap. The conditions of EBW were preserved the same as in welding of butts without inserts.

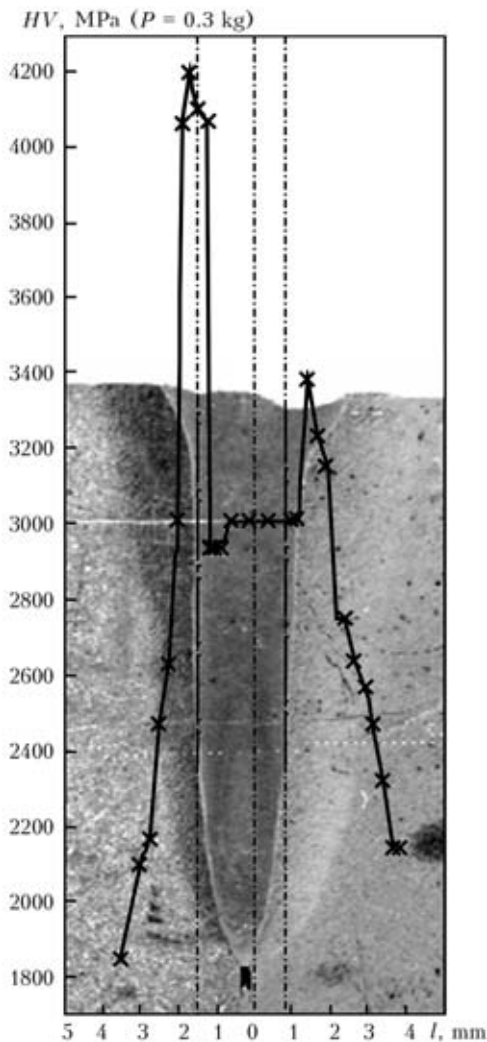


Figure 4. Cross section and distribution of hardness in welded joint of steels 40KhN and 14Kh3MNA in modifying using zirconium

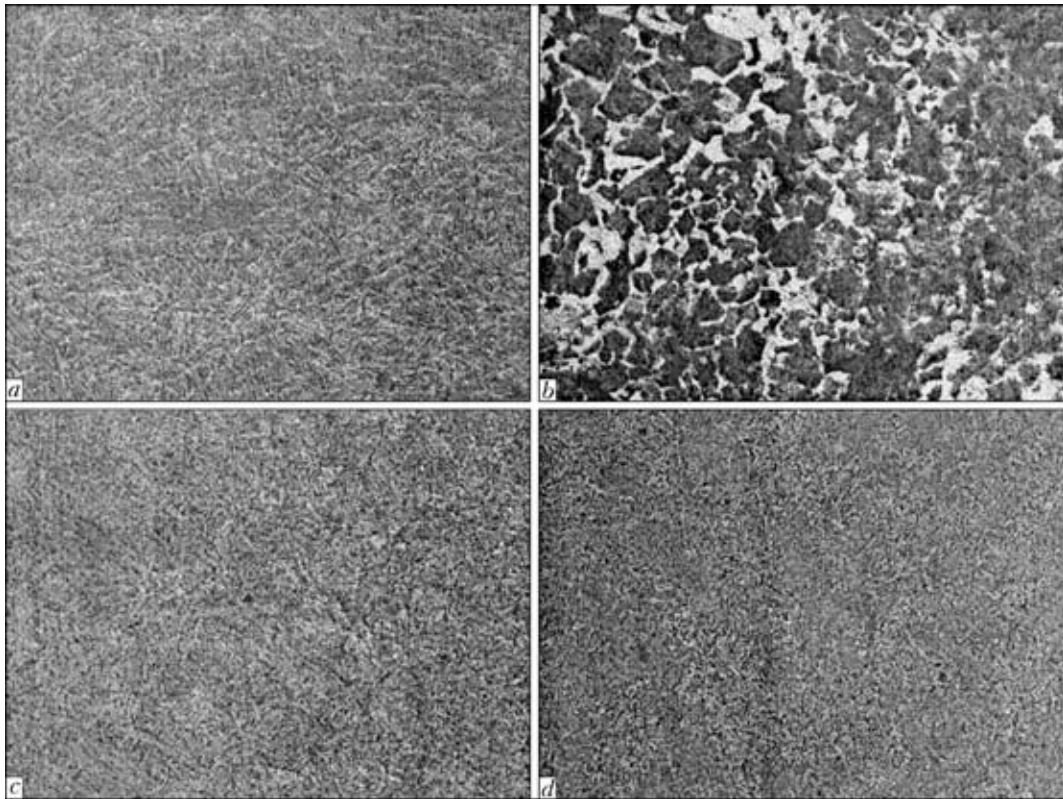


Figure 5. Microstructures of welded joint of steels 40Kh and 14Kh3MNA with insert of zirconium: *a* – weld metal ($\times 200$); *b* – area of large grain ($\times 200$); *c* – area of incomplete recrystallisation ($\times 200$); *d* – coarse grain area on the side of steel 14Kh3MNA ($\times 200$)

The adding of zirconium into weld metal facilitates the formation of hard-to-dissolve carbides in austenite. Their influence on the properties of joints is revealed in a form of refining grains, decreasing threshold of cold-shortness and decrease of sensibility to stress concentrators [4].

The distribution of hardness on the transverse sections shows its decrease in average by $HV0.1-800$ MPa (Figure 4) which evidence the producing the more ductile welded joints.

The microstructure of a weld with insert of zirconium is bainite-martensite with hardness $HV0.1-4410-4570$ MPa (Figure 5, *a*). At coarse and fine grain area the microstructure on the side of steel 40KhN represents classical fine acicular martensite with hardness of up to $HV0.1-4800$ MPa (Figure 5, *b*). At the area of partial recrystallisation the areas of ferrite and pearlite structure (Figure 5, *c*) appear

which decreases hardness down to $HV0.1-2320$ MPa. At the area of coarse grain on the side of 14Kh3MNA the microstructure is composed of mixture of upper and lower bainite with hardness of $HV0.1-3750$ MPa (Figure 5, *d*). The cracks in welded joints are not observed.

Thus, weld metal modifying using zirconium in EBW of steels 40KhN and 14Kh3MNA in designs of new types of drilling bits provides formation of welded joints without cracks.

1. Keloglu, Yu.P., Zakharevich, K.M., Kartashevskaya, M.I. (1977) *Metals and alloys*. Kishinyov: Kartya Moldavenyashke.
2. Grabin, V.F., Denisenko, A.V. (1978) *Metals science of welding of low- and med-alloy steels*. Kiev: Naukova Dumka.
3. Nesterenkov, V.M., Protosej, N.E., Arkhangelsky, Yu.A. (2009) Technological features of electron beam welding of drill bits. *The Paton Welding J.*, **5**, 8-14.
4. Hrivnak, I. (1984) *Weldability of steels*. Ed. by E.L. Makarov. Moscow: Mashinostroenie.

FLUX-CORED WIRES OF FMI SERIES FOR COATING DEPOSITION BY ELECTRIC ARC SPRAYING (Review)

V.I. POKHMURSKY¹, M.M. STUDENT¹, V.M. GVOZDETSKY¹ and A.V. POKHMURSKAYA²

¹H.V. Karpenko Physico-Mechanical Institute, NASU, Lvov, Ukraine

²Institute of Materials Science, Chemnitz University of Technology, Chemnitz, Germany

The paper gives a brief review of flux-cored wires developed by the H.V. Karpenko Physico-Mechanical Institute of the NAS of Ukraine for electric arc spraying. It is shown that development and utilisation of special flux-cored wires as electrode materials widened the application fields for electric arc metallising and allowed, in many cases, deposition of coatings with properties at a level of the best plasma and other thermal spraying ones at lower costs.

Keywords: *electric arc metallization, coating deposition by spraying, flux-cored wire, repair of worn surfaces, coating structure, properties*

Electric arc metallization is one of the thermal processes of coating deposition. In terms of technology it is the simplest and most efficient method, not requiring any expensive equipment, which is readily introduced into production. One of the essential disadvantages of this process is a limited range of applied consumables, namely solid wires. Therefore, application of flux-cored wires as electrode materials for coating deposition by electric-arc spraying allowed a broad variation of coating composition, dramatic expansion of their applications, and in many cases also producing coatings with the properties on the level of the best plasma and supersonic thermal coatings, but at 5 to 10 times lower cost. At present flux-cored wires for electric arc spraying are batch-produced both abroad (Metco, Castolin, TAFA, Nanosteel), and in Ukraine. The greatest contribution into development and intro-

duction of electric-arc coatings from flux-cored wires was made by the specialists of the E.O. Paton Electric Welding Institute (PWI) [1–8], H.V. Karpenko Physico-Mechanical Institute (FMI) [9–25], and Priazovsky State Technical University [26]. Coatings deposited with flux-cored wires are used in many fields of technology for reconditioning and protection from abrasive and gas-abrasive wear at room and elevated temperatures right up to 700 °C, for repair of various parts of machines and units operating under the conditions of boundary friction.

FMI developed flux-cored wires of 1.8 mm diameter for electric-arc metallization (Table), pilot-production batches of which were manufactured at PWI. Results of investigations devoted to flux-cored wire development, studying structure formation and service properties of various-purpose electric-arc coatings are set forth in [1–10, 26], and developed flux-cored wire compositions are protected by patents of Ukraine [21–25].

Flux-cored wires and their purpose

Wire grade	Alloying system	HRC, HV, σ_t , σ_{coh}	Applications
FMI-2	Kh6Yu8R3	HRC 40 HV 650 $\sigma_t = 130$ MPa $\sigma_{coh} = 40$ MPa	Reconditioning of medium-loaded crankshafts, cam shafts, abrasive wear protection of printing equipment
FMI-5	50Kh6Yu3G2M2S2	HV 350 $\sigma_t = 180$ MPa $\sigma_{coh} = 40$ MPa	Reconditioning of bearing seats of parts
FMI-6	Kh6Yu6R3N4	HRC 40 HV 1000 $\sigma_t = 60$ MPa $\sigma_{coh} = 45$ MPa	Protection from gas corrosion and gas-abrasive wear at high temperatures (up to 700 °C)
FMI-7	70Kh6Yu6R3W4	HRC 40 HV 1150 $\sigma_t = 120$ MPa $\sigma_{coh} = 45$ MPa	Protection from gas corrosion at high temperatures (up to 600 °C)
FMI-8	50Kh6Yu2G2T2M2	HV 500 $\sigma_t = 180$ MPa $\sigma_{coh} = 40$ MPa	Reconditioning of journals of medium-loaded crank shafts, cam shafts

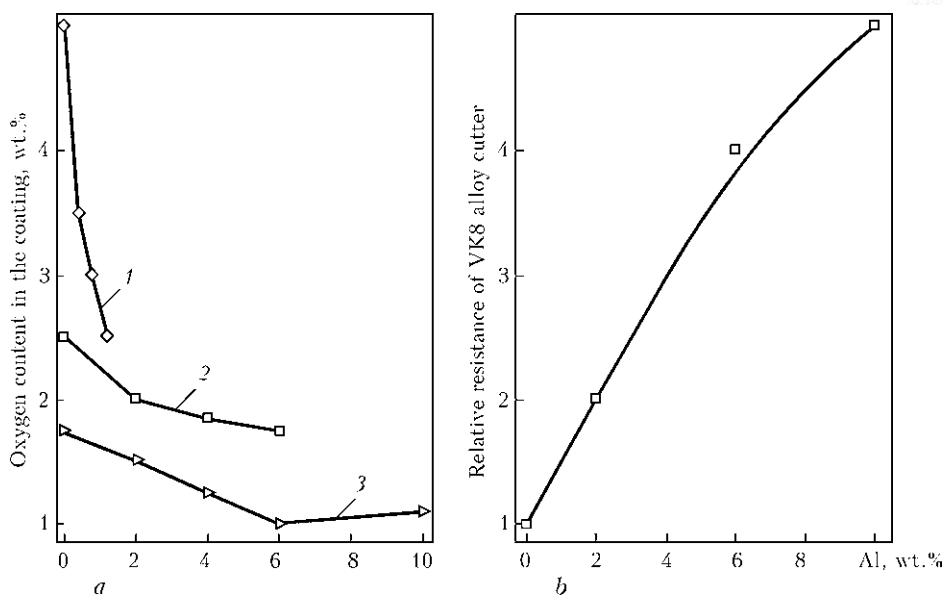


Figure 1. Influence of the quantity of carbon (1), chromium (PP 80Kh (0–6) (2) and aluminium (PP 80Kh6Yu (0–10)) (3) in flux-cored wire charge on the quantity of oxygen in the coatings (a) and relative resistance of the cutter from VK8 alloy (b) at treatment of coatings from PP 80Kh6Yu (0–10 Al) flux-cored wires

Repair coatings are used for repair of worn surfaces of shaft-type parts with subsequent mechanical treatment of coatings predominantly by machining tools. Therefore, the most important feature for such coatings is their high wear resistance and efficiency at machining. These conditions are ensured at formation of coatings with hardness HV 300–400, the structure of which contains a minimum quantity of the oxide phase.

Minimum amount of oxygen in the coatings on the level of 2 wt.% is provided in the presence of 0.8 % C, 6 % Cr and 6 % Al in the flux-cored wire charge (Figure 1).

With increase of aluminium content the quantity of martensite decreases, but ferrite content in the coating rises. Here, coating hardness decreases at simultaneous increase of its adhesion strength. Optimum coating hardness in the range of HV 300–400 is achieved in the presence of 6–12 wt.% Al in the wire. Matrix phase of such coatings is ferrite, alloyed by chromium and aluminium. Flux-cored wires with an increased content of aluminium are applied in power engineering for reconditioning the seats of shafts of electric motor rotors, brake drums of lorries, etc. (Figure 2).

The following requirements are made of coatings applied for parts operating under the conditions of

abrasive wear: high hardness, low level of stresses of the first kind, and high wear resistance. It is established that with increase of coating hardness up to HV 700–800 their wear resistance rises, and above HV 800 it decreases, which is related to initiation of microcracks in the coatings. Coating wear results from growth of the already formed cracks along the lamella boundaries with their subsequent spallation. It is found that high wear resistance of coatings at testing by fixed abrasive is ensured by harder lamels and hard aluminium oxides on lamel boundaries. Therefore, in this case coatings should be formed, first, with a high microheterogeneity, so as to provide in them a low level of tensile stresses, and secondly, with thin lamels (high dispersity of the coating), so as to increase oxide content on interlamellar boundaries. At testing for wear by unfixed abrasive the weak links of the coatings are lamels with the lowest hardness and interlamellar boundaries. In this case, a coating with a low microheterogeneity and maximum thickness of the lamels should be formed, so as to minimize the number of boundaries between the lamels. Coatings of Fe–Cr–B–Al system of FMI grades became widely accepted for protection from abrasive wear in printing industry (Figure 3).

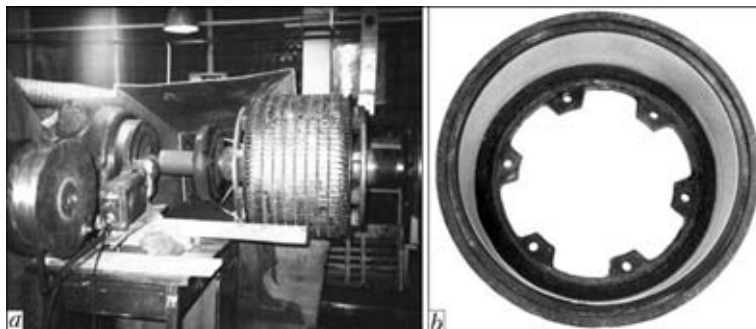


Figure 2. Reconditioning of the shaft of electric motor rotor (a) and lorry brake drum (b)

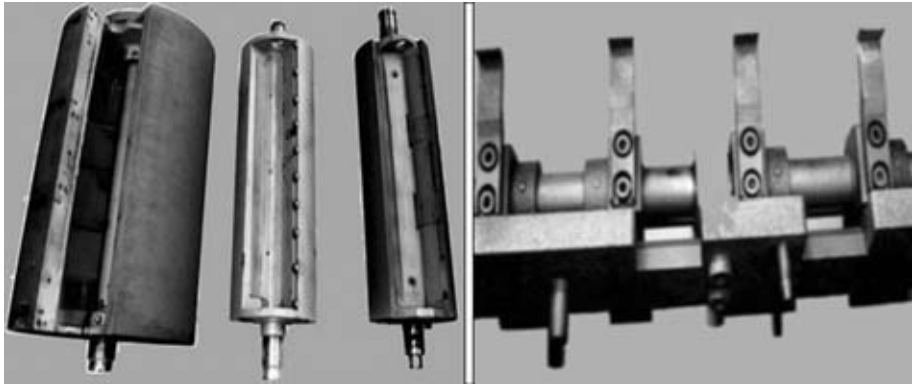


Figure 3. Reconditioned parts of sheet-drawing system of printing machine

Coating hardness for parts operating under the conditions of boundary friction should be not lower than *HV* 600. Machining of such coatings is performed by grinding to the required size. Here the coating structure often develops microcracks, which may lead to coating fracture in operation. To ensure the required coating characteristics, chromium, carbon, boron and aluminium are added to the composition of flux-cored wire charge in such amounts that martensite were the coating matrix phase. Such a structure provides a minimum level of tensile stresses in the coating not higher than 50 MPa.

At specific loads above 14 MPa catastrophic wear of the rider occurs in the coating – rider friction pair. Metallographic, spectral and X-ray structural analyses revealed that this is due to the presence of cracks on the coating ground surface, the open edges of which act as cutters, up to 0.3 μm high protrusions formed by aluminium oxides and carbides. Protrusions from carbides above the ground surface of the coatings form as a result of incomplete dissolution of coarse carbides from the charge in the flux-cored wire melt.

To remove intensive wear of the rider in the friction pair with the coating, methods of coating optimization were proposed, which consist in the following:

- provision of conditions for complete dissolution of carbides in flux-cored wire melt, using for this purpose finer carbide particles in the flux-cored wire charge or application of increased arc voltage (34–38 V) at spraying;
- reduction of air content in flux-cored wire charge by its compaction and addition of powder containing titanium compounds to it, which interacts with oxygen in the vapour phase in the melt zone, forming finer titanium oxides, which are by 1–2 orders of magnitude smaller than Al_2O_3 particles.

The ground surface of the coating, produced from flux-cored wire with an optimized charge composition, does not have any microprotrusions, and its roughness is essentially lower. More over, titanium and magnesium in the composition of flux-cored wire charge promote absorption of 2–3 wt.% N from the air, contained in the charge pores, that leads to formation of titanium nitride particles of 200–500 nm in the coating.

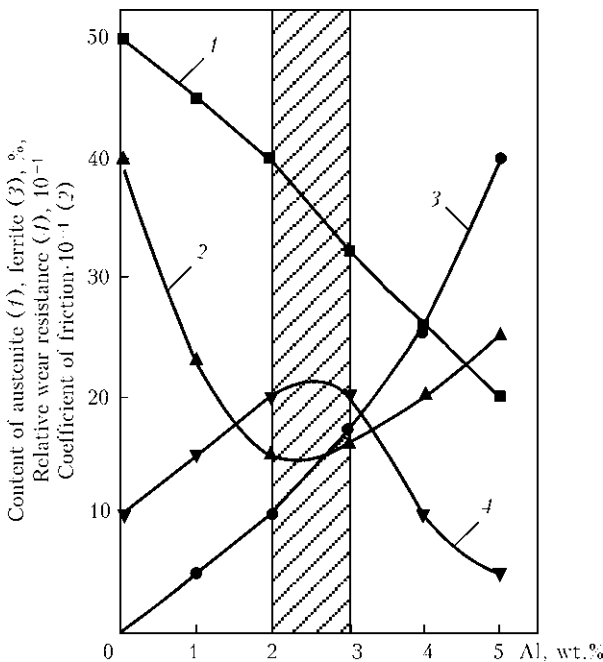


Figure 4. Influence of aluminium content in PP 50Kh6T2M2Yu2 flux-cored wire on tribological characteristics of coatings with a three-phase structure at boundary friction at specific load $P = 7$ MPa

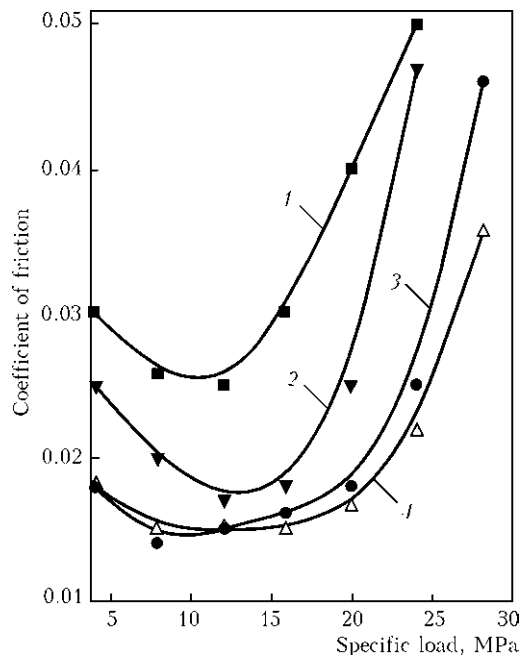


Figure 5. Dependence of coefficient of friction in diesel oil M14V2 on specific load for friction pairs of coating from flux-cored wire – bronze BrS-30: 1 – Kh6Yu6R3; 2 – ShKh15 steel (*HRC* 62); 3 – 50Kh6G2T2M2 + Kh6R3Yu6T2; 4 – 50Kh6T2M2Yu2

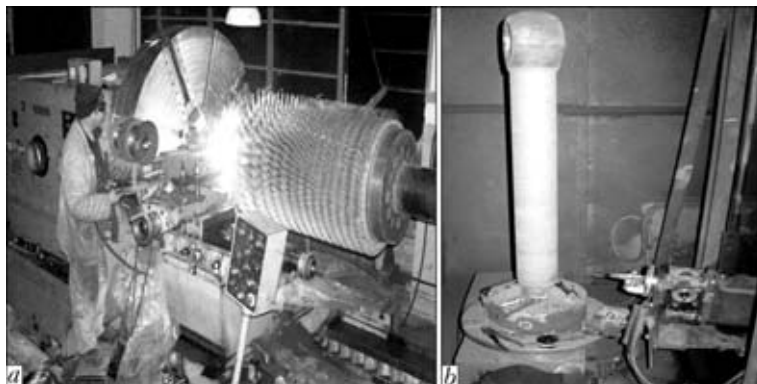


Figure 6. Spray-deposition of coating on supporting journal of turbine shaft (a) and hydraulic cylinder rod (b)

As a result of non-equilibrium of the coating structure and phase composition of coatings at friction, conditions can be in place in them, which are favorable for self-organizing of the surface layer.

Methods of small-angle roentgenography of the coating revealed that optimum conditions for self-organization of the surface develop in a three-phase coating with the matrix phase of martensite (~50%), austenite (~30%) and ferrite (~20%). At high specific loads (Fe, Cr)₂₃C₆ carbides precipitate from austenite, and part of it transforms into tempered martensite with heat absorption.

It is supposed that nanosized graphite particles (10–20 nm) precipitate in ferrite. At friction carbon diffuses to the friction surface and forms a continuous graphite film on it. Optimum ferrite content in the coating structure is equal to 10–20%. Coefficient of friction and wear of the friction pair are minimum (Figures 4 and 5). Such a content of ferrite in the coating is provided in the presence of 2–3 wt.% Al in it.

Wires of FMI series became accepted for reconditioning of support journals of rotors and shafts of compressor turbines for gas pumping in repair enterprises of «Ukrenergoservis», and rods of hydraulic cylinders of shaft equipment (Figure 6).

For coatings from flux-cored wire of Fe–Cr–B–Al system for spray-deposition of coatings operating under the conditions of higher temperatures in the case of gas-abrasive wear, a stable high hardness at long-term operation (several years) at high temperature is important. To ensure a high hardness and high-temperature resistance of coatings, such elements as chromium, boron, aluminium, magnesium, nickel and tungsten, which can initiate dispersion hardening at higher temperature, were added to the composition of flux-cored wire charge. Phase and spectral analyses determined that dispersion hardening of the coatings is provided by precipitation of (FeCr)₂B borides, CrN and AlN nitrides, as well as FeAl₃, Ni₃Al and Fe₇W₆ intermetallics in their structure. At up to 550 °C operating temperature the greatest hardening effect is provided by precipitation of Fe₇W₆ intermetallics, and above 550 °C – precipitation of Ni₃Al.

Coatings from flux-cored wire increase the wear resistance of 12Kh1MF steel by 30 times. Unlike monolithic materials, coatings are prone to both outer from the surface and internal interlamellar oxidation. Oxygen can penetrate along the lamel boundaries and along the microcracks to the steel base and form oxide

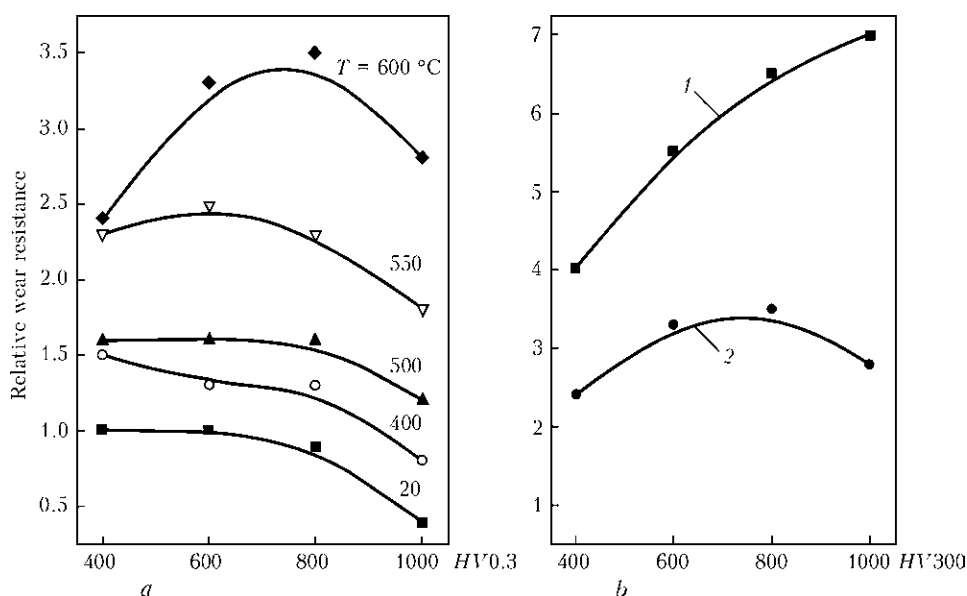


Figure 7. Relative wear resistance of coatings from flux-cored wires of Fe–Cr–B–Al system (filled signs) and reference samples from 12Kh1MF steel at different temperatures (preliminary soaking of samples for 50 h at testing temperature) (a) and relative wear resistance of coatings from the same materials at testing temperature of 600 °C (b) and duration of preliminary soaking of samples for 100 (1) and 50 (2) h

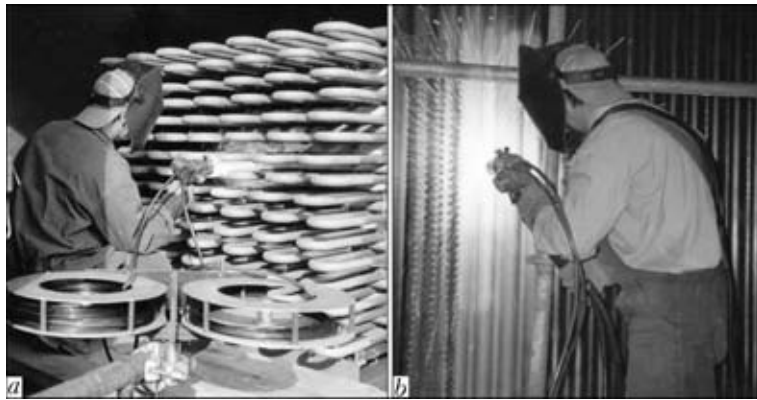


Figure 8. Spray-deposition of coatings from flux-cored wire on economizer pipe (a) and water-wall tubes (b) of TP-100 boiler for protection from gas abrasive wear at higher temperatures

films there. Intensity of gas-abrasive wear depends on coating hardness and level of stresses in them.

At room temperature coating wear resistance decreases with increase of its hardness and becomes lower than hardness of the standard — 12Kh1MF steel. With temperature rise, coating wear resistance increases, and the longer the high-temperature exposure, the higher the coating wear resistance (Figure 7). This is due to stresses of the first kind, forming in the coating. At long-term exposures at 500–600 °C temperatures two opposite processes proceed in the coating. First, disperse phases precipitate in the coating, which results in a rapid reduction of its volume and tensile stresses in it grow, while, at the same time, internal oxidation takes place in the coating and its volume increases, whereas tensile stresses decrease. As a result, at the exposure of about 1000 h, tensile stresses in the coatings are replaced by compressive stresses.

Coatings, in the structure of which dispersion hardening occurs, are applied for TPS boiler heating elements for protection from gas-abrasive wear (Figure 8).

Thus, flux-cored wires developed by H.V. Karpenko Physico-Mechanical Institute of NASU can become accepted for electric arc spraying for various purposes.

1. Borisov, Yu.S., Korzhik, V.N. (1995) Amorphous thermal coatings: theory and practice. *Avtomatich. Svarka*, **4**, 3–12.
2. Borisova, A.L., Mits, I.V., Kajda, T.V. et al. (1991) Structure and properties of electric arc coatings on the base of ferrobore produced using flux-cored wires. *Ibid.*, **9**, 66–68.
3. Borisova, A.L., Klejman, A.Sh., Andrejchuk, V.K. et al. (1989) Effect of technological parameters of electric arc metallizing on cohesive strength and structure of coatings using flux-cored wires on the base of FeCr + Al. In: *Abstr. of 10th All-Union Conf. on Theory and Practice of Thermal Spraying of Coatings*, Vol. 2.
4. Borisova, A.L., Klejman, A.Sh. (1990) Effect of rare-earth metals and calcium on structure and physico-mechanical properties of electrometallized coatings deposited with flux-cored wires with ferrobore filler. In: *Strength of parts of agricultural machinery*. Kishinev: KSKhI.
5. Borisov, Yu.S., Koziakov, I.A., Korzhik, V.N. (1996) Structure and properties of thermal coatings produced using flux-cored wires of Fe–Cr–B, Fe–Cr–B–C system. *Avtomatich. Svarka*, **5**, 21–24.
6. Borisov, Yu.S., Borisova, A.L., Koziakov, I.A. et al. (1996) Influence of spraying conditions on structure of coatings produced with flux-cored wire Amotek 101. *Ibid.*, **1**, 21–30.
7. Koziakov, I.A., Korzhik, V.N., Borisov, Yu.S. (1996) Resistance of amorphized thermal coatings deposited with Fe–B system flux-cored wires under the conditions of gas-abrasive wear. *Ibid.*, **9**, 27–29.
8. Koziakov, I.A., Korzhik, V.N., Borisov, Yu.S. (1996) Tribological characteristics of amorphized thermal coatings sprayed with flux-cored wires of Fe–B system. *Ibid.*, **10**, 24–28.
9. Pokhmursky, V.I., Student, M.M., Dovgunyk, V.M. et al. (2005) *Electric arc restoration and protective coatings*. Lviv: FMI.

10. Pokhmursky, V.I., Student, M.M., Dovgunyk, V.M. et al. (1999) Application of electric-arc metallizing with flux-cored wire of Fe–Cr–Al system. *Mashynoznavstvo*, **1**, 13–18.
11. Sydorak, I.J., Student, M.M., Dovgunyk, V.M. et al. (2000) Influence of abrasive-spray treatment on adhesion of anticorrosion and repair electric-arc metallized coatings. *Fiz.-Khimich. Mekhanika Materialiv*, **1**, 458–460.
12. Student, M.M., Dovgunyk, V.M., Sydorak, I.J. et al. (2000) Effect of friction on phase transformations in surface layers of thermal coating FeCrB + Al. *Ibid.*, **36**(4), 109–111.
13. Dovgunyk, V.M., Student, M.M., Sydorak, I.J. et al. (2000) Effect of friction on structural-phase transformations in sub-surface layer of FeCrB + Al + C thermal coating. *Ibid.*, **5**, 113–116.
14. Pokhmurska, A., Student, M., Bielanska, E. et al. (2002) Tribological properties of arc sprayed coatings obtained from FeCrB and FeCr based powder wires. *Surface & Coating Techn.*, **151/152**, 490–494.
15. Pokhmursky, V.I., Student, M.M., Dovgunyk, V.M. et al. (2002) Flux-cored wires of FeCrB + Al and FeCr + Al + C systems for electric arc metallizing. *The Paton Welding J.*, **3**, 28–31.
16. Pokhmursky, V.I., Student, M.M., Sydorak, I.I. et al. (2003) Structure and tribotechnical characteristics of coatings produced by electric arc metallizing using flux-cored wires. *Ibid.*, **8**, 12–16.
17. Pokhmursky, V.I., Student, M.M., Ryabtsev, I.A. et al. (2006) Influence of electric-arc metallizing modes and compositions of applied flux-cored wires on structure and abrasive wear resistance of coatings. *Ibid.*, **7**, 26–30.
18. Pokhmurskii, V., Dovgunyk, V., Student, M. et al. (2008) Triboelektroche miczne vlasivnosti powlok natryskiwanich lukowo na stopy aluminium. *Inzynieria Powierzchni*, **1**, 9–13.
19. Student, M., Dzyoba, Yu., Gvozdetsky, V. et al. (2008) High-temperature corrosion of electric arc coatings of flux-cored wires on the base of Fe–Cr–B–Al system. *Fiz.-Khimich. Mekhanika Materialiv*, **5**, 93–97.
20. Pokhmursky, V.I., Student, M.M., Dzyoba, Yu.V. et al. *Flux-cored wire for producing wear-resistant electric arc coatings*. Pat. 40722 Ukraine. Int. Cl. C23C 4/00, B22F 7/00, B32B 15/00. Filed 03.11.2008. Publ. 27.04.2009.
21. Student, M.M., Pokhmurska, G.V., Sirak, Ya.Ya. et al. *Flux-cored wire for producing wear-resistant electric arc coatings*. Pat. 40723 Ukraine. Int. Cl. C23C 4/00, B22F 7/00, B23B 15/00. Filed 03.11.2008. Publ. 27.04.2009.
22. Pokhmursky, V.I., Romaniv, M.S., Student, M.M. et al. *Flux-cored wire for producing of electric-arc coatings dispersion-hardened due to elevated temperatures*. Pat. 47456 Ukraine. Int. Cl. C23C 6/00. Filed 01.06.2009. Publ. 10.02.2010.
23. Markovych, S.I., Pokhmursky, V.I., Mazhejko, O.J. et al. *Method of producing of composite coatings*. Pat. 19967 Ukraine. Int. Cl. C 23 C 4/00. Filed 16.05.2006. Publ. 15.01.2007.
24. Pokhmursky, V.I., Pokhmurska, G.V., Student, M.M. et al. *Flux-cored wire for producing of composite thermal coatings*. Pat. 20013 Ukraine. Int. Cl. C23C 4/04, C3C 4/12. Filed 05.06.2007. Publ. 15.01.2007.
25. Pokhmursky, V.I., Student, M.M., Dzyoba, Yu.V. et al. *Flux-cored wire for producing wear-resistant electric arc coatings*. Pat. 40721 Ukraine. Int. Cl. C23C 4/00, B22F 7/00, B23B 15/00. Filed 03.11.2008. Publ. 27.04.2009.
26. Royanov, V.A. (1990) *Theoretical principles of development and industrial application of sparsely-alloyed flux-cored wires for electric-arc spraying of wear-resistant coatings with improved service properties*: Syn. of Thesis for Dr. of Techn. Sci. Degree. Minsk.



DEVELOPMENT OF VERSATILE TRANSPORT SHIPS AND OCEAN ENGINEERING FACILITIES

S.S. RYZHKOV¹, V.S. BLINTSOV¹, G.V. EGOROV², Yu.D. ZHUKOV³, V.F. KVASNITSKY¹, K.V. KOSHKIN¹, I.V. KRIVTSUN⁴, V.A. NEKRASOV¹, V.V. SEVRYUKOV⁵ and Yu.V. SOLONICHENKO⁶

¹Admiral S.O. Makarov National Shipbuilding University, Nikolaev, Ukraine

²«Marine Engineering Bureau» Ltd., Odessa, Ukraine

³«Aker Yards Design Ukraine» Ltd., Nikolaev, Ukraine

⁴E.O. Paton Electric Welding Institute, NASU, Kiev, Ukraine

⁵Classification Society «The Shipping Register of Ukraine», Kiev, Ukraine

⁶OJSC «Vadan Yards Ocean», Nikolaev, Ukraine

The paper presents a cycle of integrated works performed by scientists and specialists from a number of organisations and aimed at designing of competitive ships and providing of Ukrainian shipyards with the advanced technologies for their construction.

Keywords: welded structures, shipbuilding, transport ships, ocean engineering facilities, projects, advanced welding technologies

Shipbuilding of Ukraine is functioning under conditions of a shortage of innovation financial support. Profitability of enterprises in a competitive environment can be achieved due to a high level of practicability and productivity of the applied technical facilities, providing the required quality of products. Therefore, investment attractiveness of the domestic shipbuilding can be ensured through comprehensive development of the designing methods and technologies, as well as dramatic reduction of the terms of construction of ships.

The present work nominated by the Admiral S.O. Makarov National Shipbuilding University for the 2011 State Prize in Science and Technology was dedicated to addressing this complex national scientific-and-technical problem.

Participating in the work were specialists of the Admiral S.O. Makarov National Shipbuilding University (Nikolaev), companies «Marine Engineering Bureau» (Odessa) and «Aker Yards Design Ukraine» (Nikolaev), E.O. Paton Electric Welding Institute (Kiev), Classification Society «The Shipping Register of Ukraine» (Kiev) and OJSC «Vadan Yards Ocean» (Nikolaev).

The efforts of the team were focused on two areas — development of projects of the efficient and reliable competitive ships, and development of the advanced technologies and arrangement of construction of the ships at the Ukrainian shipyards. Research in the field of development, design, technological preparation and production technology, management

of construction of ships and marine engineering facilities resulted in finding of a solution to the complex scientific-and-technical problem of building of the high-efficiency versatile transport ships and ocean engineering facilities for the transportation industry, exploration and extraction of sea resources of Ukraine.

The main results of the work* are as follows:

- development of scientific principles of modern marine engineering and their implementation on a base of integrated approach to development, design and construction of ships, as well as building of the project platforms providing direct communication with databases of different shipyards and on-line solving of issues related to development, design, construction and fitting-out of ships with these shipyards;
- working out and implementation of a new development and design methodology based on the theories elaborated by the authors for ensuring technical sta-

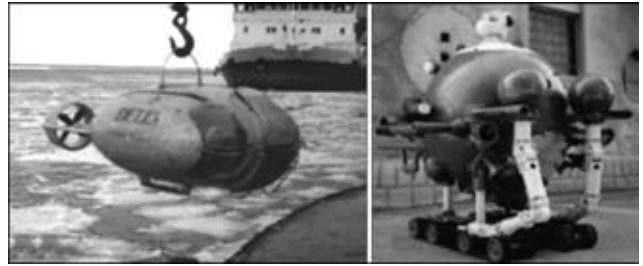


Ship «Ukrainets» of project 005RSD03

* Ryzhkov, S.S., Blintsov, V.S., Egorov, G.V. et al. (2011) Development of versatile transport ships and ocean engineering facilities. Mykolaiv: Adm. S.O. Makarov NShU. — 340 pp.



Train-ferry of project 002CA01



Appearances of underwater vehicles Delta and MTK-200

bility, reliability and efficiency of the ships, evaluation of their price and maritime safety characteristics, including further application of the programs aimed at supporting stages of lifetimes of the ships by using CALS technologies and PLM solutions;

- elaboration of theoretical fundamentals of designing, manufacturing and application of high-efficiency ocean engineering facilities for exploration and development of the sea shelf, monitoring of the technical state of off-shore and port engineering structures, and estimation of the level of safety of waterways;

- development and mastering of advanced metal-working and assembly-welding technologies and equipment for construction of ships, which will provide their competitiveness in the world market, and, in particular, application of the methods of air-plasma cutting with an addition of water to the plasma and underwater plasma cutting of metal, assembly and welding of large-size sections without the use of beds, mechanised and automatic flux-cored and solid wire welding in a mixture of gases using ceramic backings for the back weld formation, hybrid laser-arc and laser-plasma welding and materials treatment technologies, theoretical principles and technologies for upgrading of equipment, and thermal cutting machines in particular, manufacture of laser-arc and laser-plasma equipment, quasi-resonant-mode power supplies, and specialised equipment for metal treatment in hard-facing of marine shafts;

- elaboration of theoretical bases and development of mechanisms and devices for ensuring a high level of environmental safety in construction and operation of ships, and human life protection on and off shore;

- formation of a base of national standards on classification and building of practically all types of ships (from small coastal and river service to sea-going ships);

- development of computerised integrated plants and their application in the Ukrainian shipbuilding industry, and, in particular, development of methods and new software for optimisation management of domestic shipyards, i.e. management of operations on timely deliveries of materials and equipment from domestic and foreign manufacturers, sequences of operations on assembly and welding of sections, units and ship as a whole, this providing elimination of long-lasting building activities as a main obstacle in a way to entering the world market.

This integrated solution of the critical national problem has allowed 130 ships to be designed and constructed at the Ukrainian and foreign shipyards since 2002. 10 ships are now fitted out, and 24 ships are at building berths.

Since 2002 and up to now the «Ocean» (Kherson), Kiliysky and «Yuzhny Sevastopol» shipyards have built a series of ships by orders of Damen Shipyards Hoogezand and other Dutch companies, Briese Schif-fahr (Germany), STX Norway Offshore AS and other Norwegian companies, STX Pan Ocean (Korea), some Ukrainian companies, such as Joint Stock Shipping Company «Ukrrechflot», «Black Sea Shipping Management Co. Ltd.», «NIBULON Ltd.», State Enterprise «Ukrvodshlyakh» etc., as well as 10 Russian companies.

The world level of the works performed is confirmed by their acknowledgement by foreign companies. Versatile transport ships of projects 006RSD05, RSD17 and RSD19 have been included by RINA, the Royal Institution of Naval Architects, on the list of «Significant Ships». As recognized by UNESCO, owing to the ocean engineering facilities built, Ukraine has ranked on a par with the countries — world leaders in the field of high underwater technologies.

FOUNDATION OF THE E.O. PATON CHINESE-UKRAINIAN WELDING INSTITUTE

To widen and increase efficiency of international scientific-and-technical cooperation, the E.O. Paton Electric Welding Institute of the NAS of Ukraine (PWI) acted as a founder of the E.O. Paton Chinese-Ukrainian Welding Institute (CUWI). Foundation of the Institute was supported by the Ministry of Science and Technology of the People's Republic of China, National Academy of Sciences of Ukraine and State Agency on Science, Innovations and Information of Ukraine.

The goal of CUWI is to perform collaborative R&D in order to develop advanced welding and related technologies and equipment on the basis of the innovation scientific-and-technical achievements of PWI, apply them at industrial enterprises of China, and arrange joint production ventures.

Participants in foundation of CUWI from the Chinese side were the Guangdong General Research Institute of Industrial Technology and Guangdong Provincial Department of Science and Technology. The corresponding agreement between them and PWI was signed on 24 February 2011. Foundation of CUWI was validated by the documents officially registered at the State authorities of China. The Institute was named after E.O. Paton – founder of the Electric Welding Institute in Ukraine.

At present, arrangement and activities of the E.O. Paton CUWI are at a level of intergovernmental relations between Ukraine and the People's Republic of China. Thus, within the framework of the visit to Ukraine by Chinese President Hu Jintao on 8–20 July 2011, foundation of the joint Institute became one of the results of development of the strategic partnership relations between Ukraine and China.

It is planned that activities of CUWI will lie in the following areas:

- modern welding equipment;
- advanced welding consumables;
- mechanised and automatic welding technologies;
- advanced technologies for surface engineering (coating) and materials treatment;
- repair welding technologies;
- fundamental research in the field of metallurgy of arc welding and special electrometallurgy, strength and extension of service life of welded structures, and mathematical modelling of welding and related processes;
- materials and technologies for soldering and brazing;
- instruments and equipment for welding in medicine;



Ceremonial signing of the Agreement on foundation of the E.O. Paton Chinese-Ukrainian Welding Institute: *at the centre* – Prof. B.E. Paton, Director of the E.O. Paton Electric Welding Institute of the NAS of Ukraine; *to the right* – Mr. Gong Guo Ping, Deputy Director General of the Guangdong Provincial Department of Science and Technology; *to the left* – Prof. Qiu Xianyang, President of the Guangdong General Research Institute of Industrial Technology

- electric arc and plasma technologies and equipment for processing of materials and environmentally clean recycling of wastes, including with production of alternative raw material resources and power supplies;

- methods for non-destructive testing and technical diagnostics, foundation of a centre for non-destructive testing of welded joints and certification of welding technologies;

- technological auditing of welding production and scientific-and-technical supervision of fabrication of welded structures;

- training of personnel and scientific-and-technical staff.

Geographically, CUWI is situated in Guangzhou, on a base of the Guangdong General Research Institute



Main administration building of the Guangdong General Research Institute of Industrial Technology

of Industrial Technology. To fulfil the above tasks, this Institute provides office, laboratory and production facilities, as well as ground areas.

Commitments of the participants within the specified activities of the joint Institute are distributed as follows:

- the Chinese side will provide financing of the activities of CUWI, including procurement of research and technological equipment, payment of salaries to the personnel and other costs, and will promote application of the joint scientific-and-technical developments at industrial enterprises of China and other countries;

- the Ukrainian side will form the program of the activities of CUWI, participate in developments under the joint projects, and delegate specialists and experts to perform the above scientific-and-technical projects.

The main areas of the activities of CUWI will be determined by the CUWI Board consisting of ten people. The honorary chairmen of the Board are Prof. B.E. Paton, President of the National Academy

of Sciences of Ukraine, representing the Ukrainian side, and Mr. Cao Jian-lin, Vice-Minister of the Ministry of Science and Technology of the People's Republic of China, representing the Chinese side. Current activities of the joint Institute are run by the Board of Directors. Director from the Ukrainian side is Dr. V.N. Korzhik, Head of the Department of thermal-electric processes for materials treatment, and Director from the Chinese side is Prof. Yang Yongqiang, Acting President of the Guangdong General Research Institute of Industrial Technology.

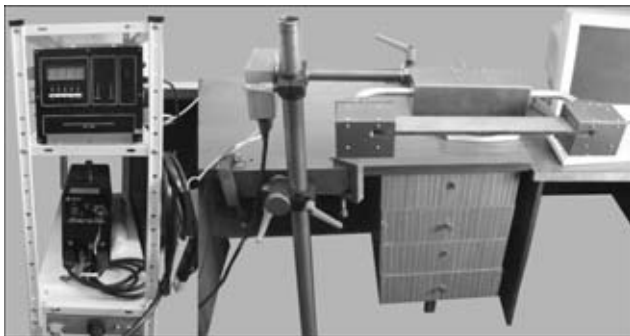
At present, the E.O. Paton Chinese-Ukrainian Welding Institute has started working on the first collaborative projects in the field of development of new technologies and equipment for welding and surfacing of large-size power engineering structures, development and production of new welding consumables (flux-cored wires and powders), flash butt welding, and new plasma and laser technologies.

Prof. V.N. Korzhik

NEWS

WELDER'S TRAINER

E.O. Paton Electric Welding Institute developed a trainer, which is used to perform training on the real processes of coated electrode manual arc (MMA) welding and inert-gas nonconsumable electrode manual arc (TIG) welding with filler wire feed and without it, as well as monitoring and documenting the



main welding mode parameters on optical, magnetic and paper carriers.

Welder's trainer TSDS-06M is designed for application as technical means of teaching, training, qualification improvement, testing, admission check and certification of arc welding operators.

TSDS-06M trainer consists of:

- manipulator-positioner, which is designed for fixing the welded sample and its placing in different positions – downhand, vertical, overhead, inclined, horizontal on a vertical plane;
- technological interface module providing on-line control, recording and processing of data of the measured main parameters of arc welding process;
- DC inverter type welding arc power source;
- welding tool – holder for MMA welding and torch for TIG welding;
- adapter ensuring tool connection to the technological interface module and power source;
- head phones (ear-phones) for verbal prompting during welding;
- personal computer;
- specialized software.